UNIVERSITY OF CALIFORNIA
Los Angeles

Mathematical Models of T-cell Population Dynamics in Aging and Immune Disease

A dissertation submitted in partial satisfaction
of the requirements for the degree
Doctor of Philosophy in Mathematics

by

Stephanie Marissa Lewkiewicz

2018

© Copyright by
Stephanie Marissa Lewkiewicz
2018

ABSTRACT OF THE DISSERTATION

Mathematical Models of
T-cell Population Dynamics
in Aging and Immune Disease

by

Stephanie Marissa Lewkiewicz
Doctor of Philosophy in Mathematics
University of California, Los Angeles, 2018
Professor Tom Chou, Chair

In this dissertation, we use birth-death-immigration systems of ordinary differential equations to study the dynamics of human naive T-cell populations in healthy aging and disease of the immune system. We derive a model that tracks both total cell counts and counts of clones (groups of genetically identical cells) of a particular size; from the latter, we compute the total clone count, or "diversity", which provides a quantitative measure of the extent to which the T-cell pool can cope with invading pathogens. We first formulate a nonautonomous model of T-cell birth and replenishment throughout an individual's lifetime, and use it to assess the relationship between the immune tissue damage, T-cell loss and dysfunction, and weakened immune response all observed simultaneously in aging. We identify tissue loss in the thymus as a fundamental cause of diminished T-cell counts, and also that diversity loss can only underlie weakened immune effectiveness in aging if small clones are ineffective against pathogen. Using a short-time, autonomous version of the same ODE, we then study changes to the T-cell pool during an instance of acute thymic atrophy and recovery. We identify equilibrium solutions that arise at different rates of T-cell production, and derive analytic approximations to the eigenvalues and eigenvectors of the linearization around the equilibria. From the forms of the eigenvalues and eigenvectors, we are able to estimate rates at which different size-segregated groups of clones converge to equilibria–that is, "adjust" to the changing rate of T-cell production. Finally, we formulate a total cell count model of populations of HIV-immune and HIV-susceptible cells of the T-cell lineage in the bone marrow, thymus, and peripheral

blood after transplant of HIV-immune bone marrow into an HIV-infected individual. We show that independent of assumptions about the homeostatic mechanism in the periphery, the ratio of HIV-immune to HIV-susceptible T-cells in each immune region should asymptotically approach the ratio of HIV-immune to HIV-susceptible stem cells that results after bone marrow transplant with no infection present. We show that with virus introduced into the system, the asymptotic ratio of HIV-immune to HIV-susceptible peripheral T-cells is highly sensitive to parameters affecting the body's ability to clear the virus.

The dissertation of Stephanie Marissa Lewkiewicz is approved.

Joseph M. Teran

Luminita Aura Vese

Otto Orlean Yang

Tom Chou, Committee Chair

University of California, Los Angeles

2018

For my protégée,

Charlotte,

who always reminds me of

what is truly important

TABLE OF CONTENTS

1 Introduction **1**

1.1 Biological Background 1

1.2 Modeling Background 4

2 T-cell Populations in Healthy Aging **6**

2.1 Introduction 6

2.2 Mathematical Models and Analysis 9

2.2.1 Total T-cell Population Model 9

2.2.2 Clonotype Abundance Distributions 14

2.2.3 Diversity of the Naive T-cell Repertoire 17

2.2.4 Sampling Statistics 19

2.3 Discussion 20

2.4 Summary and Conclusions 24

2.5 Appendix: Implementation of Numerical Truncation 25

2.6 Appendix: Steady States of the Autonomous Equations 26

2.7 Appendix: Convergence and Stability of c_k when $\gamma(t) \to 0$ 31

2.8 Appendix: Computation of Expected Sample Clonal Size Distribution . . 35

3 T-cell Populations During Acute Thymic Atrophy and Other Diseased States of the Immune System **43**

3.1 Introduction 43

3.2 Mathematical Model and Analysis 46

3.3 Solution Analysis in the Case $\gamma > 0$ (functioning thymus) 49

3.3.1 Analytic Solution of the Infinite Dimensional System 49

3.3.2 Equilibrium Solution and Linearization 51

3.3.3 Behavior of the Linearized and Fully Nonlinear Systems 58

3.4 Solution Analysis in the Case $\gamma = 0$ (full thymic cessation) 59
3.4.1 Analytic Solutions 59
3.4.2 Equilibrium Solutions and Linearization 60
3.4.3 Behavior of the Linearized and Fully Nonlinear Systems 70
3.5 Special Cases and Simulations 71
3.5.1 The Logistic Model 72
3.5.2 Constant Proliferation, Varying Death 73
3.5.3 Regulation of Proliferation and Death 75
3.6 Discussion and Conclusions 76
3.7 Appendix: Solution of Recurrence Relation 77

4 T-cell Populations During HIV Infection and Treatment 83
4.1 Introduction 83
4.2 Mathematical Model and Analysis 84
4.2.1 Stage 1: Population of Lymphoid Tissues with T-cells Before HIV Infection 84
4.2.2 Stage 2: Infection with HIV 87
4.2.3 Stage 3: After Treatment 95
4.2.4 Asymptotic Behavior in the Absence of Infection. 102
4.2.5 Asymptotic Behavior with Virus Present 110

References 112

LIST OF FIGURES

2.1 Qualitative behavior of the total T-cell population model (Eqs. 2.1, 2.2) . . . 38

2.2 Comparison of thymic export and cell population evolution time scales . . . 39

2.3 Simulation of c_k, effect of truncation . . . 40

2.4 Simulation of R_q . . . 41

2.5 Simulation of N and R_1 with rise in proliferation rate . . . 42

3.1 Eigenvalues and eigenvectors of $L_{\tilde{S}}$, $\gamma > 0$ . . . 56

3.2 Eigenvalues and eigenvectors of $L_{\tilde{S}}$, $\gamma > 0$, varying μ . . . 57

3.3 Computation of c_k from method of characteristics, comparison with truncated system . . . 61

3.4 Eigenvalues and eigenvectors of $L_{\tilde{S}}$, $\gamma = 0$ . . . 68

3.5 Dominant eigenvalue, $\tilde{\lambda}_1^S$, of $L_{\tilde{S}}$, plotted against γ, Case 1 . . . 73

3.6 Dominant eigenvalue, $\tilde{\lambda}_1^S$, of $L_{\tilde{S}}$, plotted against γ, Case 2 . . . 74

3.7 Dominant eigenvalue, $\tilde{\lambda}_1^S$, of $L_{\tilde{S}}$, plotted against γ, case 3 . . . 76

4.1 Simulation of Stage 3 with virus . . . 111

LIST OF TABLES

4.1 Stage 1 Functions and Parameters 86

4.2 Stage 2 Functions and Parameters 89

4.3 Roots of $b(\overline{y}_2)$ 94

4.4 Stage 3 Functions and Parameters 97

ACKNOWLEDGMENTS

I would first like to thank my advisor, Tom Chou, for all his guidance and support, and for introducing me to the field of immune system modeling, which I have come to love over the last few years. He really molded me into a confident, independent thinker, and helped me learn to believe in myself. I would never have grown into the researcher that I am today without him generously imparting his skill and expertise to me. I also thank him for his financial support over the years. I am also deeply indebted to my collaborator, Yao-li Chuang, who really poured time into explaining the fundamental connections between mathematics and biology to me. I can't express how much I appreciate his knowledge, patience, and eagerness to help. I would also like to thank Maria D'Orsogna for allowing me to participate in her neuroendocrine modeling project, and for financial support at the end of my time here.

I would like to thank my committee members, Joseph Teran, Luminita Vese, and Otto Yang, for their support of my research. I would especially like to thank Professor Vese for being exceptionally caring and supportive of me, for the interesting classes she taught, and for all the advice and motivation she provided me in my research. I thank Itay Neeman, who was the graduate vice chair at the start of my time here, and showed me much compassion in a time of personal hardship. I thank Michael Hitrik for an immense amount of advice, guidance, and support in the later years of my PhD. I thank Russ Caflisch for supervising me in my first (very enjoyable!) research project here, and for financial support. I would also like to thank Rachel Hegemann, who really acted as a mentor and friend to me in my first year at UCLA.

Thank you to all the great teachers I have had at every level, especially Fred Greenleaf at NYU, whose beautiful introductory analysis course made me fall in love with abstract mathematics. Thank you to John Rinzel at NYU, who gave me my first taste of mathematical research. Dziękuję Mariannie Chodorowskiej-Pilch i Romanowi Koropeckyjemu, że Państwo uczyli mnie języka polskiego. Nasze zajęcia były najlepszą częścią każdego tygodnia, i będę tęskniła za nimi po moim czasie w Los Angeles. Thank you to the staff in the math department, especially Martha and Maida, for all their help and kindness over the years.

Thank you to my late mother, Helen, for being wonderful to me when I was a child, and giving me everything I needed to thrive. I hope that I've made you proud. Thank you to my late aunt and grandmother, Elfriede and Helene, who cared for me in her absence. I miss you all very much, and hope that I see you again someday. Thank you to my father, John, who convinced me of the beauty of science and mathematics at a very young age, and has always believed that girls rule the world. Thank you to my uncle, Richie, for helping us through difficult times. Thank you to my parents and grandparents for paying my tuition to NYU, without which I would never have made it to UCLA.

For my nearest and dearest, in no particular order: Thank you, Steve and Jamaul, for always lifting my spirits. Thank you, Stelanie, for truly being my heart and soul. Thank you, Brian L., for being a ton of fun and helping me with my problems constantly. Thank you, Laurent, for being the best officemate ever, and an even better friend (on both the math side of life and the fun side of life!). Thank you, Vinay, for your unwavering kindness, and for being you, just in general. Thank you, Melissa and Josie, for our little sisterhood, and for lightening the mood. Thank you, Jasmine, for being the best person to laugh with, and always caring about me. Thank you to my late friend, Ilya, who always believed in me. (The memories I have of us learning math together at Courant at all hours of the night are among my very fondest.) Thank you to my wonderful academic brothers, Bhaven and Lae, for tons of emotional and biomathematical support. Thank you, Alexis, for your sweetness, maturity, and wisdom. Thank you, Shauna and Bryan, for carrying me when I couldn't walk on my own. Thank you to my favorite students, Charlotte and Isabelle, for our fun times in tutoring sessions. Thank you to everyone else who made graduate school better: Adam and Shaked, Julian G., Jacob and Michael, Justyna, Daniela, Ken, Farzin, Ian, Bryon, Lilian, Renaud, Tim and Connie, Mauricio, Alfonso, Gabe, Julian L., Vicky, Chris.

Last, but certainly not least, I thank my best friend, Ben–the person to whom this dissertation most owes its existence, and I my most sincere gratitude. You are a great mathematician and–more importantly–person, and a true ally of women and minorities in STEM and beyond. We are all lucky to have you, and I only hope that one day I can pay forward everything you have done for me.

Chapter 2 is a version of *A mathematical model of the effects of aging on naive T-cell*

population diversity, which has been submitted for publication. Chapter 3 is a version of *T-cell receptor diversity during acute thymic atrophy and resumption*, which is in preparation. Both are joint work with Yao-li Chuang and Tom Chou.

VITA

2018	Graduate Student Instructor, UCLA Math 33B: Differential Equations
2011–2018	Teaching Assistant, University of California, Los Angeles.
2010	NYU Mathematics Award
2010	B.F.A. (Mathematics and Theatre), New York University.

PUBLICATIONS

Lewkiewicz, S.M., Chuang, Y.L., Chou, T. (2018). *A mathematical model of the effects of aging on naive T-cell population diversity.* Manuscript submitted for publication.

Lewkiewicz, S.M., Chuang Y.L., Chou, T. (2018). *T-cell receptor diversity during acute thymic atrophy and resumption.* Manuscript in preparation.

CHAPTER 1

Introduction

1.1 Biological Background

Essentially all living organisms rely on an immune system for protection against foreign pathogens–the viruses, bacteria, fungi, and other microorganisms capable of causing harm to our bodily tissues. The human immune system, like that of most other vertebrate animals, is naturally divided into three major components: the skin, the innate immune system, and the adaptive immune system. The skin provides an immediate physical barrier to the outside world, acting as a first line of defense against invading pathogens. A pathogen that manages to breach this barrier first encounters the innate immune system, the agents of which are various cells and proteins only capable of distinguishing "foreign" objects from "self" objects, indiscriminately destroying anything of the former type. Almost all living things possess this type of immunity, and it is highly effective, as most pathogens that enter an organism are destroyed by the innate immune system. The few pathogens that manage to evade detection by the innate immune system are then dealt with by the more sophisticated adaptive immune system. The agents of the adaptive immune system, unlike those of the innate immune system, are tailored to respond to the specific pathogen the system has detected. In this dissertation, we will study the population dynamics of the most crucial component of the adaptive immune system: the T-lymphocyte, or T-cell. T-cells are truly the linchpin of the adaptive immune system, in the sense that they participate in the elimination of pathogen-infected cells and cancer cells, and also direct the action of many other immune agents throughout the course of an infection. We will construct and study ordinary differential equations models of human T-cell population dynamics during healthy aging, acute disease of the thymus, and bone marrow transplant treatment for HIV infection, each of which is associated with T-cell loss and/or dysfunction. We begin now with general background information about the

processes by which T-cells are made, compete to survive, and are destroyed, and the role T-cells play in the immune response. Background information pertaining specifically to T-cells in healthy aging (Chapter 2), acute thymic disease (Chapter 3), and bone marrow transplant during HIV infection (Chapter 4), will be provided at the start of each chapter.

A pool of nearly 10^{12} T-cells circulates in a human's peripheral bloodstream and lymphoid tissue at any given time. They circulate in a dormant state, awaiting stimulation by "antigen"–small pieces of protein, potentially derived from pathogenic microorganisms. Certain immune cells, referred to as antigen-presenting cells (APCs), consume pathogen and digest them into such protein pieces. The antigen is then affixed to an MHC molecule, and the antigen-MHC complex is transported to the surface of the APC, which presents the antigen to T-cells in the ambient environment. If the antigen-MHC complex on the APC binds to the T-cell receptor (TCR), a protein structure on the surface of a nearby T-cell, the T-cell becomes activated. In a sense, the T-cell has become alerted to the presence of pathogen in the organism, and enters an "effector" state. Once activated, the T-cell begins a period of rapid proliferation, building up a large colony of identical T-cells, which then work to clear the pathogen. It is important to note that not all antigen-MHC complexes are capable of binding to any given T-cell receptor, because the TCRs themselves are highly unique. Even though the thousands of TCRs on any given T-cell are identical to one another, the common TCR present on a given cell is unlikely to be detected on the surface of many other T-cells in the immune compartment (if any at all). The number of distinct TCRs present on cells in an individual's immune compartment is referred to as the "T-cell richness", and is one of many measures of the "diversity" of the T-cell pool. The greater the T-cell pool's diversity, the greater its capacity to deal with a wide range of pathogens. (In this dissertation, the word diversity refers specifically to richness, unless stated otherwise.)

T-cells originate from hematopoietic stem cells (HSCs) in the bone marrow. The process of creating a new T-cell begins when an HSC divides into two daughter cells, one of which commits to the T-cell lineage, thereby becoming a "T-cell progenitor" or "precursor", while the other retains the stem cell phenotype. Such T-cell precursors migrate from the bone marrow into the thymus, a small organ located above the heart, to begin the process of developing into a fully functioning T-cell. T-cells arrive in the thymus

in an immature state, and much of the maturation process consists of the acquisition of the TCR and other cell-surface molecules that allow it to communicate and interact with its ambient environment. Distinct TCRs are generated during development in the thymus through a process called recombination, during which genes that encode the TCR are rearranged to produce highly variable protein structures (the α and β chains, or δ and γ chains, which together constitute the TCR). Estimates indicate that $\sim 10^{15} - 10^{20}$ distinct TCRs can be constructed via this process, creating a highly diverse T-cell pool. Due to the small likelihood that recombination would by chance produce the same TCR twice, it is assumed that repeat TCRs in the periphery result from cellular division– or "proliferation"–which produces two identical daughter T-cells from one parent cell. Indeed, maturing T-cells undergo proliferation at several stages during their development in the thymus, and those released into the peripheral bloodstream undergo homeostatic proliferation to maintain ideal cell counts. The thymic environment vets the TCRs of developing T-cells for proper functionality. Stromal cells, which constitute the internal architecture of the thymus, stimulate the TCRs of developing T-cells with "self-antigens"– antigens derived not from a pathogen, but from the organism itself. A suitable TCR should react strongly enough to a self-antigen to indicate an ability to function during the immune response, but not so strongly that the TCR falsely identifies the self-antigen as a foreign target. The $1 - 5\%$ of T-cells maturing in the thymus that achieve this delicate balance are exported from the thymus into the peripheral bloodstream. At the time of export, a T-cell is said to be in a mature, but "naive", state, in reference to the fact that it has been deemed functionally competent, but has not yet been activated by antigen. If a naive T-cell is activated and proliferates to form a clone of identical effector cells, the infection is cleared and most of the cells in the clone die off, as they are no longer needed. Several cells from the clonal lineage remain in the system, and evolve (or "differentiate") into what is called a memory T-cell. This type of cell exists to retain a record of the encountered pathogen, so that the immune response may proceed more efficiently should the pathogen ever invade the organism again. The human body hosts a large pool of both naive and memory T-cells, and each population is subject to separate and communal mechanisms of homeostatic regulation.

1.2 Modeling Background

In this dissertation, we study the population dynamics of naive T-cells. Population models are among the oldest and most canonical in mathematical biology, originating from the simple exponential ODE, $x'(t) = \lambda x(t)$, which assumes that populations change at a rate proportional to the number of individuals present. Over time, they evolved to capture further nuances, notably that of population regulation based on feedback mechanisms, as well as immigration of new individuals to–and emigration of existent individuals from–the population. We will consider birth-death-immigration models, which account for changes to the population due to immigration of new T-cells from the thymus, and regulation-driven cellular proliferation and death in the peripheral blood and lymphatic tissue. T-cells have been modeled in this way for many years [MPF96, MPF97]. Previous modeling efforts include analysis of data pertaining to the thymic export rate of new T-cells [RP07, BTY09, HLC13], assessment of the relative importance of homeostatic maintenance and thymic export in sustaining the T-cell pool at different ages [BAC09, MKH03], and investigation of the influence of certain chemical resources in T-cell survival [RCL13]. As in this previous work, we use single population models to describe the total T-cell count, and also expand on the total cell count model by deriving a system of ODEs that describes the dynamics of individual T-cell clones or groups of clones. Such a model is advantageous when desiring to distinguish T-cell clones with certain attributes, such as a particular level of responsiveness to activation or suitability for survival, or those of a particular size [GKC15, DMM17]. We direct our attention to the last attribute, studying a model that tracks the total number of T-cell clones of a given size. As the size of a clone potentially correlates with its effectiveness in the immune response, the behavior of size-segregated T-cell groups informs predictions about immune effectiveness during disease. In this sense, we create a model that follows the T-cell population on a macroscopic and microscopic level, as it responds to changes induced by immune disease and throughout the course of human aging. For simplicity, we treat the different T-cell subgroups (CD4 versus CD8 cells) as one unified population; for modeling purposes, we regard the behavior of the average T-cell in a given context as an average of the behaviors of a CD4 and CD8 cell in that context.

The chapters in this thesis are more or less self-contained, so that they may be read individually without reference to other chapters.

CHAPTER 2

T-cell Populations in Healthy Aging

2.1 Introduction

Immunosenescence underlies poor health outcomes in the aging population, including diminished vaccine efficacy ([PLM10, MD08, FE08]), increased susceptibility to disease (including irregular presentation, intensified symptoms, longer recovery times, and increased mortality) ([TMA12]), and a heightened risk of cancer ([GLC01]). The aging of the human immune system is a highly degradative process, which originates from extensive fundamental changes to the size and functionality of immune cell pools, and the structure of lymphatic tissues in which they develop and operate ([SRD13]).

Among the many changes associated with immunosenescence ([GE00]), the T-cell compartment is arguably the most damaged ([WDB00, GHS07]). The T-cell pool is comprised of subpopulations of antigen-inexperienced naive cells and antigen-experienced memory cells, the latter of which retain immunological record of previous infections. The human immune compartment maintains $\sim 10^{12}$ T-cells in total, of which $\sim 10^{11}$ are naive ([JCM09, Tre74]). During aging, the population of naive T-cells declines in overall size, while the population of memory T-cells undergoes extensive proliferation, thereby reversing the balance of naive and memory T-cells that had persisted at younger ages ([GE00, FVP00]). The expansion of memory T-cells further enhances immunological memory of previously-encountered antigens, reinforcing existent immune protection. Many memory T-cells, however, experience senescence, whereby the ability to proliferate and function properly is lost. The remaining naive pool experiences loss of T-cell receptor (TCR) "structural diversity" ([GLW07, GQO15])–the number of distinct TCR complexes present across the entire naive pool. The diversity of T-cell clones, or "immunoclones", provides the extent of antigen specificity, with higher diversity corresponding to stronger

responsiveness to a larger number of pathogens. Unique TCR complexes are generated during T-cell development in the thymus, via recombination of genes encoding the V and J domains of the TCRα chain and the V, J, and D domains of the TCRβ chain, along with additional insertion and deletion of nucleotide fragments ([Mur12]). Combinatorially, a possible $\Omega_0 \sim 10^{15} - 10^{20}$ unique TCR complexes may be assembled via this rearrangement process ([LBA15]), but only $\Omega \sim (0.05) \times \Omega_0$ of those rearrangements are functionally viable ([Yat14]), as determined by positive and negative selection tests in the thymus, which screen for appropriate reactivity to self-peptide/MHC molecules. Each TCR is activated by at least one peptide fragment presented via MHC molecules on the surface of an antigen-presenting cell, thus loss of naive TCR structural diversity limits the number of new antigens to which the full naive T-cell pool can respond. Naive cells are also suspected to suffer major functional deficiencies in aging, such as diminished binding affinity and proliferative capacity after antigenic stimulation ([MAL13]). These effects have mostly been studied using murine models to date ([AS14]), and are not yet well understood in humans, thus beyond the scope of this thesis.

The total abundance of naive T-cells, which inhabit both blood and lymphatic tissue, can be reliably estimated from measurements in small samples ([WP90, BAC09]). Recently, Westera *et al.* [WHD15] estimated an $\sim 52\%$ decrease in the size of the naive T-cell population in aging. In contrast, accurate estimation of full-organism TCR structural diversity is currently impeded by experimental imprecision and the inability to extrapolate small sample data to the full organism ([LBA15]). Experimentation typically entails DNA sequencing of the TCRα or–more commonly–β chain, in particular the complimentarity-determining region 3 (CDR3), which is the site of TCR binding to antigenic peptide and most significant source of diversity ([Mur12]).

Increasingly sophisticated deep sequencing methods have improved estimates of a lower bound on TCR diversity, but its direct estimation remains a challenge due to various experimental complications, such as the inability to detect rare clonotypes, sequencing errors, and inaccurate measurement of clonotype frequencies resulting from inconsistencies in polymerase chain reaction (PCR) amplification ([LBA15]). Predicting full-organism TCR diversity from a small sample is typically formulated as an "unseen species problem", and one of many canonical solutions of such a problem is employed

in conjunction with experimental data ([Cha84, CL92, CC94]), but the true relationship between sample and full diversity is fundamentally elusive.

Despite variations in experimental measurements of TCR diversity, its age-related loss has been consistently observed. An early study conducted by Naylor *et al.* [NLV05] predicted a TCRβ chain diversity of $\sim 2\times10^7$ that persisted in donors through age 60, before dropping by two orders of magnitude to $\sim 2\times10^5$ at age 70. More recently, Britanova *et al.* [BPS14] collected samples from donors of all ages and observed an approximately linear decrease in TCRβ CDR3 diversity from $\sim 7\times10^6$ in youth $(6-25$ years) to $\sim 2.4\times10^6$ in advanced age $(61-66$ years). Qi *et al.* [QLC14] obtained a particularly high lower bound estimate of $\sim 10^8$ unique TCRβ sequences in youth $(20-35$ years), which declined two- to five-fold in advanced age $(70-85$ years).

Note that only the TCRβ chain is sequenced in these experiments. Sequencing of both the α and β chains together would potentially produce a more accurate measure of TCR diversity, but the same experimental limitations preclude complete analysis. The measurement of diversity is further complicated by the potentially complex relationship between structural diversity and "functional diversity"–that is, the number of antigens to which the T-cell pool is capable of responding. Due to the potential for crossreactivity, in which one TCR might respond to many structurally similar peptide fragments, it is possible that actual TCR diversity is much higher than structural diversity indicates. It has been speculated that one TCR might respond to as many as 10^6 different peptide epitopes ([Mas98]).

To obtain lifetime estimates of TCR structural diversity, and develop an informed context for discussion of functional diversity, we introduce a mechanistic mathematical model of the generation and replenishment of the lymphocyte pool from birth through the end of life. Although experimental assessments of full-system information remain challenging, measurements for the dynamics of each component related to the T-cell population can be found throughout the literature. Our mathematical approach combines the knowledge of these individual components to study their interplay, leading to an understanding of the full-system dynamics. By extending previous model studies of total cell counts ([MPF96, MPF97, RP07, BAC09, BTY09, HLC13, MKH03, RCL13]), our multi-component formulation is able to efficiently track the total number of distinct T-

cell clones, allowing for a full-system assessment of TCR structural diversity.

2.2 Mathematical Models and Analysis

We develop our mathematical model by first constructing the equation governing the total population size of the naive T-cell pool in Sec. 2.2.1, through which we quantitatively constrain the primary parameters of our model using experimental measurements found in previous literature. The model that describes the evolution of immunoclones is derived in Sec. 2.2.2, allowing us to define and estimate the diversity of the T-cell population in Sec. 2.2.3. In Sec. 2.2.4, we derive a method for computing full-organism diversity from the diversity measured in small samples.

2.2.1 Total T-cell Population Model

There are three fundamental immunological mechanisms that sustain the naive T-cell pool: 1) export of mature naive T-cells from the thymus, 2) peripheral proliferation (which is regulated by a mechanism separate from that which regulates memory cells), and 3) cell removal from the naive pool due to death or phenotypic changes. These basic mechanisms constitute a birth-death-immigration process described by the ordinary differential equation,

$$\frac{\mathrm{d}N(t)}{\mathrm{d}t} = \gamma(t) + pN(t) - \mu(N)N(t), \tag{2.1}$$

where $N(t)$ denotes the total T-cell count, $\gamma > 0$ denotes the rate of thymic output, $p > 0$ denotes the rate of proliferation, and $\mu(N) > 0$ denotes the rate of population-dependent regulated cellular death or loss of naive phenotype.

While more complex feedback mechanisms have been proposed in the context of the thymus ([MPF97]), other experiments have shown that thymic export is independent of naive T-cell counts ([RP07, BBM98, Met63]), and it is well-established that the export rate decays consistently throughout the human lifespan ([MKH03]). The lifelong decline of the thymic export rate is caused by thymic involution, the degradation of the structural

integrity and functional capacity of the thymus with age ([SKM85]). The age dependence of the rate of thymic export of newly-trained T-cells is often approximated by an exponentially decaying function, $\gamma(t) = \gamma_0 e^{-at}$, where $\gamma_0 > 0$ is the maximum rate of thymic output that arises in early years, and $a > 0$ is the rate of decrease in thymic output.

The immune systems of vertebrates maintain a healthy naive T-cell count through complex homeostatic mechanisms, which include controlled production and distribution of common gamma chain cytokines, particularly IL-7, to the naive pool ([FM05]). IL-7 is secreted by stromal and endothelial cells in the thymus, bone marrow, and lymphatic tissue, providing T-cells with necessary survival signals. In lymphoreplete conditions, competition for this limited resource regulates population size ([BHS05, TDL01, VBM01]), but in lymphopenic conditions, high levels of IL-7 resulting from low T-cell counts can even stimulate cellular proliferation. While IL-7 concentration may be explicitly formulated in a mathematical model of the peripheral T-cell population, as in the work of Reynolds *et al.* [RCL13], most models incorporate IL-7 regulation implicitly in the form of carrying capacity, assuming quick equilibration in a state of competition for IL-7 in the presence of a given number of T-cells. Such simplification commonly leads to the dependence on total cell counts of both cell proliferation and cell death rates, considering the cytokine's dual role under lymphoreplete and lymphopenic conditions described above. Our model assumes cell-count dependence of the cell death rate only, focusing on scenarios of *healthy* aging, i.e., lymphoreplete conditions. We thus assume an N-dependent cell death rate of the form

$$\mu(N) = \mu_0 + \frac{\mu_1 N^2}{N^2 + K^2}, \tag{2.2}$$

where the first term, $\mu_0 > 0$, is the basal rate of cellular death. The second one describes the IL-7-mediated regulation of cell death, with $\mu_1 > 0$ representing the maximal increase to the death rate as $N \to \infty$. The quantity K is analogous to a "carrying capacity" and dictates the population at which signalling induced death starts to limit the population. The constant rate of cellular proliferation under healthy conditions is supported by recent studies of Westera *et al.* [WHD15], showing nearly identical naive proliferation rates in youth and advanced age during moderate age-related non-lymphopenic loss of naive cells. IL-7 induced proliferation can arise in *unhealthy* lymphopenic conditions typically found

in severe disease of the immune system ([BMS14]), cytotoxic drug use ([Ger99]), radiation treatment ([GEC15]), or other abnormal situations. These scenarios are, however, beyond the scope of our analysis.

Our model has six adjustable parameters, γ_0, a, p, μ_0, μ_1 and K. The first four are biologically inherent to the mechanism of T-cell homeostasis, and have been measured experimentally in humans and rodents. The last two have to be constrained via parameter sweeps to match relevant experimental observations. Fig. 2.1(a) illustrates four qualitatively distinct trajectories of $N(t)$ that may arise from simulations of the model in the presence of a decaying thymic export rate $\gamma(t)$ (gray dash-dotted curve). To non-dimensionalize Eqs. 2.1, 2.2, we use a^{-1} to rescale t and K to rescale N. The qualitative behavior of our model is thus controlled by three independent parameters: $\gamma_0 a^{-1} K^{-1}$, $(p-\mu_0)a^{-1}$, and $\mu_1 (p-\mu_0)^{-1}$. The black dashed curve arises when $\mu_1 (p-\mu_0)^{-1} < 1$. In this case cell proliferation always exceeds cell death, leading to unbounded expansion of the naive T-cell population. This scenario is unrealistic, except perhaps during a period of lymphopenia. For $\mu_1 (p-\mu_0)^{-1} \geq 1$, cell death is able to balance cell proliferation at a homeostatic carrying capacity $N = N_{ss}(\gamma = 0)$, defined by $\mu(N_{ss}(\gamma = 0)) = p$, as $\gamma \to 0$. As illustrated by the green dotted curve, $N(t)$ rises and asymptotically converges towards $N_{ss}(\gamma = 0)$ provided that $\gamma_0 a^{-1} K^{-1} \ll 1$. We refer to this parameter regime as "proliferation-driven", given that the cell population is driven to $N_{ss}(\gamma = 0)$ primarily by homeostatic proliferation. The model's behavior makes a transition from proliferation-driven to "thymus-driven" if we increase $\gamma_0 a^{-1} K^{-1}$. As shown by the blue solid curve, $N(t)$, driven by increased thymic export, overshoots and approaches $N_{ss}(\gamma = 0)$ asymptotically from above as $\gamma(t) \to 0$. Finally, the red dash-dotted curve arises when $(p-\mu_0)a^{-1} \leq 0$. In this case, cell death always exceeds cell proliferation as $\gamma(t) \to 0$, and $N(t) \to 0$. As stated earlier, in this paper we focus on scenarios of healthy aging (lymphoreplete) conditions, which immediately rules out the scenarios of unbounded growth (black dashed curve) and complete collapse of the T-cell population (the red dot-dashed curve), effectively constraining our parameters to the physiologically reasonable values $\mu_1 (p-\mu_0)^{-1} \geq 1$ and $(p-\mu_0)a^{-1} > 0$.

We can further quantitatively calibrate the parameter values using experimental measurements in the literature. The constant peripheral proliferation rate p has been mea-

sured by Westera *et al.* [WHD15] as 0.05% day^{-1}, or equivalently $p = 0.18$ year^{-1}. The basal death rate μ_0 can be estimated from the lifespan of T-cells. Based on data from Vrisekoop *et al.* [VBB08], De Boer and Perelson [dP13] obtain an average naive CD4$^+$ T-cell lifespan of ~ 5 years and an average naive CD8$^+$ lifespan of ~ 7.6 years. Given the normal CD4$^+$:CD8$^+$ ratio of 2:1, the average combined naive T-cell clearance rate is $\mu_0 = \frac{1}{5.9}$ year^{-1} $= 0.17$ year^{-1}. Thymic involution with age can be quantified by measuring the decrease in thymic epithelial volume ([Ste86]), based on which Murray *et al.* [MKH03] showed that thymic output decreases by an average of 4.3% per year between ages 0 and 100, implying a decay factor of $a = |\ln(0.957)| \simeq 0.044$. The rate of thymic export has recently been measured in young adults ($20-25$ years old) at $\sim 1.6\times10^7$ trained cells daily, or equivalently 5.8×10^9 per year ([WHD15]). Assuming that this rate is $\gamma(t)$ at $t = 25$ years, we can back-calculate $\gamma_0 = (5.8 \times 10^9) \times \left(\frac{100}{33.3}\right) \approx 1.75 \times 10^{10}$ cell exports/year. Note that these values of p, μ_0, and a satisfy the constraint $(p - \mu_0)\, a^{-1} > 0$ that prevents the T-cell population from completely collapsing.

While direct experimental measurements of μ_1 and K are not available in the literature, further inspection of Fig. 2.1(a) reveals that μ_1 and K determine whether thymic export or homeostatic proliferation dominates the evolution of $N(t)$. Through the dimensionless parameters, $\gamma_0 a^{-1} K^{-1}$ and $\mu_1\,(p - \mu_0)^{-1}$, the time at which $N(t)$ peaks and the speed at which it declines from the peak vary with changes to the values of μ_1 and K. Recently, Westera *et al.* [WHD15] reported a 52% decrease in total naive T-cell counts between young adults and elderly individuals, which we can use to quantitatively constrain μ_1 and K. Let us define individuals of an age between $t = 20$ and 30 years as young adults, and those between $t = 70$ and 80 as the elderly. Assuming that interpersonal heterogeneity unrelated to age averages out over large sample sizes in clinical data, we may evaluate $\bar{N}_{\rm y} = \frac{1}{10}\int_{20}^{30} N(t)\mathrm{d}t$ and $\bar{N}_{\rm o} = \frac{1}{10}\int_{70}^{80} N(t)\mathrm{d}t$ as the average naive T-cell counts in the young and the elderly, respectively, as illustrated by the shaded areas under the thymus-domination curve in Fig. 2.1(a). The relative change in the naive T-cell count between youth and advanced age can thus be evaluated as

$$\Delta(\bar{N}) = \frac{(\bar{N}_{\rm o} - \bar{N}_{\rm y})}{\bar{N}_{\rm y}}. \tag{2.3}$$

Fig. 2.1(b) plots $\Delta(\bar{N})$ as a function of $\gamma_0 a^{-1} K^{-1}$ and $\mu_1 (p - \mu_0)^{-1}$, with $a = 0.044$ year^{-1} for converting the dimensionless time to years to compute $\bar{N}_{\rm y}$ and $\bar{N}_{\rm o}$. When $\gamma_0 a^{-1} K^{-1} \lesssim 1$ and $\mu_1 (p - \mu_0)^{-1} \lesssim 2$, $\Delta(\bar{N}) > 0$. Note that the homeostatic carrying capacity when $\gamma(t) = 0$ is $N_{ss}(\gamma = 0) = K \left(\mu_1 (p - \mu_0)^{-1} - 1\right)^{-1}$. A small $\gamma_0 a^{-1} K^{-1}$ value represents a relatively low thymic export rate, and the carrying capacity increases rapidly as $\mu_1 (p - \mu_0)^{-1} \to 1$, both of which make it challenging for thymic output to fill up the T-cell pool to carrying capacity before $\gamma(t)$ considerably decays before $t \sim a^{-1}$. As a result, $N(t)$ does not reach a peak value in youth and continues increasing into old age. The $\approx 52\%$ decrease in naive T-cell counts reported by Westera *et al.* [WHD15] is depicted by the black dotted curve. If we set $\mu_1 (p - \mu_0)^{-1} = 4$, our model can be calibrated to reproduce this decrease in the cell count by choosing $K = 10^{10}$ ($\gamma_0 a^{-1} K^{-1} \simeq 41$ with $\gamma_0 = 1.8 \times 10^{10}$ and $a = 0.044$). In contrast, $K = 10^{12}$ yields $\gamma_0 a^{-1} K^{-1} \simeq 0.41$, leading to an increase in the cell count ($\Delta(\bar{N}) \simeq 0.63$). In between, $K = 10^{11}$ results in a moderate decrease in the cell count ($\Delta(\bar{N}) \simeq -0.33$). For the rest of the paper, we fix $K = 10^{10}$ and $\mu_1 (p - \mu_0)^{-1} = 4$, or equivalently $\mu_1 = 0.04$, given that $p = 0.18$ and $\mu_0 = 0.17$, so that the age-related decline of $N(t)$ in our model is consistent with the results of Westera *et al.* [WHD15].

Note that there exist two intrinsic timescales in Eq. 2.1; thymic export decays at rate a, while the homeostatic time scale is controlled by p, μ_0, and μ_1. If homeostasis is much faster than thymic involution, the solution $N(t)$ will quickly converge to the quasisteady-state solution as $\gamma(t)$ evolves. We compare these two solutions in Fig. 2.2(a), where the quasisteady-state solution is obtained by solving for the steady-state solution, $N_{\rm ss}$, of Eq. 2.1 with fixed $\gamma(t)$ at each time t, and $N_{\rm ss}(\gamma(t))$ (black dashed curve) decreases monotonically with age due to the continuous decline of $\gamma(t)$. In contrast, $N(t)$ (blue solid curve) slowly rises from the initial condition $N(1) = 10^{11}$ and does not approach the quasisteady-state level until age ≈ 20 years. The trajectory of $N(t)$ then overshoots the declining $N_{\rm ss}(\gamma(t))$, reaches a peak value, and reverses course to follow $N_{\rm ss}(\gamma(t))$. However, $N(t)$ doesn't catch up with $N_{\rm ss}(\gamma(t))$ before the latter reaches a steady-state representing a very low cell count. That $N(t)$ keeps lagging behind $N_{\rm ss}(\gamma(t))$ indicates that the timescale on which the full model solution converges to the local steady-state is slower than that on which the nonautonomous term $\gamma(t)$ evolves. The results here

suggest that steady-state solutions cannot adequately describe the temporal evolution of the T-cell population in the biologically relevant range of parameter values that we have implemented. It is necessary to numerically compute the time-dependent solutions of the full nonautonomous equation.

Indeed, we find a disparity in the rates at which thymic export decays and the steady state solutions evolve. The latter is provided by the inverse of the linearization of Eq. 2.1 around $N = N_{ss}(\gamma(t))$. The eigenvalue takes the form $\lambda_1 = p_0 - (\mu_0 + \mu_1((3N_{ss}^2K^2 + N_{ss}^4)/((K^2 + N_{ss}^2)^2))$. Simulations in Fig. 2.2(b) show that for the biologically relevant parameter values we have implemented, the cell-population evolution timescale, $|\lambda_1|^{-1}$ (red solid curve), is generally longer than the timescale of thymic involution ($a^{-1} \simeq 22.7$ years for $a = 0.044$, as denoted by the horizontal black dotted line). Hence the nonautonomous solutions $N(t)$ are expected to lag behind the thymus-driven steady-state solutions N_{ss}. For $N(t)$ to be reasonably well-approximated by N_{ss}, the cell population has to evolve much faster than thymic involution. This occurs when μ_1 is very large (the blue dash-dotted curve), and cell death is extremely sensitive to the cell population size.

2.2.2 Clonotype Abundance Distributions

We now wish to formulate a model that captures the behavior of individual clones. Assign to each clone an index i, with $i \in \mathbb{N}$. Assuming the same population dynamics for each T-cell clonotype, the evolution of the expected cell count, $n_i(t)$, of the i-th clone may be deduced from Eq. 2.1 and take the following generalized form,

$$\frac{\mathrm{d}n_i}{\mathrm{d}t} = \frac{\gamma(t)}{\Omega} + pn_i - \mu(N)n_i, \tag{2.4}$$

where $\gamma(t)/\Omega$ represents thymic export of naive T-cells of *each* TCR type (the total thymic export rate divided by the total number of viable TCR combinations Ω), and $N(t) = \sum_i n_i(t)$. Within the framework of these "neutral" models, basic qualitative behaviors of T-cell population dynamics have been investigated, particularly for scale-invariant properties that can be studied in a reduced system ([LCH16, DMW15]). Indeed, the total number of T-cell clonotypes, Ω, in rodent or human bodies is prohibitively large for

direct numerical simulation of the full system using Eq. 2.4. It is thus common to reduce the full system to a more manageable size with the assumption that the phenomena under investigation are scale-invariant. However, it is sometimes difficult to assert whether a certain property really does not change in a re-scaled system, as nonlinear phenomena, such as the Allee effects, often arise in population dynamics and cast doubt on the scalability of the system. Moreover, some properties, such as the thymic export rate, $\gamma(t)$, are naturally scale dependent. It is not always clear how these quantities should be re-scaled in a reduced system, and they have typically been omitted by simplification arguments in previous models, which limits the applicability of these models.

To facilitate a more manageable full-system model, we consider a formulation that tracks how the expected number of clones of a given size changes with time. By focusing on the clone count rather than the count of cells of each distinct clonotype, we are able to effectively reduce the number of tracked variables and thus the dimension of the model. This representation was used by Ewens in population genetics [Ewe72], by Goyal *et al.* [GKC15] in the context of hematopoietic stem cell population dynamics, and by Desponds *et al.* in the context of T-cells [DMM17]. We define $\hat{c}_k(t)$ to be the number of clones represented by exactly k naive T-cells in the organism at time t:

$$\hat{c}_k(t) = \sum_{i=1}^{\Omega} \delta_{n_i(t),k}, \tag{2.5}$$

where the Kronecker delta function, $\delta_{x,y}$, satisfies $\delta_{x,y} = 1$ when $x = y$ and $\delta_{x,y} = 0$ otherwise. By lumping clones of a common size into one single variable, $\hat{c}_k$, we can efficiently describe changes to the full system TCR diversity, albeit at the expense of the ability to distinguish individual clonotypes ([MCB14, MW16]). Individual clone information is lost, and $n_i(t)$ cannot be recovered from $\hat{c}_k(t)$ after the transformation in Eq. 2.5. Nonetheless, the amount of computation can be significantly reduced by truncating $\hat{c}_k(t)$ at a reasonably large k, as few large clones exist in realistic scenarios, and $\hat{c}_k(t)$ for large k is negligible. Letting $c_0(t) \equiv \langle \hat{c}_0(t) \rangle$ denote the expected number of all possible (thymus-allowed) clonotypes unrepresented in the periphery at time t, and $c_k(t) \equiv \langle \hat{c}_k(t) \rangle$ the expected number of clones of size k at time t, a closed set of equations governing the

evolution of $c_k(t)$ can be derived from Eq. 2.4 in the mean-field limit,

$$\frac{\mathrm{d}c_k(t)}{\mathrm{d}t} = \frac{\gamma(t)}{\Omega}\left[c_{k-1} - c_k\right] + p\left[(k-1)c_{k-1} - kc_k\right] + \mu(N)\left[(k+1)c_{k+1} - kc_k\right], \qquad (2.6)$$

where $N(t) = \sum_i^\infty n_i(t) = \sum_{\ell=1}^\infty \ell c_\ell(t)$. The expected values $c_k(t)$ are also called species abundances in the ecology literature. The number of unrepresented clones is $c_0 = \Omega - \sum_{k=1}^\infty c_k$, and summing Eq. 2.6 multiplied by k over $k = 1, 2, \cdots$ recovers Eq. 2.1. The mean-field assumption is articulated in terms such as $\mu(\sum_\ell \ell\hat{c}_\ell)\hat{c}_k$ that involve higher-order products of $\hat{c}_k$ rather than correlations of products of $\hat{c}_k$.

We have found that this mean-field approximation breaks down only when $\gamma/\mu < 1/\Omega \ll 1$ (unpublished results). With this parameter relationship, the total population is proliferation driven and the quasistatic configuration is $N \sim K$ and all $c_k \sim 0$ except c_M, where M is the finite index at which the ODE system is truncated. Thus, we reasonably assume that $\gamma(t) > \mu/\Omega$ allowing the use of the mean-field equations 2.6.

In Eq. 2.6, the terms $(\gamma(t)/\Omega)c_k$, pkc_k, and $\mu(N)kc_k$ respectively represent the effects of thymic export, homeostatic proliferation and cell death on a T-cell clone consisting of k cells in the peripheral blood. Adding one cell via thymic export or homeostatic proliferation moves one clone from the c_k-compartment to the c_{k+1}-compartment, while the death of one cell shifts one clone from the c_k-compartment to the c_{k-1}-compartment. Proliferation and thymic export thus reduce c_k and increase c_{k+1}, while death reduces c_k and increases c_{k-1}.

In a healthy, aging adult, the TCR repertoire is mostly comprised of small clones, and the probability of finding a clone of size k decreases as k increases. To solve Eq. 2.6 numerically, we thus truncate the model at a maximum clone size $M \gg 1$, beyond which the probability of finding a clone is assumed negligible. For our implementation of the truncation, please see Appendix 2.5. In Fig. 2.3(a) we examine the effect of changes to M on solution behavior. We find that for $M \gtrsim 30$, increases to M produce effectively no change in $c_{10}(t)$ at $t = 40$ and 70, indicating that inclusion of clones of size larger than 30 has little effect on the solution for $t \lesssim 70$ years. For numerical simulations of Eq. 2.6 in this chapter, we set $M = 200$ to ensure minimal truncation errors.

Fig. 2.3(b) shows the temporal evolution of $c_k(t)$ for $k = 2$, 19, and 59. As k increases, the overall magnitude of $c_k(t)$ decreases, and the age at which $c_k(t)$ peaks increases. For example, $c_2(t)$ peaks in the region $t \lesssim 20$ years, and there are many fewer clones of size 2 in old age than there are in youth. In contrast, $c_{19}(t)$ peaks around age 55, and the number of clones of size 19 is roughly the same in old age as it was in youth, while the number of clones of size 59 ($c_{59}(t)$) keeps increasing into old age.

That $c_k(t)$ peaks earlier when k is smaller is expected, considering that new single-cell clones are introduced into the peripheral circulation primarily by the thymus, which starts to involute shortly after birth. When k is larger, thymic export has less of an influence–and homeostatic proliferation more of an influence–on $c_k(t)$. Recalling that the rate of thymic involution is faster than the time scale on which homeostasis drives the clonal population towards equilibrium, the fast collapse of the rare clone population leaves room for larger clones to expand.

To accompany the steady state N_{ss}, we compute analogous fixed-γ_0 steady state solutions of the full system, c_k^{ss}, in Appendix 2.6. The steady-states satisfy $c_k^{ss} \to 0$ as $\gamma_0 \to 0$ for all $1 \leq k \leq M$. We show that despite the fact that $c_k^{ss} \to 0$ as $\gamma_0 \to 0$, Eq. 2.6 asymptotically yields a positive total cell count, with $\lim_{\gamma_0 \to 0} \lim_{M \to \infty} \sum_{k=1}^{M} k c_k^{ss} > 0$, indicating qualitative consistency with the positive, stable steady-state of Eq. 2.1. Moreover, we prove in Appendix 2.7 that solutions $c_k(t)$ of the full nonautonomous system satisfy $c_k(t) \to 0$ for all $1 \leq k \leq M$ as $t \to \infty$, independent of M. This result is completely independent of the assumed functional forms of the proliferation and death rates, suggesting that manipulation of homeostatic regulatory mechanisms cannot prevent the extinction of small T-cell clones caused by the decay of $\gamma(t)$ to 0. We thus conclude that TCR diversity cannot be preserved in the context of an involuting thymus.

2.2.3 Diversity of the Naive T-cell Repertoire

From the functions c_k that track the number of clones consisting of k cells, we are able to observe how TCR diversity changes over the course of a human lifespan. TCR structural diversity, or "richness", is the total number of distinct clones present in the immune compartment. To explore the nuances of the notion of TCR diversity, we define a "threshold" TCR richness diversity,

$$R_q(t) = \sum_{k \geq q} c_k(t), \tag{2.7}$$

where $q \in \mathbb{N}$, and $R_q(t)$ represents the number of clones of size at least q present in the immune compartment at time t. There are several reasons to consider omitting clones smaller than a minimal size threshold. The initiation of the adaptive immune response requires physical contact between a T-cell and another immune cell capable of activating it, and the likelihood of such a collision intuitively decreases with clone size, suggesting the possibility that sufficiently small clones are unlikely to engage the immune response. Moreover, when measuring TCR diversity in humans experimentally, small clones are likely to evade detection during sampling. The ability to neglect small clones in our diversity measure thus allows us to paint a more accurate picture of immune responsiveness and experimental results.

As shown in Fig. 2.4(a), $R_q(t)$ increases in youth, peaks in childhood or early adulthood, and declines afterwards. As q increases, the time t at which $R_q(t)$ peaks increases. This behavior is consistent with that of the individual functions $c_k(t)$, as shown in Fig. 2.3(b).

To compare values of $R_q(t)$ in youth and advanced age, we adopt the same measure used to study total cell counts. Defining $\bar{R}_{\mathrm{y}}(q) \equiv \frac{1}{10}\int_{20}^{30} R_q(t)\mathrm{d}t$, and $\bar{R}_{\mathrm{o}}(q) \equiv \frac{1}{10}\int_{70}^{80} R_q(t)\mathrm{d}t$, we quantify the loss of richness by computing its relative change,

$$\Delta(\bar{R}_q) \equiv \frac{(\bar{R}_{\mathrm{o}}(q) - \bar{R}_{\mathrm{y}}(q))}{\bar{R}_{\mathrm{y}}(q)}. \tag{2.8}$$

Using the same parameter values as in Fig. 2.4(a), we plot $\Delta(\bar{R}_q)$ with respect to μ_1 in Fig. 2.4(b), and with respect to q in Fig. 2.4(c). In Fig. 2.4(b), $\Delta(\bar{R}_q)$ decreases monotonically with increasing μ_1, suggesting that an upregulated death rate exacerbates the age-related loss of richness, with the impact more significant at larger q. Fig. 2.4(c) shows that when $K = 10^{10}$, $\Delta(\bar{R}_q) < 0$ for $q \leq 4$. The lifetime decrease in R_q for small q generally agrees with the loss of diversity observed in recent experiments where measurements were taken from individuals at many ages ([QLC14, BPS14]). For $q = 5, 6,$

$\Delta(\bar{R}_q) \approx 0$, and R_q is nearly unchanged between youth and advanced age. For $q \geq 7$, $\Delta(\bar{R}_q) > 0$, indicating that R_q actually increases with age. Generally, $R_q(t)$ presents a lifetime decrease for small q, and a lifetime increase for large q, in agreement with our discussion of Fig. 2.3(b) and Fig. 2.4(a). This phenomenon indicates that loss of diversity is primarily due to the extinction of rare clones, which is consistent with the observation made by Naylor *et al.* [NLV05]. In contrast, the number of larger clones increases over time, leading to the lifetime increase to $R_q(t)$ at higher q.

Recent TCR-β sequencing studies have attempted to estimate the change in the naive T-cell repertoire richness with age. Even though these studies produce estimates of TCR diversity that differ from one another by up to several orders of magnitude, they all agree that there is a dramatic loss of richness with age. For example, Britanova *et al.* [BPS14] estimated a diversity of $\sim 7\times10^6$ distinct clonotypes in youth (ages $6-25$), and $\sim 2.4\times10^6$ in aged individuals (ages $61-66$), a roughly 66% decrease. Similar measurements were also reported by Qi *et al.* [QLC14], in which a two-to-five-fold decline (i.e., a 50% – 80% drop) between youth (ages $20-35$) and advanced age (ages $70-84$) was observed. These results are quantitatively consistent with our computation of $\Delta(\bar{R}_1)$ for $K = 10^{10}$ – $10^{11.5}$ and $0.03 \leq \mu_1 \leq 0.05$ in Fig. 2.4(d), whereas the decline of R_q for $q \geq 2$ is not as pronounced as that observed in these experiments.

2.2.4 Sampling Statistics

Considering that naive T-cell richness is often assessed via small blood samples, let us next use the same framework to examine the relationship between the detected clone sizes in small samples and the true clone sizes in the full organism. As before, denote by N the total number of naive T-cells in the human's immune compartment, and $Y \leq N$ the number of cells collected during sampling from among the N total. We assume that the N total cells consist of R distinct clones, which we number from 1 to R. In this section, we denote by c_k^N the mean number of clones of size k from among the N total cells in the full organism (denoted by c_k in the previous simulations), and by c_k^Y the mean number of clones of size k in the sampling of Y cells taken from the N total cells. Then the expectation of c_k^Y, denoted by $\mathbb{E}[c_k^Y]$, is,

$$\mathbb{E}[c_k^Y] = \sum_{j=1}^{R} jP\left(c_k^Y = j\right), \tag{2.9}$$

where $P\left(c_k^Y = j\right)$ represents the probability that there are precisely j clones of size k in the sampling. Then $\mathbb{E}[c_k^Y]$ may be expressed explicitly in terms of the c_k^N as:

$$\mathbb{E}[c_k^Y] = \sum_{l=k}^{R} \frac{1}{\binom{N}{Y}} c_l^N \binom{l}{k}\binom{N-l}{Y-k}. \tag{2.10}$$

(See Appendix 2.8 for the detailed proof.) The collection of expressions given by Eq. 2.10 for $k = 1, 2, \cdots, R$, yields a linear system of equations solvable for c_k^N, using sampled data for the quantities $\mathbb{E}[c_k^Y]$. More specifically, if we define the vectors $\widehat{\mathbf{E}} := (\mathbb{E}[c_1^Y], \mathbb{E}[c_2^Y], \cdots, \mathbb{E}[c_R^Y],)$ and $\mathbf{E} := (c_1^N, c_2^N, \cdots, c_R^N)$, Eq. 2.10 can be written as $\widehat{\mathbf{E}} = \mathbf{A}\mathbf{E}$, where $\mathbf{A}$ is a constant matrix that has non-zero elements only in the upper triangle, with non-zero diagonal entry $\frac{1}{\binom{N}{Y}}\binom{N-k}{Y-k}$ in position (k, k). The equation can always be solved uniquely for $\mathbf{E}$ given $\widehat{\mathbf{E}}$. Thus the full size distribution $\mathbf{E}$ can be uniquely reconstructed from the expected mean sample size distribution $\widehat{\mathbf{E}}$ measured experimentally, provided that the latter can be reliably estimated through a sufficient number of repeated samplings.

2.3 Discussion

We have formulated a model of lifetime human naive T-cell population dynamics, which traces T-cell lineages on the level of individual clones. It accounts for exponentially decaying lifetime thymic export, a constant rate of cellular proliferation, and variable cellular death rate that adjusts to present cell counts and availability of survival resources. It depicts the generation of the naive T-cell pool in early life via thymic export, and long-term maintenance of the population via peripheral turnover after thymic export has waned. Values of most of the model's parameters can be found in previous literature, while the few exceptions are obtained by fitting some basic results of the model, such

as age-related T-cell loss, to previous experiments. Our analysis serves two important purposes: to map the thymic machinery, identifying which components do and do not contribute to age-related cellular loss, and then to interpret the nuanced role of that cellular loss in immunosenescence.

First, we compare simulations of the nonautonomous N-ODE in Eq. 2.1 with quasisteady-state solutions $N_{SS}(\gamma(t))$, over the course of age-related thymic export erosion. We find that the nonautonomous solution lags behind the changing quasisteady-state solutions, suggesting that thymic export decays on a faster timescale than that on which solutions of the frozen-coefficient autonomous ODE converge to steady-state. Mathematically, this result reveals that the evolution of the T-cell population within the human lifespan is a rather dynamical phenomenon, which may not be well-described by quasistatic solutions, requiring evaluation of the fully nonautonomous system. Biologically, our results indicate that the loss of T-cell diversity is a delayed response to thymic involution, and we may predict the health of the immune system by assessing the level of thymic function.

We have found that if thymic export is assumed to decay exponentially to zero, then all compartments $c_k(t)$ (with $1 \leq k \leq M$) deplete as $t \to \infty$, independent of essentially any restrictive assumptions about the homeostatic mechanism in the periphery. Concretely, for any choice of proliferation and death rates $p(N), \mu(N)$, that satisfy $p(0), \mu(0) > 0$, and with the choice $\gamma(t) = \gamma_0 e^{-at}$ with $\gamma_0, a > 0$, there exists a sufficiently small $\delta > 0$ such that $c_k(t) \to 0$ as $t \to \infty$ for all $1 \leq k \leq M$, if $\sum |c_k(1)| \leq \delta$. Although this result only ensures that trajectories $c_k(t)$ initialized sufficiently close to zero converge to zero, simulation indicates that the basin of attraction to this "zero state" is actually quite large. In fact, for the typical initial conditions used throughout this chapter, simulation suggests convergence of all compartments c_k to zero in infinite time. Although full depletion of the c_k compartments only occurs in infinite time, the drop in richness diversity observed during the human lifespan corresponds to the initial phase of this asymptotic process. Most importantly, we are able to identify the exponentially-diminishing thymic export rate as a fundamental cause of age-related diversity loss, in the sense that the T-cell pool cannot survive if the rate of thymic export decays to zero, independent of the functional forms of the homeostatic rate coefficients $p(N), \mu(N)$. Even a particularly

strong homeostatic mechanism (say, one with $p(0) \gg \mu(0)$) cannot rescue a plunging diversity. This, in turn, suggests that in searching for treatments of age-induced loss of diversity, efforts should be directed at the thymus, in particular to maintaining thymic productivity into advanced age.

Although peripheral division cannot salvage the T-cell population on a long time scale, we suspect that a higher basal proliferation rate may at least delay the erosion of the T-cell compartment, sustaining acceptable effectiveness of the immune system within the human lifespan ([NLV05]). With that in mind, we use a modified form of our model to investigate the feasibility of artificially increasing the basal proliferation rate to combat immune dysfunction. For simplicity, we take the death rate to be constant ($\mu(N) = \mu_0 > 0$), and adopt a logistic growth rate, $p(N,t) = p(t)(1 - N/K)$, in which a jump increase in the proliferation rate is incorporated into $p(t)$. We let $p(t) = p_0(1 + rH(t - T))$, with $p_0 > 0$ the early-life basal cellular proliferation rate, and $H(t)$ the Heaviside function, with T the age at which the proliferation rate increases. The constant r specifies the magnitude of the increase to the proliferation rate. (Full simulation details are given in the caption of Fig. 2.5.) In addition to modeling treatment with, for instance, a chemical agent to induce heightened cellular proliferation, this formulation could also describe a natural increase to the basal proliferation rate. We assumed a constant lifetime rate of proliferation, but alternative research suggests that such an inherent proliferation rate increase may, in fact, occur ([NLV05]). This alternate description of the homeostatic mechanism thus serves the dual purpose of exploring an alternate model formulation, to which the perturbation analysis outlined in Appendix 2.5 does not apply, and also to investigate manipulation of the homeostatic mechanism as a treatment option. By varying r, simulation under these alternate hypotheses indicates that increased basal proliferation rates do lead to notably higher total cell counts (Fig. 2.5(a)), but have little effect on diversity (Fig. 2.5(b)). These results further affirm that heightened peripheral proliferation is unlikely to rescue the eroding naive T-cell diversity, despite the increased cell count. If diversity loss is the main cause of immunosenescence (an idea still up for debate in the medical community), peripheral proliferation may not be the sensible target of treatment.

Although artificial increases to the basal proliferation rate are unable to salvage the declining diversity, it is possible that the increase they cause to the total cell count may

itself boost immune health, considering that most of the clones extinguished as diversity wanes are very small, and may not effectively participate in the immune response to begin with. In this regard, the viability of treating immunosenescence by increasing peripheral proliferation depends on the elucidation of the T-cell pool's *effectiveness clone size*–that is, the size a clone must have attained to effectively guarantee activation of the clone when its cognate antigen infiltrates the organism. The effectiveness clone size is intrinsically linked to true functional TCR diversity; if we can identify a threshold integer q^*, such that clones of size at least q^* are reliably activated in the presence of their cognate antigen(s), but that smaller clones are not, then $R_{q^*}(t)$ is naturally the most useful measure of diversity, because it accounts for precisely those clones actively participating in the adaptive immune mechanism. The larger the "correct" choice of q^* is, the more effective treatments that increase cellular proliferation in the periphery will be. Moreover, an increase to the total cell count may also strengthen the immune response despite the loss of TCR diversity if the degree of T-cell crossreactivity high enough that each T-cell is capable of responding to a wide array of pathogens.

The effectiveness clone size is also significant to the question of whether diversity loss is the driving factor in immunosenescence. Using the parameter values that we found in the literature, $R_q(t)$ decreases from youth to advanced age for $q \leq 4$, stays nearly constant for $q = 5, 6$, and increases for $q \geq 7$. The extinction of small clones allows the surviving clones to expand in size, causing the richness of large clones to increase into advanced age. If the effectiveness clone size is large, the diversity of such "effective" clones may actually increase with age, strengthening the immune response. We may conclude that either the effectiveness clone size is low, or the weakened immune response in advanced age is caused primarily by other mechanisms. For example, functional deficiencies acquired by naive T-cells in aging are one possible alternative cause of the weakened immune response. Such functional deficiencies have been studied heavily in mouse models, but research in humans is still lacking ([AS14]). Diminished naive T-cell effector responsiveness and proliferative capacity have been observed in aged mice ([MAL13]), and it is possible that similar changes occur in humans. On the other hand, experiments on mice have directly shown that loss of TCR diversity does have an actively detrimental effect on immune responsiveness ([YAL08]), supporting the notion that loss of TCR diversity is a

significant contributor to immunosenescence.

Our model illustrates the feasibility of several different scenarios, in which loss of diversity contributes to immunosenescence on drastically different levels. There is clearly a strong need to investigate the effects of both age-related structural diversity loss and diminished T-cell functionality in human subjects *in vivo*, to better understand the causes of immunosenescence. Moreover, our model indicates that the effectiveness clone size and crossreactivity *in vivo* are valuable pieces of missing information, the elucidation of which would allow for the identification of effective options to treat immunosenescence.

2.4 Summary and Conclusions

We have simulated the time evolution of the functions $c_k(t)$, which represent the number of naive T-cell clones of size k present in a human's immune compartment at time t. We determined that under essentially any realistic assumptions about homeostatic proliferation and death, all clones deplete in infinite time if thymic export is assumed to decay exponentially. This implicates thymic export as a fundamental cause of age-associated diversity loss. We simulated our model under the assumption that a carrying capacity is regulated by homeostatic proliferation and death through N-dependent rates. We found that the manipulation of homeostatic proliferation and death rates to raise the carrying capacity, and thus the total cell count, was unable to save falling diversity as an individual ages. It affirms the vital role of thymic output in age-related diversity loss, and indicates that boosting the proliferation rate is unlikely to be an effective solution. However, if only large clones are sufficiently effective in the immune response, boosting proliferation rates might raise average clone sizes and help to mitigate the effects of lost diversity. We simulated "threshold richness diversity", $R_q(t)$, which counts the total number of clones of size q or larger. We found that by increasing q, $R_q(t)$ goes from presenting a lifetime decrease to a lifetime increase. From this trend, we concluded that if only large clones are effective, the effective richness would actually increase with age, suggesting that it is important to identify the minimal effectiveness clone size in order to determine whether the loss of TCR diversity is the primary mechanism driving the immune dysfunction seen in advanced age. Lastly, we derived a one-to-one mapping between the full-sample

diversity c_k^N of N cells and the expected measurement of diversity $\mathbb{E}[c_k^Y]$ in samples of Y cells. Our formulation provides a rigorous method for accurately inferring the statistical distribution of clonal sizes from small-sample measurements.

2.5 Appendix: Implementation of Numerical Truncation

The most straightforward way to truncate Eq. 2.6 at $k = M$ is to neglect the exchange terms between c_M and c_{M+1}, assuming that c_k is negligible for $k > M$ and essentially imposing a "no-flux" boundary condition. This leads to the following equation for the boundary term $c_M(t)$:

$$\frac{\mathrm{d}c_M(t)}{\mathrm{d}t} = \frac{\gamma(t)}{\Omega} c_{M-1} + p(M-1)c_{M-1} - \mu(N)Mc_M. \tag{2.11}$$

This formulation, however, introduces a disparity between $N(t)$ as the solution of Eq. 2.1, and the conceptual definition $N(t) = \sum_{k=1}^{M} kc_k(t)$, with which it should agree. An alternative implementation of the truncation that preserves the relation $N(t) = \sum_{k=1}^{M} kc_k(t)$ is:

$$\frac{\mathrm{d}c_M(t)}{\mathrm{d}t} = \frac{\gamma(t)}{\Omega}\left(c_{M-1} + \frac{c_M}{M}\right) + p(M-1)c_{M-1} + pc_M - \mu(N)Mc_M, \tag{2.12}$$

However, the truncation in Eq. 2.12 introduces an error in the number of clonotypes, $\Omega = \sum_{k=0}^{M} c_k$–a quantity which had been preserved by Eq. 2.11. In the limit as $M \to \infty$, the truncation errors for both implementations go to zero at $\sim 1/M$, and the two implementations become more or less equivalent. Assuming sufficiently large M, the truncation errors can be negligible when $\gamma(t) > 0$, or have minimal cumulative effects within the relatively short duration of the human lifespan, on which our investigations in this paper have primarily focused.

In this paper, we use, for simplicity, Eq. 2.11 to numerically truncate Eq. 2.6. Note that this choice may seem "natural" if one regards M as the carrying capacity, making

it reasonable for the clones accounted for in the function c_M to proliferate at rate zero. However, the mechanism that governs the T-cell carrying capacity is quite sophisticated, and its nuances cannot be described fully by merely eliminating the proliferation term in the ODE for c_M. Not only should the c_M clones proliferate at rate zero, the proliferation rates of the other c_k should also depend on k. The k dependence may be weak for small k, but as $k \to M$, the proliferation rate should attenuate significantly. Such a k-dependent proliferation rate would yield a natural truncation threshold at the carrying capacity. However, this type of sophisticated k-dependence of the proliferation rate is beyond the scope of this analysis. Our assumption here is simply that the truncation errors introduced by Eq. 2.11 are numerically negligible and not biologically significant.

2.6 Appendix: Steady States of the Autonomous Equations

If we fix $\gamma(t) = \gamma_0$, Eqs. 2.1, 2.6, and 2.11 become autonomous and admit the following steady state solution,

$$c_1^{ss} = \gamma_0 \left[\frac{\gamma_0}{\Omega} \sum_{i=1}^{M} \frac{1}{i!\mu(N_{ss})^{i-1}} \left(\prod_{j=1}^{i-1} \left[\frac{\gamma_0}{\Omega} + jp \right] \right) + \mu(N_{ss}) \right]^{-1}, \tag{2.13}$$

$$c_k^{ss} = \frac{c_1^{ss}}{k!\mu(N_{ss})^{k-1}} \left(\prod_{n=1}^{k-1} \left[\frac{\gamma_0}{\Omega} + np \right] \right), \tag{2.14}$$

where N_{ss} is the total population at steady state, given by the unique positive root of the cubic,

$$c(N;\gamma_0) = (p_0 - (\mu_0 + \mu_1))\, N^3 + \gamma_0 N^2 + (p_0 - \mu_0)K^2 N + \gamma_0 K^2. \tag{2.15}$$

Taking $\gamma_0 = 0$, $c(N;0)$ has three real roots, $N = 0, \pm\sqrt{((p-\mu_0)K^2)/(\mu_0 + \mu_1 - p)}$. The positive steady state solution, which we denote by $N_{ss}(0)$, is stable, and the zero solution unstable, under the parameter restrictions described in Section 2.2.1. We now demonstrate that even though Eqs. 2.13, 2.14 indicate that each $c_k^{ss} \to 0$ as $\gamma_0 \to 0$, the

quantity $\lim_{M\to\infty}\sum_{k=1}^{M} kc_k^{ss}$ converges to a positive value qualitatively consistent with $N_{ss}(0)$ as $\gamma_0 \to 0$.

Proposition 2.6.1. *The steady state solutions c_k^{ss}, as given in Eqs. 2.13, 2.14, satisfy,*

$$\lim_{\gamma_0\to 0}\lim_{M\to\infty}\sum_{k=1}^{M} kc_k^{ss} > 0.$$

Proof. We seek to derive upper and lower bounds, $U(\gamma_0)$, $L(\gamma_0)$, which satisfy,

$$L(\gamma_0) \leq \lim_{M\to\infty}\sum_{k=1}^{M} kc_k^{ss} \leq U(\gamma_0),$$

for $\gamma_0 > 0$, and $\lim_{\gamma_0\to 0} U(\gamma_0) \geq \lim_{\gamma_0\to 0} L(\gamma_0) > 0$. We first establish two small results, which will be used later on:

Proposition 2.6.2. *For $\mu = \mu(N_{ss}(\gamma_0))$, $\lim_{\gamma_0\to 0}\frac{d\mu}{d\gamma_0} > 0$.*

Proof. Recalling that $\mu = \mu(N_{ss}(\gamma_0)) = \mu_0 + \mu_1(N_{ss}(\gamma_0)^2/(N_{ss}(\gamma_0)^2 + K^2))$, we have:

$$\begin{aligned}
\frac{\mathrm{d}\mu}{\mathrm{d}\gamma_0} &= \frac{\mathrm{d}\mu}{\mathrm{d}N_{ss}}\frac{\mathrm{d}N_{ss}}{\mathrm{d}\gamma_0} \\
&= \frac{2\mu_1 K^2 N_{ss}}{(N_{ss}^2+K^2)^2}\left[\frac{-(N_{ss}^2+K^2)}{3(p_0-(\mu_0+\mu_1))N_{ss}^2 + 2\gamma_0 N_{ss} + (p_0-\mu_0)K^2}\right] \\
&= \frac{-2\mu_1 K^2 N_{ss}}{(N_{ss}^2+K^2)\left[3(p_0-(\mu_0+\mu_1))N_{ss}^2 + 2\gamma_0 N_{ss} + (p_0-\mu_0)K^2\right]}
\end{aligned}$$

where we computed the derivative $\frac{\mathrm{d}N_{ss}}{\mathrm{d}\gamma_0}$ implicitly from the expression $c(N_{ss}(\gamma_0);\gamma_0) = 0$. From the explicit form $N_{ss}(0) = \sqrt{(p_0-\mu_0)K^2/((\mu_0+\mu_1)-p_0)}$, we have:

$$\begin{aligned}\lim_{\gamma_0 \longrightarrow 0} \frac{\mathrm{d}\mu}{\mathrm{d}\gamma_0} &= \frac{-2\mu_1 K^2 N_{SS}(0)}{(N_{SS}(0)^2 + K^2)\left[3(p_0 - (\mu_0 + \mu_1))N_{SS}(0)^2 + (p_0 - \mu_0)K^2\right]} \\ &= \frac{-2\mu_1 K^2 N_{SS}(0)}{(N_{SS}(0)^2 + K^2)\left[-2(p_0 - \mu_0)K^2\right]} \\ &> 0\end{aligned}$$

□

Proposition 2.6.3. *For* $f(p/\mu(N_{ss}(\gamma_0)); \gamma_0) = \frac{\gamma_0}{p\Omega}\left(1 - \frac{p}{\mu(N_{ss}(\gamma_0))}\right)^{\frac{-\gamma_0}{p\Omega}-1}$, *we have* $\lim_{\gamma_0 \to 0} f(p/\mu(N_{ss}(\gamma_0)); \gamma_0) > 0$.

Proof. We write the function $f(p/\mu(N_{\mathrm{ss}}(\gamma_0)); \gamma_0)$ as a product of two functions as follows:

$$\begin{aligned}f(p/\mu(N_{\mathrm{ss}}(\gamma_0)); \gamma_0) &= \frac{\gamma_0}{p\Omega}\left(1 - \frac{p}{\mu(N_{\mathrm{ss}}(\gamma_0))}\right)^{\frac{-\gamma_0}{p\Omega}-1} \\ &= \left(1 - \frac{p}{\mu(N_{\mathrm{ss}}(\gamma_0))}\right)^{\frac{-\gamma_0}{p\Omega}} \cdot \frac{\gamma_0}{p\Omega}\left(1 - \frac{p}{\mu(N_{\mathrm{ss}}(\gamma_0))}\right)^{-1} \\ &:= A(\gamma_0) \cdot B(\gamma_0)\end{aligned}$$

We define $A_0 := \lim_{\gamma_0 \to 0} A(\gamma_0)$ and $B_0 := \lim_{\gamma_0 \to 0} B(\gamma_0)$, and compute A_0 and B_0:

$$
\begin{aligned}
\ln(A_0) &= \lim_{\gamma_0 \longrightarrow 0} \frac{-\gamma_0}{p\Omega} \ln\left(1 - \frac{p}{\mu(N_{\rm ss}(\gamma_0))}\right) \\
&= \frac{-1}{p\Omega} \lim_{\gamma_0 \longrightarrow 0} \frac{\ln\left(1 - \frac{p}{\mu(N_{\rm ss}(\gamma_0))}\right)}{\gamma_0^{-1}} \\
&= \frac{-1}{p\Omega} \lim_{\gamma_0 \longrightarrow 0} \frac{\left(1 - \frac{p}{\mu(N_{\rm ss}(\gamma_0))}\right)^{-1} \frac{\rm d}{{\rm d}\gamma_0}\left(-\frac{p}{\mu(N_{\rm ss}(\gamma_0))}\right)}{-\gamma_0^{-2}} \\
&= \frac{1}{p\Omega} \lim_{\gamma_0 \longrightarrow 0} \gamma_0^2 \left[1 - \frac{p}{\mu(N_{\rm ss}(\gamma_0))}\right]^{-1} \left[p\mu(N_{\rm ss}(\gamma_0))^{-2} \frac{{\rm d}\mu}{{\rm d}\gamma_0}\right] \\
&= \frac{1}{p\Omega} \lim_{\gamma_0 \longrightarrow 0} \left[\frac{\gamma_0^2 p \frac{{\rm d}\mu}{{\rm d}\gamma_0}}{\mu(N_{\rm ss}(\gamma_0))^2 - p\mu(N_{\rm ss}(\gamma_0))}\right] \\
&= \frac{1}{\Omega} \lim_{\gamma_0 \longrightarrow 0} \left[\frac{2\gamma_0 \frac{{\rm d}\mu}{{\rm d}\gamma_0} + \gamma_0^2 \frac{{\rm d}^2\mu}{{\rm d}\gamma_0^2}}{(2\mu - p)\frac{{\rm d}\mu}{{\rm d}\gamma_0}}\right] \\
&= \frac{1}{\Omega} \left[\frac{2\gamma_0 \lim_{\gamma_0 \to 0} \frac{{\rm d}\mu}{{\rm d}\gamma_0} + \gamma_0^2 \lim_{\gamma_0 \to 0} \frac{{\rm d}^2\mu}{{\rm d}\gamma_0^2}}{p \lim_{\gamma_0 \to 0} \frac{{\rm d}\mu}{{\rm d}\gamma_0}}\right],
\end{aligned}
$$

where we used that $\mu(N_{\rm ss}(\gamma_0)) \to p$ as $\gamma_0 \to 0$. From Proposition 2.6.2, $\lim_{\gamma_0 \longrightarrow 0} \frac{{\rm d}\mu}{{\rm d}\gamma_0} > 0$, and a similar computation shows that $\lim_{\gamma_0 \to 0} \frac{{\rm d}^2\mu}{{\rm d}\gamma_0^2} \in \mathbf{R}$. Thus, $\ln(A_0) \in \mathbf{R}$, and $A_0 > 0$. Now,

$$
\begin{aligned}
B_0 &= \lim_{\gamma_0 \to 0} \frac{\gamma_0}{p\Omega} \left(1 - \frac{p}{\mu(N_{\rm ss}(\gamma_0))}\right)^{-1} \\
&= \lim_{\gamma_0 \to 0} \frac{(\gamma_0/p\Omega)}{\left(1 - \frac{p}{\mu(N_{\rm ss}(\gamma_0))}\right)} \\
&= \lim_{\gamma_0 \to 0} \frac{(1/p\Omega)}{p\mu(N_{\rm ss}(\gamma_0))^{-2}\frac{{\rm d}\mu}{{\rm d}\gamma_0}} \\
&= \lim_{\gamma_0 \to 0} \frac{\mu(N_{\rm ss}(\gamma_0))^2}{p^2\Omega\frac{{\rm d}\mu}{{\rm d}\gamma_0}} \\
&> 0.
\end{aligned}
$$

Thus, $\lim_{\gamma_0 \to 0} \frac{\gamma_0}{p\Omega}\left(1 - \frac{p}{\mu(N_{\rm ss})}\right)^{\frac{-\gamma_0}{p\Omega}-1} = A_0 B_0 > 0.$ □

We now resume the proof of Proposition 2.6.1. We first derive upper and lower bounds on the term c_1^{ss}, to simplify calculations. From the nonnegativity of the parameters and coefficient functions, and the form in Eq. 2.13, $c_1^{ss} \leq \gamma_0/\mu_0$, independent of M. To derive an M-independent lower bound on c_1^{ss}, we observe that the sum in the denominator of Eq. 2.13 satisfies,

$$\begin{aligned}
&\frac{\gamma_0}{\Omega}\sum_{i=1}^{M}\frac{1}{i!\mu(N_{\rm ss}(\gamma_0))^{i-1}}\left(\prod_{j=1}^{i-1}\left[\frac{\gamma_0}{\Omega}+jp\right]\right)\\
&\leq \sum_{i=1}^{M}\frac{1}{(i-1)!\mu(N_{\rm ss}(\gamma_0))^{i-1}}\left(\prod_{j=0}^{i-1}\left[\frac{\gamma_0}{\Omega}+jp\right]\right)\\
&= p\sum_{i=1}^{M}\frac{1}{(i-1)!}\left(\prod_{j=0}^{i-1}\left[\frac{\gamma_0}{p\Omega}+j\right]\right)\left(\frac{p}{\mu(N_{\rm ss}(\gamma_0))}\right)^{i-1}
\end{aligned}$$

and that the sum on the right above is the M-th Taylor polynomial, S_{M,γ_0}, for the function $f(x;\gamma_0) = \frac{\gamma_0}{p\Omega}(1-x)^{\frac{-\gamma_0}{p\Omega}-1}$ expanded around $x=0$ and evaluated at $x = \frac{p}{\mu(N_{\rm ss}(\gamma_0))}$. The function $f(x;\gamma_0)$ is analytic in x away from $x=1$, and in particular, the S_{M,γ_0} increase monotonically to $f(p/\mu(N_{\rm ss}(\gamma_0));\gamma_0)$. It follows that,

$$\frac{1}{p}\sum_{i=1}^{M}\frac{1}{i!\mu(N_{\rm ss}(\gamma_0))^{i-1}}\left(\prod_{j=0}^{i-1}\left[\frac{\gamma_0}{\Omega}+jp\right]\right) \leq S_{M,\gamma_0} \leq f\left(\frac{p}{\mu(N_{\rm ss}(\gamma_0))};\gamma_0\right) := f_{\gamma_0}$$

and thus that $c_1^{ss} \geq \gamma_0/(pf_{\gamma_0}+\mu_0+\mu_1)$. After using the c_1^{ss} bounds in the expression for c_k^{ss}, we have:

$$\begin{aligned}
&\frac{p\Omega}{pf_{\gamma_0}+\mu_0+\mu_1}S_{M,\gamma_0} \leq \sum_{k=1}^{M}kc_k^{ss} \leq \frac{p\Omega}{\mu_0}S_{M,\gamma_0}\\
\longrightarrow &\lim_{M\to\infty}\frac{p\Omega}{pf_{\gamma_0}+\mu_0+\mu_1}S_{M,\gamma_0} \leq \lim_{M\to\infty}\sum_{k=1}^{M}kc_k^{ss} \leq \lim_{M\to\infty}\frac{p\Omega}{\mu_0}S_{M,\gamma_0}\\
\longrightarrow &\frac{p\Omega}{pf_{\gamma_0}+\mu_0+\mu_1}f_{\gamma_0} \leq \lim_{M\to\infty}\sum_{k=1}^{M}kc_k^{ss} \leq \frac{p\Omega}{\mu_0}f_{\gamma_0}
\end{aligned}$$

Now we let $L(\gamma_0) = \frac{p\Omega}{pf_{\gamma_0}+\mu_0+\mu_1} f_{\gamma_0}$ and $U(\gamma_0) = \frac{p\Omega}{\mu_0} f_{\gamma_0}$. From Proposition 2.6.3, $\lim_{\gamma_0 \to 0} f_{\gamma_0} > 0$, so $\lim_{\gamma_0 \to 0} L(\gamma_0), \lim_{\gamma_0 \to 0} U(\gamma_0) > 0$, and Proposition 2.6.1 follows. □

2.7 Appendix: Convergence and Stability of c_k when $\gamma(t) \to 0$

In this section we will prove that solutions c_k to our ODE system initialized sufficiently close to $\overrightarrow{0}$ converge to $\overrightarrow{0}$ as $t \to \infty$. Denote by (P) the "perturbed" ODE system given by Eqs. 2.6, 2.11, with $\gamma(t) = \gamma_0 e^{-at}$, and by (U) the "unperturbed" ODE system resulting from the alternate choice $\gamma(t) \equiv 0$. For the sake of generality, we omit previous assumptions about the forms of the functions $p(N), \mu(N)$, except that $p(0), \mu(0) > 0$. Additionally, in this section, we replace the term N that appears in the ODEs with $\sum_{k \geq 1} kc_k$, and thus do not explicitly include Eq. 2.1 in our analysis, as in Appendix 2.6. (Note that the $N - \sum_{k \geq 1} kc_k \to 0$ as $M \to \infty$, validating the substitution). We begin by noting that the unperturbed system (U) has steady-state $c_k^U(t) \equiv 0$ for $k \geq 1$. To analyze the stability of this steady state, we consider the linearization of (U) around this steady state, which is represented by the $M \times M$ matrix we call $\mathbf{L_U}$ ($\mathbf{L_U} = (l_{ij})_{1 \leq i,j \leq M}$). The components l_{ij} of $\mathbf{L_U}$ are given explicitly by:

$$l_{ij} = \begin{cases} -j(p(0)+\mu(0)), & \text{if } i = j \leq M-1 \\ -M\mu(0), & \text{if } i = j = M \\ j\mu(0), & \text{if } i = j-1;\ 2 \leq j \leq M \\ jp(0), & \text{if } i = j+1;\ 1 \leq j \leq M-1 \\ 0, & \text{otherwise} \end{cases} \tag{2.16}$$

Although the matrix is tridiagonal, it is high-dimensional, and thus its eigenvalues cannot be computed analytically. However, we may nevertheless demonstrate that all eigenvalues possess strictly negative real part, indicating that the zero solution is asymptotically stable. To do this, we use Gershgorin's circle theorem to show that if there exists an eigenvalue $\lambda \in \mathbb{C}$ satisfying $Re(\lambda) \geq 0$, then $\lambda = 0$. We then verify that $\lambda = 0$ is never

an eigenvalue of $\mathbf{L_U}$, by directly demonstrating that $\mathbf{L_U}$ has linearly independent rows.

Proposition 2.7.1. *All eigenvalues $\lambda \in \mathbb{C}$ of the matrix $\mathbf{L_U}$ satisfy $Re(\lambda) < 0$, so that the zero-solution of (U) is asymptotically stable.*

Proof. We first apply Gershgorin's circle theorem to the columns of the matrix $\mathbf{L_U}$ to conclude that all eigenvalues $\lambda \in \mathbb{C}$ of the truncated system (finite M) are contained within the following union of disks:

$$\{\lambda \in \mathbb{C} : |\lambda + (M-1)(p(0)+\mu(0))| \leq (M-1)(p(0)+\mu(0))\}$$
$$\bigcup \{\lambda \in \mathbb{C} : |\lambda + M\mu(0)| \leq M\mu(0)\},$$

where we have used the fact that $\{\lambda \in \mathbb{C} : |\lambda + D| \leq D\} \subset \{\lambda \in \mathbb{C} : |\lambda + (D+\epsilon)| \leq D+\epsilon\}$ for $D, \epsilon > 0$. Given the assumption that $p(0), \mu(0) > 0$, each of these disks is tangent to the line $Re(\lambda) = 0$ at $\lambda = 0$, and otherwise lies entirely in the half plane $Re(\lambda) < 0$. Thus, $\mathbf{L_U}$ can only possess an eigenvalue λ satisfying $Re(\lambda) = 0$ if $\lambda = 0$ is itself an eigenvalue. We next verify that $\lambda = 0$ is never an eigenvalue of $\mathbf{L_U}$ directly, by establishing the linear independence of the rows of $\mathbf{L_U}$.

Denote by $(\mathbf{L_U})^i$ the i-th row of the matrix $\mathbf{L_U}$, and assume that there exist scalars $a_1, a_2, \ldots, a_M$, such that $\sum_{i=1}^{M} a_i(\mathbf{L_U})^i = 0$. By directly comparing the M-th components of the vectors on either side of the expression $\sum_{i=1}^{M} a_i(\mathbf{L_U})^i = 0$, we find that $a_{M-1}M\mu(0) - a_M M\mu(0) = 0$, so that $a_{M-1} = a_M$. From this, it then follows from inspection of the $M-1$-st components of the aforementioned expression that $a_{M-2}(M-1)\mu(0) - a_M(M-1)(p(0)+\mu(0)) + a_M(M-1)p(0) = 0$, which implies that $a_{M-2} = a_{M-1} = a_M$. Continuing inductively, we arrive at the conclusion that $a_j = a_1$ for all $j \geq 2$, from which it follows that if $a_1 \neq 0$, then $\sum_{i=1}^{M}(\mathbf{L_U})^i = 0$. However, we conclude by direct comparison of the first components on either side of the expression $\sum_{i=1}^{M}(\mathbf{L_U})^i = 0$ that $-\mu(0) = 0$, contradicting the assumption that $\mu(0) > 0$. Thus, $a_j = 0$ for all $k \geq 1$, and the rows of $\mathbf{L_U}$ are linearly independent, implying that $\lambda = 0$ is not an eigenvalue. Thus, we conclude that all eigenvalues λ of the matrix $\mathbf{L_U}$ satisfy $Re(\lambda) < 0$, and the zero-solution of (U) is asymptotically stable. □

We next proceed to demonstrate that the uniform asymptotic stability of the zero-solution ($c_k^U(t) \equiv 0$ for $k \geq 1$) of the unperturbed system (U) confers a similar notion of "stability" on the perturbed system (P). In particular, the uniform asymptotic stability of the system (U), in conjunction with the exponential decay of the function $\gamma(t)$, implies that solutions of the perturbed system (P) also converge to zero in magnitude, in a sense to be made more precise later on. Let us describe the ODEs more compactly by writing (U) as $\mathrm{d}\mathbf{c}/\mathrm{d}t = \mathbf{f}(\mathbf{c})$, where $\mathbf{c} \equiv (c_1, c_2, \ldots, c_M)$. The autonomous function $\mathbf{f}(\mathbf{c})$ consists of terms accounting for cellular proliferation and death. We express (P) as $\mathrm{d}\mathbf{c}/\mathrm{d}t = \mathbf{f}(\mathbf{c}) + \mathbf{g}(t, \mathbf{c})$, where the nonautonomous function $\mathbf{g}(t, \mathbf{c})$ consists of terms accounting for thymic export. We appeal to results of Strauss and Yorke in [SY67], in particular their Theorem 4.6, which we invoke to prove that the solution of the perturbed system, $\mathbf{c}^P(t)$, satisfies $\mathbf{c}^P(t) \to 0$ if the unperturbed and perturbed systems, (U) and (P), satisfy the following conditions:

1. The zero solution ($\mathbf{c}^U(t) \equiv 0$) of the unperturbed system (U) is uniformly asymptotically stable.

2. The autonomous term $\mathbf{f}(\mathbf{c})$ is C^1.

3. There exists $r > 0$ such that if $|\mathbf{c}| \leq r$, then $|\mathbf{g}(t, \mathbf{c})| \leq \eta(t)$ for all $t \geq 0$ where $G(t) := \int_t^{t+1} \eta(s)ds \to 0$ as $t \to \infty$. (Here, we use the norm $|\mathbf{c}| = \sum_{i=1}^M |c_i|$.)

We now verify Conditions 1–3 above. Condition 1 follows immediately from the previous discussion in Proposition 2.7.1, and the fact that for an autonomous system, asymptotic stability and uniform asymptotic stability are equivalent. Condition 2 is trivial. To verify Condition 3, we must construct a suitable function $\eta(t)$, from the function $g(t, \mathbf{c})$:

$$|\mathbf{g}(t,\mathbf{c})| = \left|\frac{\gamma_0 e^{-at}}{\Omega}\left(\Omega - \sum_{j=1}^{M} c_j - c_1\right)\right| + \sum_{j=2}^{M-2}\left|\frac{\gamma_0 e^{-at}}{\Omega}\left(c_j - c_{j+1}\right)\right| + \left|\frac{\gamma_0 e^{-at}}{\Omega} c_{M-1}\right| \quad (2.17)$$

$$\leq \frac{\gamma_0 e^{-at}}{\Omega}\left(|\Omega| + \left(\sum_{i=1}^{M}|c_i|\right) + |c_1|\right) + \sum_{j=2}^{M-2}\frac{\gamma_0 e^{-at}}{\Omega}\left(|c_j| + |c_{j+1}|\right) + \frac{\gamma_0 e^{-at}}{\Omega}|c_{M-1}| \quad (2.18)$$

$$\leq \frac{\gamma_0 e^{-at}}{\Omega}\left(\Omega + 3\sum_{i=1}^{M-1}|c_i|\right) \quad (2.19)$$

$$\leq \frac{\gamma_0 e^{-at}}{\Omega}\left(\Omega + 3|\mathbf{c}|\right) \quad (2.20)$$

$$= \gamma_0 e^{-at}\left(1 + \frac{3}{\Omega}|\mathbf{c}|\right) \quad (2.21)$$

Thus, $|\mathbf{g}(t,\mathbf{c})| \leq \gamma_0 e^{-at}\left(1 + \frac{3}{\Omega}|\mathbf{c}|\right)$, and for a given choice of $r > 0$, we may define $\eta_r(t) := \gamma_0 e^{-at}\left(1 + \frac{3r}{\Omega}\right)$. From the exponential form of $\eta_r(t)$, it is clear that $\lim_{t\to\infty}\int_t^{t+1}\eta_r(s)ds = 0$. Moreover, not only does there exist a single choice of $r > 0$ that produces a suitable $\eta_r(t)$, but *any* choice of r produces a suitable $\eta_r(t)$.

From Theorem 4.6 in ([SY67]), we may conclude that for any $T_0 \geq 0$, there exists a $\delta_0 > 0$ such that if $t_0 \geq T_0$ and $|\mathbf{c}^P(t_0)| \leq \delta_0$, then the solution of the perturbed problem, $\mathbf{c}^P(t)$, passing through $(t_0, \mathbf{c}^P(t_0))$ converges to zero in magnitude as $t \to \infty$. Moreover, the proof of convergence holds for any sufficiently smooth function $\gamma(t)$ that satisfies $\gamma(t) \to 0$ as $t \to \infty$. Given Eq. 2.6 truncated at an arbitrarily large threshold M, all c_k decline with the decaying thymic export rate as $t \to \infty$. While the total cell count is preserved as $c_k(t) \to 0$ due to the proliferative mechanism driving all cells past the truncation threshold and out of the finite system through truncation errors, the mean-field approximation breaks down at the limit $\gamma(t)/\mu \to 1/\Omega \ll 1$, and Eq. 2.6 no longer accurately describes the real biology. Nonetheless, our analysis here describes the decline of the number of T-cell clones with decaying $\gamma(t)$ as $t \to \infty$, before the mean-field approximation breaks down.

2.8 Appendix: Computation of Expected Sample Clonal Size Distribution

In this section, we detail the derivation of Eq. 2.10, the explicit expression for $\mathbb{E}[c_k^Y]$. We begin with Eq. 2.9,

$$\mathbb{E}[c_k] = \sum_{j=1}^{R} jP\left(c_k^Y = j\right). \tag{2.22}$$

Each term $P\left(c_k^Y = j\right)$ in Eq. 2.22 can itself be expanded as a sum over all the ways to choose the j clones that are of size k. For a sample containing exactly Z clones of size k, we introduce the following Z-tuple notation, for $Z \in \mathbb{N}$:

$$I_Z := \{\vec{i_Z} = (i_1, i_2, \ldots, i_Z) : i_j \in \{1, 2, \ldots, R\}, i_j < i_{j+1} \text{ for all } j\}, \tag{2.23}$$

where $\vec{i_Z}$ lists the indices of all the sample clones consisting of precisely k cells. Additionally, let y_i denote the size of the i-th ordered sample clone, so that $y_{i_1} = y_{i_2} = \cdots = y_{i_Z} = k$, but no other sample clone consists of k cells. Note that in $\vec{i_Z}$, clones are listed in numerical order, due to the assumption that $i_j < i_{j+1}$, in order to avoid repetition (e.g., in I_2, (i_1, i_2) should be indistinct from (i_2, i_1), and this pair should not be counted twice, as the significance is in which clone numbers are listed at all, and not the order in which they are written.) With this, let $P(\vec{i_Z}, k)$ denote the probability that there are precisely Z clones of size k in the sample, and that their clone numbers are listed in the vector $\vec{i_Z}$. Additionally, for $s \in \mathbb{N}$, denote by $I_{Z,s} \subset I_Z$ the collection of all $\vec{i_Z} \in I_Z$ such that $i_{z^*} = s$ for some $z^* \in \{1, 2, \cdots, Z\}$. Essentially, we are imposing the assumption that the s-th clone specifically belongs somewhere in the list $\vec{i_{Z,s}}$. Explicitly, we may write $I_{Z,s}$ as:

$$I_{Z,s} = \{\vec{i_{Z,s}} = (i_1, \ldots, i_{z^*-1}, i_{z^*} = s, i_{z^*+1}, \ldots, i_Z) : i_j \in \{1, 2, \ldots, R\}, i_j < i_{j+1} \text{ for all } j\ \}. \tag{2.24}$$

We define $P(\vec{i_{Z,s}}, k)$ to be the probability that there are precisely Z clones of size k, with clone numbers listed in $\vec{i_{Z,s}}$, recalling that the s-th clone is in the list. We may further simplify Eq. 2.22 with this notation, rearranging sums by strategically regrouping clone size distributions that share a common size k clone.

$$\mathbb{E}[c_k] = \sum_{j=1}^{R} jP(c_k^Y = j), \tag{2.25}$$

$$= \sum_{j=1}^{R} j \left(\sum_{\vec{i_j} \in I_j} P(\vec{i_j}, k) \right), \tag{2.26}$$

$$= \sum_{s=1}^{R} \left(\sum_{j=1}^{R} \sum_{\vec{i_{j,s}} \in I_{j,s}} P(\vec{i_{j,s}}, k) \right), \tag{2.27}$$

$$= \sum_{s=1}^{R} P(y_s = k), \tag{2.28}$$

The terms of the final sum in Eq. 2.28 give the probability that the s-th clone is of size k, independent of any other information about the sampling. This probability is easy to compute, and given by:

$$P(y_s = k) = \frac{1}{\binom{N}{Y}} \binom{n_s}{k} \binom{N - n_s}{Y - k}. \tag{2.29}$$

Inserting Eq. 2.29 into Eq. 2.28, we obtain a simple expression for the expected sample clone size distribution:

$$\mathbb{E}[c_k] = \sum_{s=1}^{R} \frac{1}{\binom{N}{Y}} \binom{n_s}{k} \binom{N - n_s}{Y - k}. \tag{2.30}$$

We can further simplify Eq. 2.30 by recognizing that the term $\binom{n_s}{k}$ is nonzero only if $n_s \geq k$. We can thus rewrite Eq. 2.30 in terms of the true clone size distribution $\{c_l^N\}_{l=1}^R$ as:

$$\mathbb{E}[c_k] = \sum_{l=k}^{R} \frac{1}{\binom{N}{Y}} c_l^N \binom{l}{k} \binom{N-l}{Y-k}. \tag{2.31}$$

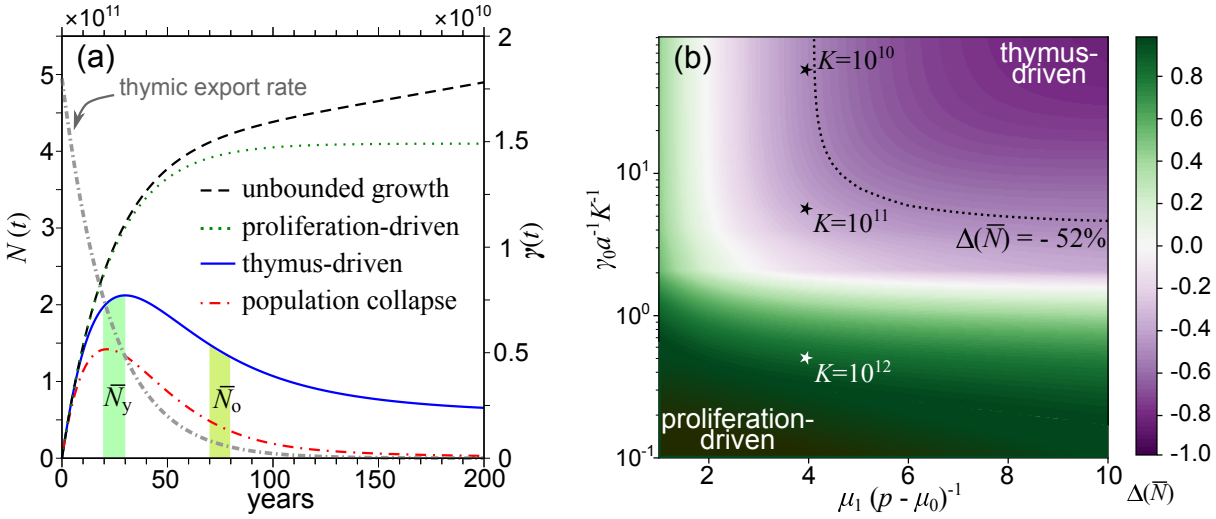

Figure 2.1: **Qualitative behavior of the total T-cell population model (Eqs. 2.1, 2.2)** (a) The total T-cell population $N(t)$ as a function of time (in years) for four qualitatively distinct scenarios. Unbounded growth arises when $\mu_1 (p-\mu_0)^{-1} < 1$, and the T-cell population collapses when $(p-\mu_0)a^{-1} < 0$. Outside of these two regimes, $N(t)$ converges asymptotically to a positive steady state as $\gamma(t) \to 0$. If $\gamma_0 a^{-1} K^{-1} \ll 1$, $N(t)$ is driven primarily by homeostatic proliferation and increases monotonically towards the constant plateau. Increasing $\gamma_0 a^{-1} K^{-1}$ leads to a transition from the proliferation-driven scenario to the thymus-driven scenario, in which $N(t)$ reaches a peak value before converging to the steady state. The decaying thymic export rate $\gamma(t)$ is plotted alongside the $N(t)$ curves as a reference. To quantify the decrease in cell counts with age, we define $\bar{N}_y$ as the average of $N(t)$ between ages 20 and 30, and $\bar{N}_o$ as the average between 70 and 80–then $\Delta(\bar{N}) = (\bar{N}_o - \bar{N}_y)/\bar{N}_y$ is the relative change in cell counts. The parameter values used are $\gamma_0 = 1.8 \times 10^{10}$, $a = 0.044$, and $K = 10^{10}$, with $p = 0.022$, $\mu_0 = 0.017$, and $\mu_1 = 0.004$ in the unbounded growth scenario, $p = 0.17$, $\mu_0 = 0.18$, and $\mu_1 = 0.04$ in the collapse scenario, $p = 0.18$, $\mu_0 = 0.17$, and $\mu_1 = 0.01001$ in the homeostasis-driven scenario, and $p = 0.18$, $\mu_0 = 0.17$, and $\mu_1 = 0.04$ in the thymus-driven case. The initial value is $N(1) = 10^{11}$ at $t = 1$ year. (b) $\Delta(\bar{N})$ as a function of $\gamma_0 a^{-1} K^{-1}$ and $\mu_1 (p-\mu_0)^{-1}$. When $\gamma_0 a^{-1} K^{-1}$ and $\mu_1 (p-\mu_0)^{-1}$ are small, $N(t)$ is driven primarily by proliferation and keeps increasing well into old age, leading to positive $\Delta(\bar{N})$ values. Conversely, for large $\gamma_0 a^{-1} K^{-1}$ and $\mu_1 (p-\mu_0)^{-1}$, thymic export dominates and $N(t)$ peaks in youth, resulting in a negative $\Delta(\bar{N})$. The black dotted curve corresponds to $\Delta(\bar{N}) = -52\%$, as previously reported by Westera *et al.* in human adults. Fixing $\mu_1 (p-\mu_0)^{-1} = 4$, we are able to reproduce this curve by setting $\gamma_0 a^{-1} K^{-1} \simeq 41$ (corresponding to $K = 10^{10}$ for our choice of parameter values). The value of $\Delta(\bar{N})$ increases with decreasing $\gamma_0 a^{-1} K^{-1}$ and become positive when $\gamma_0 a^{-1} K^{-1} \lesssim 1$. Here, we fixed $(p-\mu_0)a^{-1} = 0.2$ and $a = 0.044$.

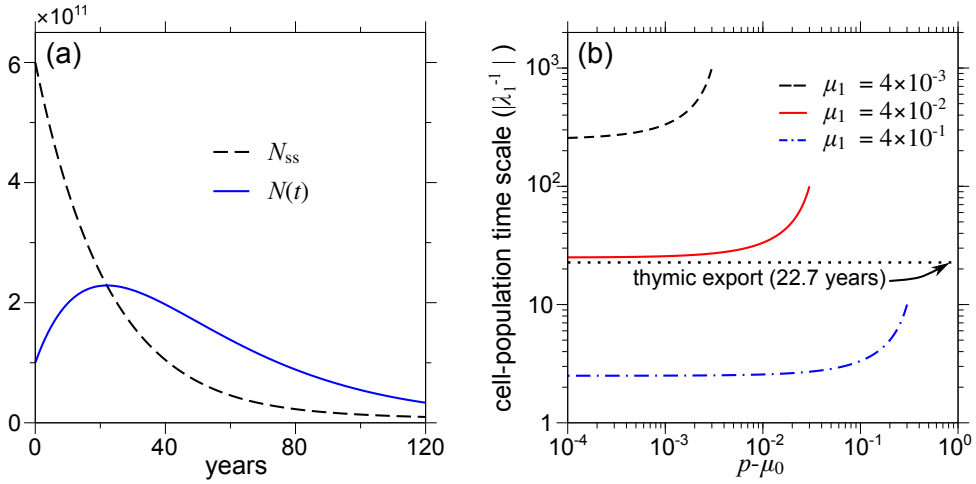

Figure 2.2: **Comparison of thymic export and cell population evolution time scales** (a) The discrepancy between $N(t)$ and N_{ss}. N_{ss} declines monotonically with the exponentially decaying thymic export, and approaches a small positive value as $\gamma(t) \to 0$. The solution $N(t)$ evolves towards N_{ss} but never catches up with it, due to the slower evolution time scale. (b) Comparison of timescales of thymic atrophy and cell population evolution. Thymic atrophy is the faster mechanism for most choices of the system's parameters. Increasing μ_1 shortens the time scale of clone evolution, indicating that steady-state solutions can be reasonable approximations to the fully time-dependent solution at very large μ_1 and very small $p - \mu_0$. Here, varying N_{ss} within the range $[10^{10}, 10^{12}]$ yields almost identical results, and the values of γ_0 and K, chosen within the reasonable parameter regime, do not affect the results significantly. Parameter values used are $\gamma_0 = 1.8 \times 10^{10}$, $a = 0.044$, $p = 0.18$, $\mu_0 = 0.17$, $K = 10^{10}$, $\Omega = 10^{16}$. For (a) $\mu_1 = 0.04$, and the initial condition is $N(1) = 10^{11}$.

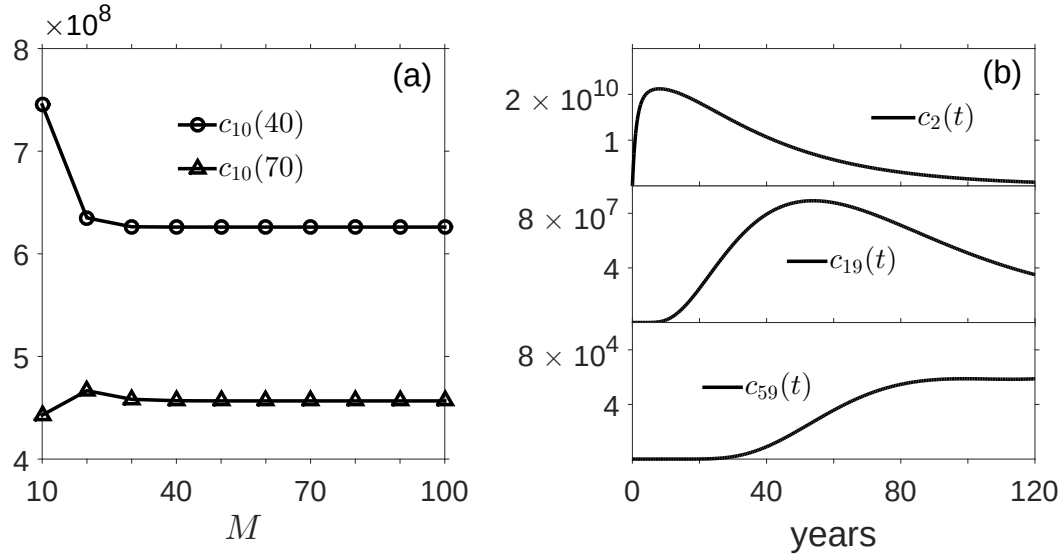

Figure 2.3: **Simulation of c_k, effect of truncation** (a) Effect of numerical truncation. We plot $c_{10}(40)$ and $c_{10}(70)$ as functions of M for $10 \leq M \leq 100$. Compartment sizes are effectively fixed when $M \gtrsim 30$. (b) Temporal evolution of $c_k(t)$. We plot $c_2(t)$, $c_{19}(t)$, and $c_{59}(t)$. Each $c_k(t)$ curve rises to a peak value and subsequently decreases. As k increases, $c_k(t)$ decreases in magnitude, and the time at which it reaches its peak value also increases. Parameter values: $\gamma_0 = 1.8 \times 10^{10}$, $a = 0.044$, $p = 0.18$, $\mu_0 = 0.17$, $\mu_1 = 0.04$, $K = 10^{10}$, $\Omega = 10^{16}$. Initial values $c_1(1) = 10^{11}$, $c_0(1) = \Omega - 10^{11}$, $c_k(1) = 0$ for all $k \geq 2$

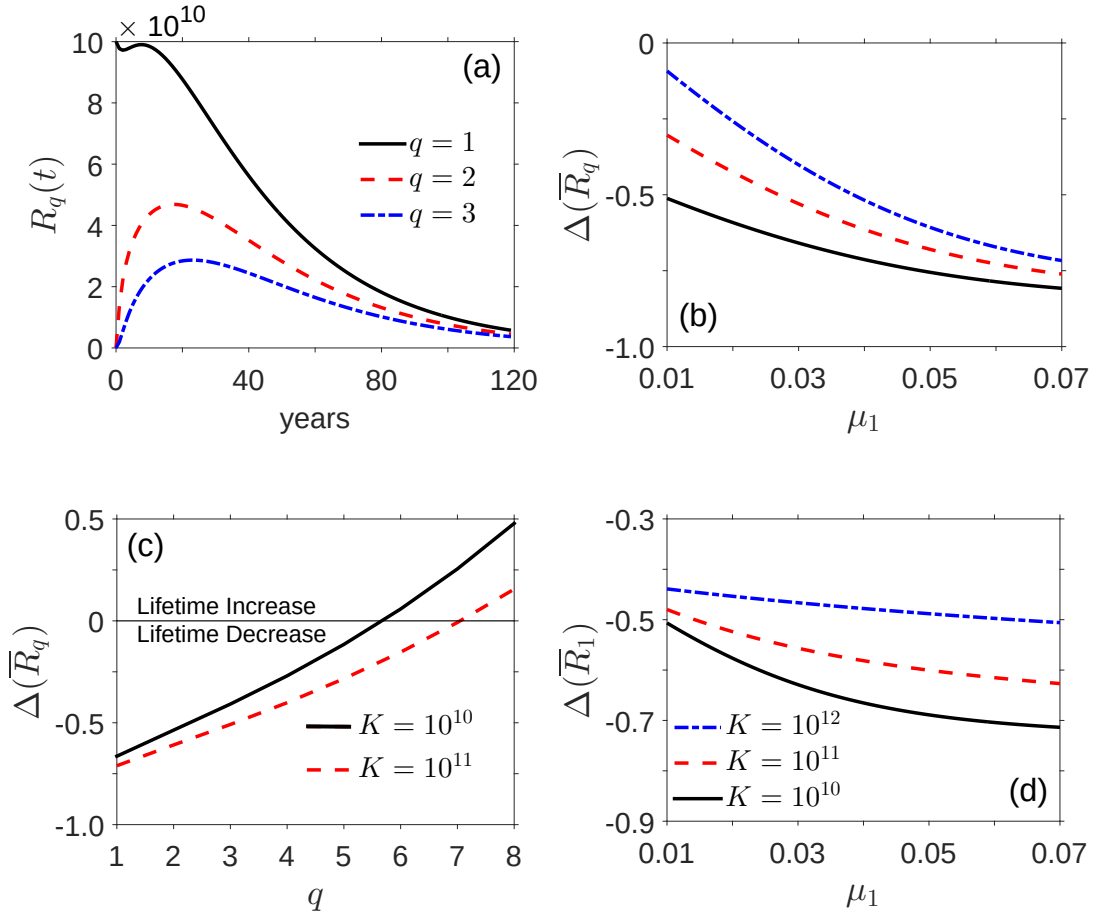

Figure 2.4: **Simulation of** R_q (a) $R_q(t)$ as a function of t, for $q = 1, 2, 3$. R_q peaks at later times as q increases. (b) $\Delta(\bar{R}_q(t))$ for varying q, μ_1. Higher μ_1 correspond to more severe loss of T-cell clones in advanced age. (c) $\Delta(\bar{R}_q)$ for varying q, K. Small values of q result in a lifetime decrease to R_q, but larger values result in a lifetime increase. This is due to the fact that R_q peaks at later times as q increases. (d) $\Delta(\bar{R}_1)$ for varying μ_1, K. Initial values $c_0(1) = \Omega - 10^{11}$, $c_1(1) = 10^{11}$ $c_k(1) = 0$ for $k \geq 2$. Parameter values, when not varying: $\Omega = 10^{16}$, $K = 10^{10}$, $p_0 = 0.18$, $\mu_0 = 0.17$, $\mu_1 = 0.04$, $a = 0.044$, $\gamma_0 = 1.8 \times 10^{10}$.

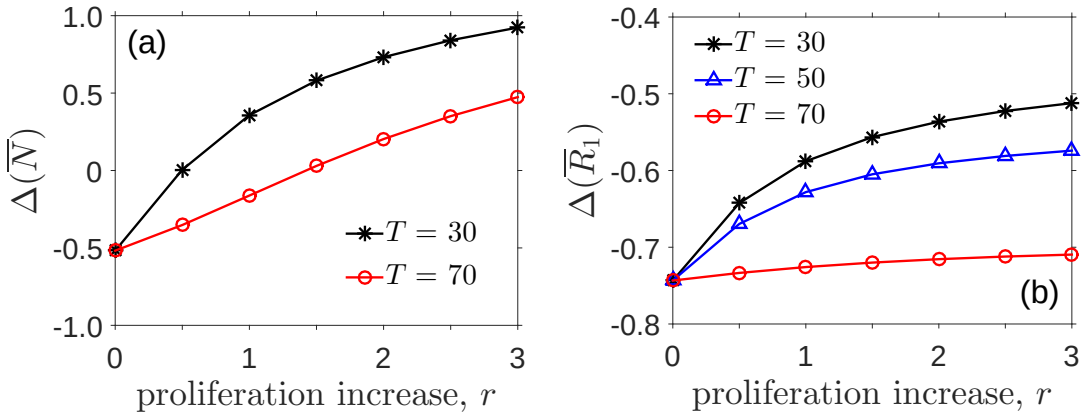

Figure 2.5: **Simulation of N and R_1 with rise in proliferation rate** Simulation of Eq. 2.6 with exponentially decaying thymic export, and peripheral homeostasis described by time-varying logistic growth. We use the thymic export rate $\gamma(t) = \gamma_0 e^{-at}$, peripheral death rate $\mu(N) = \mu_0 > 0$, and peripheral proliferation rate $p(N,t) = p(t)(1-(N/K))$, with $p(t) = p_0(1+rH(t-T))$. Here, $H(t)$ represents the Heaviside function with jump at $t = 0$. The constant r determines the magnitude of the increase to the basal proliferation rate, and T represents the time at which the jump occurs. We take the jump to occur at varying ages. (a) $\Delta(\bar{N})$ with jump at ages $T = 30$ and 70, for varying r. (Curve corresponding to $T = 50$ is omitted due to close similarity to $T = 30$ curve.) Raising the basal proliferation rate diminishes cellular loss in advanced age, with sufficiently high values of r producing a lifetime increase in total cell counts. The positive steady state solution of the autonomous total cell ODE, $\mathrm{d}N/\mathrm{d}t = \gamma_0 + p_0(1-N/K) - \mu_0 N$, is given by $N^* = (K/2)(1-\mu_0/p_0 + \sqrt{(1-\mu_0/p_0)^2 + 4\gamma_0/Kp_0})$, and can be seen to satisfy $\partial N^*/\partial p_0 > 0$ if $\gamma_0 < K\mu_0$, suggesting that increases to the basal proliferation rate are likely to increase the total cell count. (b) $\Delta(\bar{R}_1)$ with $T = 30$, 50, and 70, for varying r. Increases to the basal proliferation rate do mitigate diversity loss, but the effect is minor and potentially insignificant. Increases to the basal proliferation rate increase c_{k+1} due to a decrease in c_k, preserving additional diversity, but lifetime diversity loss is still observed, even when proliferation rates are high enough to generate a lifetime increase to the total cell count. Fixed parameter values: $\gamma_0 = 1.8 \times 10^{10}$, $a = 0.044$, $p_0 = 0.18$, $\mu_0 = 0.17$, $K_0 = 3 \times 10^{11}$, $\Omega = 10^{16}$. Initial values: $c_0(1) = \Omega - 10^{11}$, $c_1(1) = 10^{11}$ $c_k(1) = 0$ for $k \geq 1$. Eq. 2.6 is truncated at $k = 200$.

CHAPTER 3

T-cell Populations During Acute Thymic Atrophy and Other Diseased States of the Immune System

3.1 Introduction

The thymus, a small organ located above the heart in humans, is a crucial component of the primary lymphoid architecture, as the site of T-cell development [Mur12, GNV10]. The many different T-cell subpopulations together guide and assist the action of other immune agents during infection [AJL02], regulate the immune response [Cor09], and retain memory of encountered pathogens [FYR14]. As such, the thymus supplies the immune compartment with its most essential source of direction, support, and regulation. T-cells are produced when lymphocyte progenitors derived from hematopoietic stem cells in the bone marrow migrate to the thymus and begin a process of role selection, maturation, and vetting, before being exported to the peripheral blood [Tak06]. The most significant event during thymocyte development is the rearrangement of the α and β chains of the T-cell receptor (TCR) [BSA02]. The particular rearrangement a T-cell undergoes determines its antigen specificity; a naive T-cell in the peripheral pool is activated when its TCR is bound by a cognate antigen, a pathogen-derived peptide fragment capable of stimulating that particular TCR [Mas98]. The total number of distinct TCRs present across the full T-cell pool is the "TCR diversity" [NSM04], and this quantifies the breadth of the pool's antigen responsiveness [LBA15].

TCR rearrangement occurs in the thymic cortex, which is populated with both thymocyte progenitors and thymic epithelial cells (TECs), the latter of which participate in T-cell maturation by stimulating progenitors to differentiate and proliferate, and conducting positive selection of rearranged TCRs capable of successful interaction with self-peptide:self-MHC molecules [Tak06]. Thymocytes also undergo negative selection to elim-

inate cells that react too strongly to self antigens presented by resident macrophages and dendritic cells. The small number of T-cells that survive this process are deemed safe and functionally competent, and thus exported to the peripheral blood to participate in the immune mechanism.

The thymus is known to experience both chronic and acute forms of atrophy [CVD16], resulting from both normal biological processes and the presence of disease or stress. The most universal form of thymic atrophy is age-related involution, the process by which productive thymic tissue is gradually replaced with nonproductive fat [SKM85]. Involution begins at puberty and continues indefinitely, and the resulting decline in T-cell production has been implicated as a likely source of immune dysfunction in the elderly [GE00, GHS07, SAM09]. Acute atrophy can occur under a plethora of conditions associated with a state of disease or stress [GS08, DL12, Sel36], including viral, bacterial, and fungal infection [Sav06, WHL94, GFN85], malnutrition [SDV07], cancer treatment [MFB95], bone marrow transplant [SWS95], alcoholism [ASR86], psychological stress, and pregnancy [ZSK07, TDR99, RTB96]. Each condition facilitates thymic atrophy in (at least) one of several ways, among them by reducing thymic cellularity [CVD16], decreasing thymocyte proliferation and increasing apoptosis [ALV00], instigating premature export of underdeveloped thymocytes [CSA06], and inducing morphological changes to TECs and the thymic microenvironment [SMK93]. Such disturbances may consequently alter the size and composition of the peripheral T-cell pool. Decreased lymphocyte prevalence in the periphery during acute involution has been documented [GSC03, BSR89, JJU01, FJB14], and *Salmonella*, which infects the thymus itself, has been shown to disrupt positive and negative selection, producing a skewed TCR repertoire [LAG15]. The size of the peripheral pool may also be reduced for reasons other than interruption to thymic function. Radiation and chemotherapy drugs, such as temozolmide, used to treat cancer can be highly lymphotoxic, producing a lymphopenic state referred to as "treatment-related lymphopenia" (TRL). [YKG13, MGL16, CYB13] Viral infections, particularly HIV, and autoimmune disorders can induce lymphopenia by increasing peripheral cellular death and redistributing cells to inappropriate tissues, in addition to affecting production in the thymus. [Lon12]

The activation of the hypothalamic-pituitary-adrenal axis by stress stimuli and subse-

quent release of glucocorticoids, which are known to induce apoptosis in double-positive thymocytes [PML04] and inhibit their differentiation [ALV00], is likely a major underlying catalyst of this acute involution [DL12, KHC02]. Evidence suggests further that glucocorticoid release is actually necessary to affect thymic atrophy [ALV00, Sel36]. Several other chemical agents have been observed to participate in thymic atrophy, notably sex hormones [DL12], which have been shown to weaken thymocyte proliferation [ZSK07] and induce apoptosis [PMI00], and the IL-6 cytokine family, which is demonstrably thymosuppressive [GS08]. Despite this apparent sensitivity to stress, the thymus is highly plastic, and generally recovers in size and functionality after removal of the stressor [CVD16]. Studies of the thymus during and after chemotherapy treatment in cancer patients indicate a return of thymic volume and productivity during recovery from treatment [MFB95]. A recuperating thymus may even surpass its pre-treatment volume, in a phenomenon known as "thymic rebound" [CZG87, CHC80]. Such thymic recovery has also been seen after infection [DCW01] and traumatic injury [GGL72]. However, recovery is demonstrably age-dependent, with thymi of older patients reconstituting the naive T-cell compartment more weakly than those of younger patients [MFB95]. Although acute thymic atrophy has been observed extensively in humans, much has yet to be learned about it, and clear treatment protocol is lacking [CVD16].

To this end, we present a mechanistic mathematical model of fluctuations in the size and diversity of the peripheral naive T-cell compartment in response to various immunologically diseased conditions. We study how this pool's size and composition adjust to changes in the intensity of thymic cell production, and how it reconstitutes from lymphopenic states induced by a combination of cellular destruction, undesirable redistribution, and/or diminished production. We compartmentalize the peripheral T-cell pool by grouping clones–collections of T-cells with the same TCR–according to the number of cells of which they consist. We then use a high-dimensional autonomous ODE system to follow the time evolution of the number of clones in each compartment. We assume that the size of the peripheral naive T-cell pool is dictated by rates of thymic export of new T-cells, along with homeostatic proliferation and death mechanisms. We assume a piecewise constant rate of thymic export, as the atrophy/recovery cycle is known to be a rapid process, and that the proliferative and death processes are subject to homeostatic

regulation based on the total T-cell pool size. We derive analytic approximations to the dominant eigenvalues and eigenvectors of the system linearized around its equilibria in both the presence and the absence of thymic activity. From this, we assess the rates of convergence of different T-cell compartments to equilibria that result from a changing thymic export rate. We then compare the linearized and fully nonlinear models, and study several special cases. We also compute explicit representations of solutions in an infinite-dimensional extension of our model.

3.2 Mathematical Model and Analysis

Letting $N(t)$ denote the total naive T-cell count in a human's immune compartment, we begin with the canonical ODE model for dynamics of a single population,

$$\frac{\mathrm{d}N}{\mathrm{d}t} = \gamma + p(N)N - \mu(N)N, \tag{3.1}$$

where $\gamma \geq 0$ represents the rate of export of naive T-cells from the thymus, and $p(N), \mu(N) \geq 0$ are N-dependent (that is, regulation-dependent) rates of proliferation and death of naive T-cells in the peripheral bloodstream. We take $p(N)$ to be non-increasing in N, and $\mu(N)$ to be non-decreasing in N, as the proliferation rate should decrease and the death rate should increase as cell counts increase. We assume that $p(0) > \mu(0)$, as the lymphopenic proliferation rate would be higher than the lymphopenic death rate [BHS05, TDL01, VBM01, FM05]. We also assume that when a healthy, homeostatic cell count, N^*, is achieved, that $p(N^*) - \mu(N^*) < 0$, to prevent continued exponential growth of the population. In order to compute the peripheral naive T-cell diversity, we couple this ODE in the total cell count with a system of ODEs that describes the time evolution of the size-segregated subpopulations of the peripheral naive T-cell pool. Let $c_k(t)$ denote the number of clones of size k at time $t \geq 0$. We then assert that the functions $c_k(t)$ for $k \geq 1$ evolve according to the following system of ODEs:

$$\frac{\mathrm{d}c_1}{\mathrm{d}t} = \frac{\gamma}{\Omega}\left[\Omega - \sum_{i=1}^{M} c_i - c_1\right] - p(N)c_1 + \mu(N)\left[2c_2 - c_1\right], \tag{3.2}$$

$$\frac{\mathrm{d}c_k}{\mathrm{d}t} = \frac{\gamma}{\Omega}\left[c_{k-1} - c_k\right] + p(N)\left[(k-1)c_{k-1} - kc_k\right] + \mu(N)\left[(k+1)c_{k+1} - kc_k\right], \tag{3.3}$$

$$\frac{\mathrm{d}c_M}{\mathrm{d}t} = \frac{\gamma}{\Omega}c_{M-1} + p(N)(M-1)c_{M-1} - \mu(N)Mc_M, \tag{3.4}$$

where $k = 2, 3, \cdots, M-1$ in Eq. 3.3, and the index M in Eq. 3.4 is the hypothetical maximum size a clone can achieve. We take M to be finite, in accordance with evidence of intraclonal competition that restricts clone sizes and preserves a balanced TCR diversity [HMK06]. Each of the ODEs in Eqs. 3.2, 3.3, 3.4 describes how c_k changes due to the effects of thymic export of new cells, and proliferation and death in the periphery. The constant $\Omega > 0$ denotes the total number of clonotypes that can potentially be assembled in and exported from the thymus.

In Eq. 3.3, the term $\frac{\gamma}{\Omega}$ represents the rate at which cells of a given clonotype are exported to the periphery from the thymus, and thus $\frac{\gamma}{\Omega}c_k$ represents the export rate of cells of clonotypes already represented by size-k clones in the periphery. As the addition of a new cell to a clone transfers the clone from the size-k compartment to the size-$(k+1)$ compartment, this is equivalent to the rate at which clones move from c_k to c_{k+1} due to thymic export. Similarly, $\frac{\gamma}{\Omega}c_{k-1}$ in Eq. 3.3 provides the rate at which clones move from c_{k-1} to c_k due to thymic export. We assume that clones can only move among adjacent compartments, so that the expression $\frac{\gamma}{\Omega}\left[c_{k-1} - c_k\right]$ in Eq. 3.3 fully accounts for changes to c_k due to thymic export. Also in Eq. 3.3, the term $p(N)kc_k$ denotes the rate at which cells in size-k clones proliferate, which in turn corresponds to the rate at which clones move from c_k to c_{k+1} due to peripheral proliferation. Analogously, $p(N)(k-1)c_{k-1}$ denotes the rate at which cells enter c_k from c_{k-1} due to proliferation, so that $p(N)\left[(k-1)c_{k-1} - kc_k\right]$ accounts for changes to c_k due to proliferation. The death term in Eq. 3.3, given by $\mu(N)\left[(k+1)c_{k+1} - kc_k\right]$ is defined analogously. In Eqs. 3.2 and 3.4, we modify Eq. 3.3 to account for appropriate "boundary conditions". In Eq. 3.2, the term $\left[\Omega - \sum_{i=1}^{M} c_i\right]$ gives the number of clonotypes unrepresented in the periphery, so that $\frac{\gamma}{\Omega}\left[\Omega - \sum_{i=1}^{M} c_i\right]$ provides the rate at which new clones enter the periphery from the thymus. Eq. 3.2 also

retains the terms from Eq. 3.3 that account for loss of clones in c_1 due to thymic export, proliferation, and death, and the addition of clones into c_1 due to death of cells in c_2. Finally, Eq. 3.4 retains terms accounting for the introduction of clones into c_M via thymic export to and proliferation within clones in c_{M-1}, as well as loss of clones from c_M due to cellular death. This represents the imposition of a "boundary condition" that allows clones to achieve, but not surpass, size M.

We now consider the relationship between the ODE in Eq. 3.1 and those in Eqs. 3.2–3.4. Since $N(t)$ represents the total cell count, it should be the case conceptually that $N(t) = \sum_{k=1}^{M} kc_k(t)$. Summing Eqs. 3.2, 3.4, and 3.3 for $k = 2, \cdots, M-1$, we find that,

$$\frac{\mathrm{d}\left(\sum_{k=1}^{M} kc_k\right)}{\mathrm{d}t} = \gamma + p(N)\left(\sum_{k=1}^{M} kc_k\right) + \mu(N)\left(\sum_{k=1}^{M} kc_k\right) - \left(p(N)Mc_M + \frac{\gamma_0}{\Omega}c_M\right), \tag{3.5}$$

so that the ODE satisfied by $N(t)$ (Eq. 3.1) and that satisfied by $\sum_{k=1}^{M} kc_k(t)$ (Eq. 3.5) differ by a factor of $\left(p(N)Mc_M + \frac{\gamma_0}{\Omega}c_M\right)$, and thus $N(t) \neq \sum_{k=1}^{M} kc_k$. Thus, a small mass of size M or larger clones, which are accounted for in Eq. 3.1, are not accounted for fully in Eqs. 3.2, 3.3, 3.4. However, large clones are quite rare, and thus contribute such a small portion of the total cell count that we regard Eq. 3.1 and Eqs. 3.2, 3.3, 3.4 as sufficiently consistent for our purposes.

We use this basic ODE system to formulate models of different single-stage and multi-stage cycles of thymic disease and recovery. As we are studying how thymic disease affects total cell counts, the parameter most crucial to our investigation is γ, the thymic export rate. To represent healthy thymic function, we take $\gamma = \gamma_0$, where γ_0 is the normal level of thymic export in an adult of a given age. To represent diminished thymic activity during atrophy, we take $\gamma \ll \gamma_0$, or even $\gamma = 0$, depending on the severity of the atrophy. As the thymus is highly plastic, the changes in γ throughout the process of atrophy and recovery tend to be rapid. With this in mind, we model such cycles of disease with a piecewise ODE system. Specifically, let us observe a human's response to disease-induced changes in thymic activity over some time interval $I = [t_0, t_{S+1}]$. We assume that this individual's

thymic export rate undergoes S abrupt changes, at times $t_1, t_2, \cdots, t_S$, where $t_0 < t_1 < t_2 < \ldots < t_S < t_{S+1}$. Letting $I_i = [t_i, t_{i+1}]$, so that $I = \bigcup_{i=0}^{S} I_i$, we assume that $\gamma = \gamma_i \geq 0$, on I_i. If the initial condition $\{c_k(t_0)\}_{k=1}^{M}$ represents the size of each c_k compartment at the start of the process, we then let $\{c_k^i(t)\}_{k=1}^{M}$ represent the solution of the ODE in Eqs. 3.1-3.4, on I_i, with $\gamma = \gamma_i$ and initial condition $\{c_k^i(t_i)\}_{k=1}^{M} = \{c_k^{i-1}(t_i)\}_{k=1}^{M}$, for $i = 1, 2, \cdots, S$. Thus, the solution $\{c_k^i(t)\}_{k=1}^{M}$ represents the time evolution of the c_k compartments after a transition to a thymic activity level γ_i. This is the most general description of our model; in practice, we will mostly take $S = 0, 1$. Further descriptions of the piecewise ODE formulation specific to certain disease patterns and particular initial conditions are included in the relevant sections below.

3.3 Solution Analysis in the Case $\gamma > 0$ (functioning thymus)

We begin by studying the behavior of solutions of our ODE model under the assumption of a strictly positive thymic export rate, γ. We conduct analysis of equilibrium solutions of Eqs. 3.1-3.4 and their stability, and also compute an explicit solution in the infinite dimensional case that arises when $M \to \infty$. At the beginning of sections 3.3.1 and 3.3.2 below, as well as in sections 3.4.1, 3.4.2, and 3.5, we focus on solutions over one individual interval in the piecewise formulation described in section 3.2 above. For simplicity when doing this, we omit the i notation that distinguishes the different subintervals, writing γ instead of γ_i, etc. When the discussion returns to the full piecewise ODE, the i notation is reintroduced.

3.3.1 Analytic Solution of the Infinite Dimensional System

We begin by computing analytic expressions for the solutions c_k of Eqs. 3.1-3.4. If we take $M \to \infty$ and consider instead the infinite dimensional system, the c_k compartments can be obtained through a generating function, defined as:

$$Q(z,t) \equiv \sum_{k=0}^{\infty} c_k(t) z^k, \tag{3.6}$$

with $z \in \mathbb{R}$ to be determined later. Note that $\partial^k Q / \partial z^k \big|_{z=0} = k! c_k$. The solution $Q(z,t)$

allows us to solve for every c_k with $k \geq 0$. In addition, $\partial Q/\partial z|_{z=1} = \sum_{k=0}^{\infty} k c_k = N$, and the total cell number can also be recovered from the generating function.

In order to derive an explicit form for $Q(z,t)$, we assume that an explicit solution $N = N(t)$ of Eq. 3.1 can be found, so that we may write p and μ as functions of t ($p = p(t)$, $\mu = \mu(t)$). By substituting Eqs. 3.2, 3.3 for $\mathrm{d}c_k/\mathrm{d}t$, the time derivative of Q can be expressed as

$$\begin{aligned} \frac{\partial Q}{\partial t} &= \sum_{k=0}^{\infty} \frac{\mathrm{d}c_k}{\mathrm{d}t} z^k \\ &= (z-1)(p(t)z - \mu(t))\frac{\partial Q}{\partial z} + \frac{\gamma}{\Omega}(z-1)Q. \end{aligned} \tag{3.7}$$

The above partial differential equation can be solved analytically using the method of characteristics. The characteristic curves are defined by

$$\frac{\mathrm{d}z}{\mathrm{d}t} = -(z-1)(p(t)z - \mu(t)). \tag{3.8}$$

Along a particular characteristic curve $z(t)$, the value of Q evolves via the following equation:

$$\frac{\mathrm{d}Q}{\mathrm{d}t} = \frac{\gamma}{\Omega}(z(t)-1)Q. \tag{3.9}$$

Eq. 3.8 leads to the following expression for $z(t)$

$$z_0 = 1 - \frac{z(t)-1}{(z(t)-1)B(t) - A(t)}, \tag{3.10}$$

where

$$A(t) \equiv \exp\left(-\int_0^t (p(s) - \mu(s))\,\mathrm{d}s\right), \tag{3.11}$$

$$B(t) \equiv \int_0^t p(s)A(s)\mathrm{d}s, \tag{3.12}$$

and $z_0 = z(0)$. The generating function $Q(z(t), t)$ is then:

$$Q(z(t), t) = \sum_{k=0}^{\infty} c_k(0) z_0^k \exp\left(\int_0^t \frac{\gamma}{\Omega}(z(s) - 1)\mathrm{d}s \right). \tag{3.13}$$

A particularly interesting scenario is that of a depleted T-cell pool being repopulated after blood transfusion. In such a scenario, the initial conditions are $c_0(0) = \Omega$, while $c_k(0) = 0$ for all $k \geq 1$, and Eq. 3.13 is subsequently simplified to

$$Q(z(t), t) = \Omega \exp\left(\int_0^t \frac{\gamma}{\Omega}(z(s) - 1)\mathrm{d}s \right). \tag{3.14}$$

To compute $c_k(t_1)$ at time $t_1 > 0$, we take the k-th order derivative of Eq. 3.14 with respect to $z(t)$ and obtain

$$c_k(t_1) = \frac{\prod_{i=0}^{k-1} (\gamma + ip(t_1))}{k! \left(\mu(t_1) - p(t_1) z(t_1)\right)^k} \exp\left(\int_0^{t_1} \frac{\gamma}{\Omega}(z(s) - 1)\mathrm{d}s \right). \tag{3.15}$$

In Eq. 3.15 the characteristic $z(t)$ is chosen such that $z(t_1) = 0$. Note that for another time point $t_2 \neq t_1$, a different characteristic curve will be selected. Moreover, $N(t_1)$ can be evaluated by taking the first order derivative of Eq. 3.14 with respect to $z(t)$ and selecting the characteristic satisfying $z(t_1) = 1$.

3.3.2 Equilibrium Solution and Linearization

Returning to the truncated formulation (finite M), we now study the equilibrium solution that results when taking $\gamma > 0$ in Eqs. 3.1-3.4. Denote such a generic equilibrium solution by $\{c_k^*(\gamma)\}_{k=1}^M$, $N^*(\gamma)$. For a given $N^*(\gamma)$, the $c_k^*(\gamma)$ have the form,

$$c_1^*(\gamma) = \gamma \left[\frac{\gamma}{\Omega} \left(\sum_{i=1}^{M} \frac{1}{i! \mu(N^*(\gamma))^{i-1}} \left(\prod_{j=1}^{i-1} \left[\frac{\gamma}{\Omega} + jp(N^*(\gamma)) \right] \right) \right) + \mu(N^*(\gamma)) \right]^{-1}, \quad (3.16)$$

$$c_k^*(\gamma) = \frac{c_1^*(\gamma)}{k! \mu(N^*(\gamma))^{k-1}} \left(\prod_{n=1}^{k-1} \left[\frac{\gamma}{\Omega} + np(N^*(\gamma)) \right] \right). \quad (3.17)$$

In the discussion below, we will write $N^*(\gamma)$ as N^* and $c_k^*(\gamma)$ as c_k^* for simplicity, unless desiring to emphasize the γ-dependence. To identify the stability of this equilibrium solution–and to identify the rates of convergence of solutions to equilibria under the linearized model later on–we consider the linearization of the system around this generic equilibrium solution, represented by the $(M+1) \times (M+1)$ matrix L_S ($L_S = (s_{ij})_{1 \le i,j \le M+1}$), with component s_{ij} given by:

$$\begin{cases} -\left(\frac{2\gamma}{\Omega}\right) - (p(N^*) + \mu(N^*)), & \text{if } i = j = 1 \\ -\left(\frac{\gamma}{\Omega}\right) + 2\mu(N^*), & \text{if } i = 1,\ j = 2 \\ -\left(\frac{\gamma}{\Omega}\right), & \text{if } i = 1;\ 3 \le j \le M \\ -\left(\frac{\gamma}{\Omega}\right) - i(p(N^*) + \mu(N^*)), & \text{if } i = j;\ 2 \le j \le M-1 \\ -M(p(N^*) + \mu(N^*)), & \text{if } i = j = M \\ -\frac{\gamma}{\Omega} + ip(N^*), & \text{if } i = j+1;\ 1 \le j \le M-1 \\ (i+1)\mu(N^*), & \text{if } i = j-1,\ 2 \le j \le M \\ p'(N^*)[(j-1)c_{j-1}^* - jc_j^*] + \mu'(N^*)[(j+1)c_{j+1}^* - jc_j^*], & \text{if } i = M+1;\ 1 \le j \le M-1 \\ p'(N^*)(M-1)c_{M-1}^* - \mu'(N^*)Mc_M^*, & \text{if } i = M+1;\ j = M \\ p'(N^*)N^* + p(N^*) - \mu'(N^*)N^* - \mu(N^*), & \text{if } i = j = M+1 \\ 0, & \text{otherwise.} \end{cases} \quad (3.18)$$

For clarity, an example of the matrix L_S with $M = 4$ is given below:

$$\begin{pmatrix} -\frac{2\gamma}{\Omega} - (p(N^*) + \mu(N^*)) & -\frac{\gamma}{\Omega} + 2\mu(N^*) & -\frac{\gamma}{\Omega} & -\frac{\gamma}{\Omega} & -p'(N^*)c_1^* \\ \frac{\gamma}{\Omega} + p(N^*) & -\frac{\gamma}{\Omega} - 2(p(N^*) + \mu(N^*)) & 3\mu(N^*) & 0 & p'(N^*)[c_1^* - 2c_2^*] + \mu'(N^*)[3c_3^* - 2c_2^*] \\ 0 & \frac{\gamma}{\Omega} + 2p(N^*) & -\frac{\gamma}{\Omega} - 3(p(N^*) + \mu(N^*)) & 4\mu(N^*) & p'(N^*)[2c_2^* - 3c_3^*] + \mu'(N^*)[4c_4^* - 3c_3^*] \\ 0 & 0 & \frac{\gamma}{\Omega} + 3p(N^*) & -4\mu(N^*) & 3p'(N^*)c_3^* - 4\mu(N^*)c_4^* \\ 0 & 0 & 0 & 0 & p'(N^*)N^* + p(N^*) - \mu'(N^*)N^* - \mu(N^*) \end{pmatrix}$$

We now apply a simplifying assumption to the matrix L_S to analytically compute its eigenvalues more readily. In general, $\frac{\gamma}{\Omega} \sim 10^{-8} - 10^{-6}$, and $p(N^*), \mu(N^*) \sim 10^{-1}$ (when rates are measured in the unit year^{-1}), so that $\frac{\gamma}{\Omega} \ll p(N^*), \mu(N^*)$. We thus omit the terms consisting of multiples of the quantity $\frac{\gamma}{\Omega}$ from the matrix L_S, resulting in the new matrix, $L_{\tilde{S}}$, ($L_{\tilde{S}} = (\tilde{s}_{ij})_{1 \leq i,j \leq M+1}$), with the component $\tilde{s}_{ij}$ given by:

$$\begin{cases} -i(p(N^*) + \mu(N^*)), & \text{if } i = j \leq M-1 \\ -M\mu(N^*), & \text{if } i = j = M \\ (i+1)\mu(N^*), & \text{if } i = j-1;\ 2 \leq j \leq M \\ ip(N^*), & \text{if } i = j+1;\ 1 \leq j \leq M-1 \\ p'(N^*)[(j-1)c_{j-1}^* - jc_j^*] + \mu'(N^*)[(j+1)c_{j+1}^* - jc_j^*], & \text{if } i = M+1;\ j \leq M-1 \\ p'(N^*)(M-1)c_{M-1}^* - \mu'(N^*)Mc_M^*, & \text{if } i = M+1,\ j = M \\ p'(N^*)N^* + p(N^*) - \mu'(N^*)N^* - \mu(N^*), & \text{if } i = j = M+1 \\ 0, & \text{otherwise} \end{cases} \tag{3.19}$$

Again for clarity, we include an example of the matrix $L_{\tilde{S}}$ described in Eq. 3.19, with $M = 4$:

$$\begin{pmatrix} -(p(N^*)+\mu(N^*)) & 2\mu(N^*) & 0 & 0 & -p'(N^*)c_1^* \\ p(N^*) & -2(p(N^*)+\mu(N^*)) & 3\mu(N^*) & 0 & p'(N^*)[c_1^*-2c_2^*]+\mu'(N^*)[3c_3^*-2c_2^*] \\ 0 & 2p(N^*) & -3(p(N^*)+\mu(N^*)) & 4\mu(N^*) & p'(N^*)[2c_2^*-3c_3^*]+\mu'(N^*)[4c_4^*-3c_3^*] \\ 0 & 0 & 3p(N^*) & -4\mu(N^*) & 3p'(N^*)c_3^*-4\mu(N^*)c_4^* \\ 0 & 0 & 0 & 0 & p'(N^*)N^*+p(N^*)-\mu'(N^*)N^*-\mu(N^*) \end{pmatrix}$$

Simulation confirms that the eigenvalues of the new matrix $L_{\tilde{S}}$ given by Eq. 3.19 are essentially identical to those of the original matrix L_S, validating our assumption that the term $\frac{\gamma}{\Omega}$ may be neglected in L_S. Note that this assumption does not cause us to omit the constant γ from the linearization matrix L_S entirely, as the steady state values N^*, c_k^* depend on γ. Denote by λ_k^S for $k = 1, 2, \cdots, M+1$ the eigenvalues of $L_{\tilde{S}}$, and note that that the entry $\tilde{s}_{(M+1,M+1)} = \frac{\mathrm{d}N}{\mathrm{d}t}|_{N=N^*} = p'(N^*)N^* + p(N^*) - \mu'(N^*)N^* - \mu(N^*)$ is an eigenvalue. We denote this eigenvalue by λ_{M+1}^S. We assume that N^* is the homeostatic population level that results at thymic export rate $\gamma > 0$, so that N^* represents an asymptotically stable equilibrium solution of Eq. 3.1. With that said, we assume that $\lambda_{M+1}^S < 0$. The eigenvalues $\lambda_1^S, \cdots, \lambda_M^S$ are those of the $(M+1) \times (M+1)$ minor of $L_{\tilde{S}}$. (In section 2.7, it was shown that the eigenvalues of $L_{\tilde{S}}$ all have strictly negative real part. Although the proof does not apply to the analogous minor of L_S, numerical computation indicates that this is also true of the eigenvalues of L_S.) Denote by $y_k = (y_k^1, \cdots, y_k^M, 0)$ the eigenvector corresponding to λ_k^S. We now derive an analytic approximation, $\tilde{\lambda}_k^S$, to λ_k^S, and an approximation, $\tilde{y}_k$, to y_k, for $k = 1, \cdots, M$. For each $k = 1, \cdots, M$, we let $\tilde{\lambda}_k^S = k(p(N^*) - \mu(N^*))$, and produce an eigenvector $\tilde{y}_k$ that satisfies $||(L_{\tilde{S}} - \tilde{\lambda}_k^S I)\tilde{y}_k|| \to 0$ as $M \to \infty$, so that at large M, the residual quantity in the eigenvalue equation is "small". (Numerical simulation verifies that at large M, $\tilde{\lambda}_k^S \approx \lambda_k^S$ and $\tilde{y}_k \approx y_k$ for small k.) We make this precise in the following Proposition:

Proposition 3.3.1. *If $p(N^*) - \mu(N^*) < 0$, the eigenvalues $\{\lambda_k^S\}_{k=1,\ldots,M}$ of the matrix $L_{\tilde{S}}$ are well approximated by the terms $\tilde{\lambda}_k^S = k(p(N^*) - \mu(N^*))$, in the sense that there exist vectors $\tilde{y}_k$ such that $||(L_{\tilde{S}} - \tilde{\lambda}_k^S I)\tilde{y}_k|| \longrightarrow 0$ as $M \longrightarrow \infty$.*

Proof. We begin by assuming that the terms $\tilde{\lambda}_k^S = k(p(N^*) - \mu(N^*))$ are themselves eigen-

values of $L_{\tilde{S}}$, and search for their corresponding eigenvectors, $\tilde{y}_k = (\tilde{y}_k^1, \tilde{y}_k^2, \cdots, \tilde{y}_k^M, 0)$. Choosing $\tilde{y}_k^1 = 1$, we then choose $\tilde{y}_k^i$ for $i = 2, \ldots, M$ inductively so as to force the i-th component of the residual vector, which we denote by $[(L_{\tilde{S}} - \tilde{\lambda}_k^S I)\tilde{y}_k]_i$, to equal zero for $i = 1, 2, \cdots, M-1$. We then verify that $[(L_{\tilde{S}} - \tilde{\lambda}_k^S I)\tilde{y}_k]_M \longrightarrow 0$ as $M \longrightarrow \infty$, so that for $M \gg 1$, $||(L_{\tilde{S}} - \tilde{\lambda}_k^S I)\tilde{y}_k|| \approx 0$, where $||\cdot||$ is any p-norm. (Trivially, $[(L_{\tilde{S}} - \tilde{\lambda}_k^S I)\tilde{y}_k]_{M+1} = 0$.)

We first note that the components $\tilde{y}_k^1, \cdots, \tilde{y}_k^M$ of the approximate eigenvector $\tilde{y}_k$ corresponding to eigenvalue $\tilde{\lambda}_k^S$ are defined by the recurrence relation,

$$i\tilde{y}_k^i = \left[(i + (k-1))\left(\frac{p(N^*)}{\mu(N^*)}\right) + (i - (k+1))\right]\tilde{y}_k^{i-1} - [i-2]\left(\frac{p(N^*)}{\mu(N^*)}\right)\tilde{y}_k^{i-2}. \tag{3.20}$$

The solution of this recurrence relation is then,

$$\tilde{y}_k^i = \sum_{n=1}^{k} \frac{\left[\prod_{j=1}^{n-1}(i-j)\right]\left[\prod_{j=1}^{k-n}(i+j)\right]}{k(-1)^{n-1}(n-1)!(k-n)!}\left(\frac{p(N^*)}{\mu(N^*)}\right)^{i-n}, \tag{3.21}$$

where we let $\prod_{j=1}^{0}(i \pm j) = 1$, whenever such a term appears in the above sum. (This is verified in Appendix 3.7.) As previously mentioned, $[(L_{\tilde{S}} - \tilde{\lambda}_k^S I)\tilde{y}_k]_i = 0$ for $i = 1, 2, \cdots, M-1$. We now compute $[(L_{\tilde{S}} - \tilde{\lambda}_k^S I)\tilde{y}_k]_M$, obtaining,

$$[(L_{\tilde{S}} - \tilde{\lambda}_k^S I)\tilde{y}_k]_M = (M-1)p(N^*)\tilde{y}_k^{M-1} - M\mu(N^*)\tilde{y}_k^M \tag{3.22}$$

$$= p(N^*)\sum_{n=1}^{k} \frac{\left[\prod_{j=0}^{n-1}(M-1-j)\right]\left[\prod_{j=1}^{k-n}(M-1+j)\right]}{k(-1)^{n-1}(n-1)!(k-n)!}\left(\frac{p(N^*)}{\mu(N^*)}\right)^{M-1-n} \tag{3.23}$$

$$- \mu(N^*)\sum_{n=1}^{k} \frac{\left[\prod_{j=0}^{n-1}(M-j)\right]\left[\prod_{j=1}^{k-n}(M+j)\right]}{k(-1)^{n-1}(n-1)!(k-n)!}\left(\frac{p(N^*)}{\mu(N^*)}\right)^{M-n}. \tag{3.24}$$

Each term in the sum above has the form $p_k(M)a^M$, where $p_k(M)$ is a polynomial of

degree k in the variable M, and $a = p(N^*)/\mu(N^*)$. Recalling that $p(N^*)/\mu(N^*) < 1$, then $\lim_{M\longrightarrow\infty} p_k(M)a^M = 0$, so that at large values of M, $[(L_{\tilde{S}} - \tilde{\lambda}_k^S I)\tilde{y}_k]_M \approx 0$. This demonstrates that $\tilde{\lambda}_k^S$ may be regarded as an approximation to the true eigenvalue λ_k^S, assuming that the eigenvalues of $L_{\tilde{S}}$ are stable under small perturbations. □

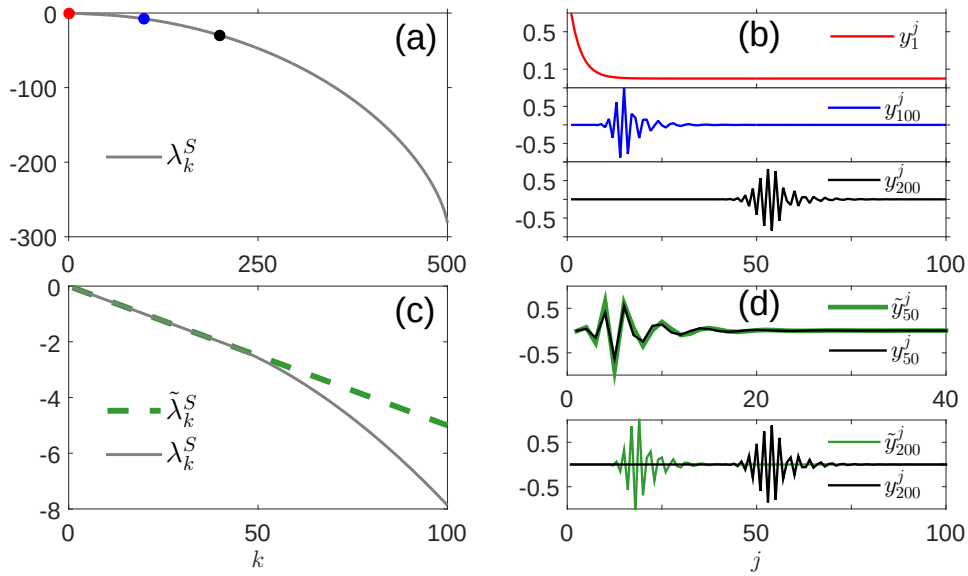

Figure 3.1: **Eigenvalues and eigenvectors of $L_{\tilde{S}}$,** $\gamma > 0$ (a) Numerically computed eigenvalue spectrum of the matrix $L_{\tilde{S}}$, with $p(N^*) = 0.12$, $\mu(N^*) = 0.17$, and $M = 500$. Dots identify the locations of the eigenvalues λ_1^S (red), λ_{100}^S (blue), λ_{200}^S (black). (b) First 100 components $(\tilde{y}_k^1, \cdots, \tilde{y}_k^{100})$ of the eigenvectors with indices $k = 1, 100, 200$, the eigenvalues corresponding to which are marked on the spectral curve in (a). (c) Comparison of true eigenvalues (λ_k^S) and approximate eigenvalues $(\tilde{\lambda}_k^S)$ for $k = 1, \cdots, 100$. Approximation is strong for $k \lesssim 50$. (d) (top) Comparison of $\tilde{y}_{50}^j$ and y_{50}^j for $j = 1, \cdots, 40$, showing that the approximation is strong. (bottom) Comparison of $\tilde{y}_{200}^j$ and y_{200}^j for $j = 1, \cdots, 100$, showing that the accuracy of the approximation breaks down, but the qualitative behavior of y_{200}^j is captured in $\tilde{y}_{200}^j$.

The solutions $\tilde{y}_k^i$, as functions of i for fixed k, are characterized by short bursts of oscillatory behavior, as shown in Fig. 3.1, which depicts numerical computations of true and approximate eigenvalues and eigenvectors of $L_{\tilde{S}}$. Fig. 3.1(a) presents a sample plot of the eigenvalue spectrum λ_k^S in the case $M = 500$; on the spectral curve, several eigenvalues are marked, the first 100 components of which are plotted in Fig. 3.1(b). As discussed previously, all eigenvalues are negative. The eigenvector plots in Fig. 3.1(b) indicate that as k increases, the period of oscillatory "mass" occurs at increasingly large values of j, so that the oscillatory "mass" of the eigenvector appears to shift down along the vector itself. Fig. 3.1(c) presents a comparison of the true eigenvalue spectrum (λ_k^S) and the

approximate eigenvalue spectrum ($\tilde{\lambda}_k^S$) of the matrix $L_{\tilde{S}}$. The eigenvalue approximation is very strong for $1 \lesssim k \lesssim (0.1)M$, and this remains true as M varies. The quantities $\tilde{\lambda}_k^S = k(p(N^*) - \mu(N^*))$ over-approximate the λ_k^S for $k \gtrsim (0.1)M$. Fig. 3.1(d) depicts a comparison of y_k and $\tilde{y}_k$ for two values of k, one below the threshold $(0.1)M$ ($k = 50$, top) and one above the threshold ($k = 200$, bottom). As expected, the eigenvector approximate is quite accurate precisely when the corresponding eigenvalue approximation is accurate. Even for $k \gtrsim (0.1)M$, the approximate eigenvectors $\tilde{y}_k$ present an appearance similar to that of the $\tilde{y}_k$ for smaller k. The diminished accuracy of the eigenvalue/eigenvector pairs at higher k (for fixed M) is attributable to the slower convergence of $[(L_{\tilde{S}} - \tilde{\lambda}_k^S I)\tilde{y}_k]_M$ to 0 as $M \to \infty$ for larger k, which is immediately apparent from the form in Eqs. 3.23, 3.24. For a system of a fixed dimension M, increasing $\mu(N^*)$ relative to $p(N^*)$ causes the approximate eigenvalues $\tilde{\lambda}_k^S$ to become increasingly valid at larger k, clearly due to the quicker convergence of the residual quantity $||(L_{\tilde{S}} - \tilde{\lambda}_k^S I)\tilde{y}_k||$ to 0 when $(p(N^*)/\mu(N^*)) \ll 1$, as indicated by Eq. 3.21. Increases to $\mu(N^*)$ relative to $p(N^*)$ also cause an intensified dampening of the oscillations in the eigenvector $\tilde{y}_k$ at lower components j, which creates the illusion of the oscillatory mass shifting to the left as $\mu(N^*)$ increases for fixed $p(N^*)$, as in Fig. 3.2(right). At the same time, the entire eigenvalue spectrum becomes more negative as $\mu(N^*)$ increases, as indicated in Fig. 3.2(left), so that increases to the death rate at homeostatic levels indicate much faster convergence to equilibrium of all c_k compartments.

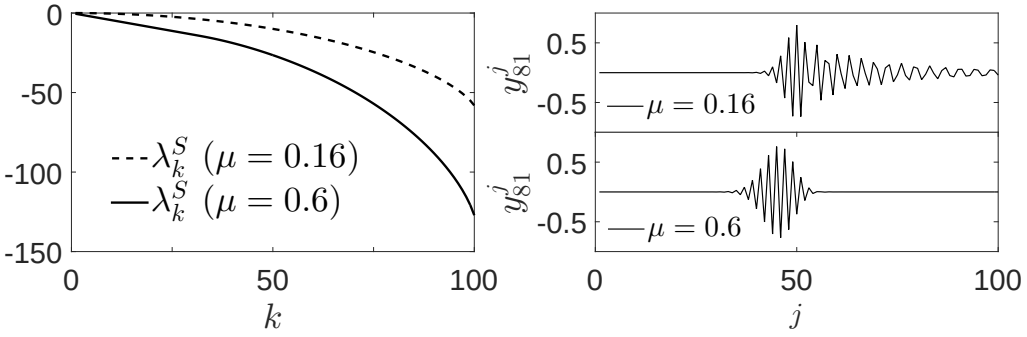

Figure 3.2: **Eigenvalues and eigenvectors of $L_{\tilde{S}}$, $\gamma > 0$, varying μ** (left) Numerically computed eigenvalues, λ_k^S, for $k = 1, \cdots, 100$, when $\mu(N^*) = 0.16$ and $\mu(N^*) = 0.6$. In both cases, $p(N^*) = 0.15$, $M = 100$. (right) Numerically computed eigenvectors x_{81}.

3.3.3 Behavior of the Linearized and Fully Nonlinear Systems

This section addresses the convergence behavior of solutions in the presence of a positive thymic export rate $\gamma > 0$. This situation represents a functioning thymus, with the possibility for many different levels of functionality, ranging from total health (high $\gamma \sim \gamma_0$) to dramatically diminished functionality (low γ). In this case, we determined that for each equilibrium solution of Eq. 3.1, the system has an equilibrium solution given by Eqs. 3.16, 3.17. If the equilibrium, $N^*(\gamma)$, of Eq. 3.1 is stable, the corresponding equilibrium $c_k^*(\gamma)$ will also be stable. (Physiologically typical forms of $p(N)$, $\mu(N)$ tend to result in one positive, stable equilibrium solution in Eq. 3.1.) Based on the eigenvalues and eigenvectors of the approximate linearization, $L_{\tilde{S}}$, of Eqs. 3.1-3.4 around this equilibrium, we study the rates at which individual compartments converge to equilibrium under the linearized model. If for some i, $\gamma_i > 0$, the solution $\{c_k^i(t)\}_{k=1}^M$, $N^i(t)$ satisfies $c_k^i(t) \to c_k^*(\gamma_i)$, $N^i(t) \to N^*(\gamma_i)$. Based on the explicit solution of the linearized problem, we naturally regard as the rate of convergence of a particular compartment c_j to zero the smallest $k \in \mathbb{N}$ for which $|\tilde{y}_k^j|$ is particularly "large" compared to the other components that lie outside the oscillatory "mass" of the eigenvector. According to our discussion in section 3.3.2, $c_k^i(t) \to c_k^*$ at the rate $p(N^*) - \mu(N^*)$ if $k \sim 1$, and $c_k^i(t) \to c_k^*$ at a rate much faster than $k(p(N^*) - \mu(N^*))$ if k is large. $N^i(t) \to N^*$ at the rate $p'(N^*)N^* + p(N^*) - \mu'(N^*)N^* - \mu(N^*)$.

In the fully nonlinear system, however, the linearized eigenvalues a priori only provide rates of convergence of solution trajectories initialized near equilibrium. The accuracy of the eigenvalues in providing convergence rates of solutions depends on the initial conditions. If the initial conditions, $c_k^i(t_i), N^i(t_i)$, satisfy $c_k^i(t_i) \sim c_k^*(\gamma_i)$, $N^i(t_i) \sim N^*(\gamma_i)$, then the solutions begin near the stable equilibrium, and the eigenvalues provide accurate rates of convergence. If the initial conditions are far from equilibrium, the eigenvalues may not provide accurate rates of convergence of the entire solution trajectory. When trajectories are far from equilibrium at time t_i, further information about the speed of convergence can be discerned from the relationship between $p(N^*(t_i)) - \mu(N^*(t_i))$ and $p(N^*(\gamma_i)) - \mu(N^*(\gamma_i))$–that is, the disparity in proliferation and death rates at the starting and terminal population levels. If these quantities differ significantly, solution trajectories are generally characterised by a transient period of fast convergence, which carries the

trajectory close enough to the stable equilibrium that convergence rates from then on are those of the linearized eigenvalues. For example, assume that an abrupt drop in thymic productivity occurs at t_i, so that $\gamma_{i-1} \gg \gamma_i$. If the person was in a state of immune health prior to atrophy, the population level $N^*(t_i)$ will represent a normal homeostatic level and satisfy $p(N^*(t_i)) - \mu(N^*(t_i)) \sim p(N^*(\gamma_{i-1}) - \mu(N^*(\gamma_{i-1})) < 0$. We can expect the quantity $p(N^*(\gamma_i)) - \mu(N^*(\gamma_i))$ to satisfy $0 > p(N^*(\gamma_i)) - \mu(N^*(\gamma_i)) > p(N^*(\gamma_{i-1})) - \mu(N^*(\gamma_{i-1}))$, as a higher thymic export rate subsequently necessitates a higher level of regulation-induced cellular death to maintain homeostatic balance. In this situation, the T-cell pool will experience a brief transient period of higher cellular death, until the total cell count falls to a level near $N^*(\gamma_i)$, at which point convergence rates correspond to the linearized eigenvalues.

3.4 Solution Analysis in the Case $\gamma = 0$ (full thymic cessation)

We now proceed to study solution behavior in the absence of thymic export ($\gamma = 0$). As in section 3.3 above, we compute equilibrium solutions of the truncated system (finite M) that arise when $\gamma = 0$, and identify the rates of convergence of the different $c_k(t)$ to equilibrium under the linearized model. We also take $M \to \infty$ and consider explicit solutions of the infinite-dimensional system.

3.4.1 Analytic Solutions

We begin, as before, by taking $M \to \infty$ and considering the generating function $Q(z,t)$ defined in Eq. 3.6, which was shown to satisfy the partial differential equation in Eq. 3.7. Taking $\gamma(t) = 0$ in Eq. 3.13, the solution $Q(z,t)$ may be written as,

$$Q(z,t) \;=\; \sum_{k=0}^{\infty} c_k(0) \left[1 - \frac{z-1}{(z-1)B(t) - A(t)}\right]^k. \tag{3.25}$$

As stated earlier, the analytic solution $c_k(t)$ for $k \geq 0$ is given by the k-th order derivative of Q with respect to z at $z = 0$. Utilizing the results previously derived in the literature [Wan05], we can write

$$c_k(t) = \left[\frac{B(t)}{A(t)+B(t)}\right]^k \sum_{i=0}^{\infty} c_i(0) \cdot \left[\sum_{j=0}^{i} \begin{pmatrix} i \\ j \end{pmatrix} \begin{pmatrix} k+j-1 \\ k \end{pmatrix} \left(1-\frac{1}{B(t)}\right)^{i-j} \left(\frac{A(t)}{B(t)\,(A(t)+B(t))}\right)^j\right] \quad (3.26)$$

Note that for depleted initial conditions $c_0(0) = \Omega$ and $c_k(0) = 0$ for $k \geq 1$, Eq. 3.26 leads to $c_0(t) = \Omega$ and $c_k(t) = 0$ for $k \geq 1$ at all times. Indeed, the T-cell pool is expected to remain empty since there is no thymic export. We can also verify that $N(t) = A(t)^{-1} \sum_{k=0}^{\infty} k c_k(0)$, which is the same as the analytical solution obtained directly from Eq. 3.1.

Fig 3.3(A) depicts a numerical computation of the solution, c_k, of the infinite-dimensional formulation, obtained from the generating function. We include values of c_k for $k = 1, 2, \cdots, 50$ at times $t = 30, 60, 90$. As a function of k, the c_k present as linear on a logarithmic scale, as expected. To compare the infinite dimensional system with the truncated system, we also compute solutions, y_k, of the truncated Eqs. 3.2, 3.3, 3.4 (not pictured). Fig. 3.3(B) depicts the relative error, $|c_k - y_k|/c_k$. As we see, the error is several orders of magnitude smaller than c_k, y_k themselves at each of the times $t = 30, 60, 90$, indicating that the infinite- and finite- dimensional systems may be used more or less interchangeably.

3.4.2 Equilibrium Solutions and Linearization

We now investigate the equilibrium solutions that arise when we take $\gamma = 0$ in Eqs. 3.1-3.4. In this case, the system has 2 equilibrium solutions. Denoting generic equilibrium solutions by $\{c_k^*\}_{k=1}^M, N^*$, the unstable solution is $c_k^* = 0$ for all $k \geq 1$ and $N^* = 0$, and the asymptotically stable solution is $c_k^* = 0$ for all $k \geq 1$ and $N^* = \tilde{N} > 0$, where $\tilde{N}$ satisfies $p(\tilde{N}) = \mu(\tilde{N})$. To verify the stability of these solutions, we consider the linearization of the system around this equilibrium, which is represented by the $(M+1) \times (M+1)$ matrix we call L_U ($L_U = (u_{ij})_{1 \leq i,j \leq M+1}$). The components u_{ij} of L_U are given explicitly by:

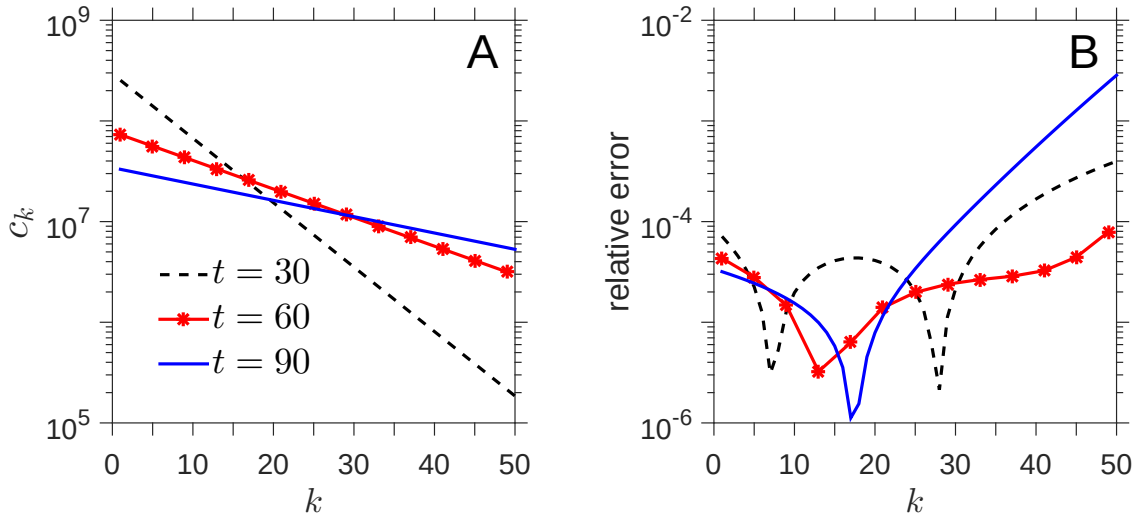

Figure 3.3: **Computation of c_k from method of characteristics, comparison with truncated system** (A) Plots of c_k for $k = 1, 2, \cdots, 50$, at times $t = 30, 60, 90$. Solutions c_k were computed numerically from the analytic method described in 3.4.1, based on the infinite-dimensional system. As a function of k, c_k presents as linear on a logarithmic scale. (B) Relative error, $|c_k - y_k|/c_k$ for $k = 1, 2, \cdots, 50$, at times $t = 30$, 60, 90, where c_k denotes the solutions depicted in (A), and y_k denotes the numerically computed solutions of the truncated system in Eqs. 3.2, 3.3, 3.4. From (B), the disparity between the solutions of the infinite dimensional systems (c_k) and the finite dimensional truncated systems (y_k) is negligible, validating our decision to use them interchangeably. Coefficient functions: $p(N) = p_0 > 0$, $\mu(N) = \mu_0 + \mu_1(N^2/(N^2 + K^2))$. Parameter values: $p_0 = 0.18$, $\mu_0 = 0.17$, $\mu_1 = 0.04$, $K = 10^{10}$, $\Omega = 10^{16}$, $M = 100$. Initial condition: $c_0(0) = 10^{16} - 10^{10}$, $c_1(0) = 10^{10}$, $c_k(0) = 0$ for $k \geq 2$.

$$\begin{cases} -j(p(N^*) + \mu(N^*)), & \text{if } i = j \leq M - 1 \\ -M\mu(N^*), & \text{if } i = j = M \\ j\mu(N^*), & \text{if } i = j - 1;\ 2 \leq j \leq M \\ jp(N^*), & \text{if } i = j + 1;\ 1 \leq j \leq M - 1 \\ p'(N^*)N^* + p(N^*) - \mu'(N^*)N^* - \mu(N^*), & \text{if } i = j = M + 1 \\ 0. & \text{otherwise} \end{cases} \tag{3.27}$$

For reference, an example of the matrix L_U, with $M = 4$, is given below:

$$\begin{pmatrix} -(p(N^*)+\mu(N^*)) & 2\mu(N^*) & 0 & 0 & 0 \\ p(N^*) & -2(p(N^*)+\mu(N^*)) & 3\mu(N^*) & 0 & 0 \\ 0 & 2p(N^*) & -3(p(N^*)+\mu(N^*)) & 4\mu(N^*) & 0 \\ 0 & 0 & 3p(N^*) & -4\mu(N^*) & 0 \\ 0 & 0 & 0 & 0 & p'(N^*)N^* + p(N^*) - \mu'(N^*)N^* - \mu(N^*) \end{pmatrix}$$

As before, $u_{(M+1),(M+1)} = p'(N^*)N^* + p(N^*) - \mu'(N^*)N^* - \mu(N^*)$ is an eigenvalue with eigenvector $(0, \ldots, 0, 1)$, and the remaining eigenvalues are those of the $(M+1) \times (M+1)$ minor of L_U. As before, all eigenvalues of the $(M+1) \times (M+1)$ minor have negative real part, and the stability of an equilibrium solution depends on the sign of $u_{(M+1),(M+1)}$. If $N^* = 0$, then $u_{(M+1),(M+1)} = p(0) - \mu(0) > 0$, as described previously, and the equilibrium $c_k^* = 0$, $N^* = 0$ is unstable. On the other hand, if $N^* = \tilde{N}$ with $p(\tilde{N}) = \mu(\tilde{N})$, then N^* represents a positive, homeostatic cell count, and $u_{(M+1),(M+1)} = \left(p'(N^*) - \mu'(N^*)\right) N^* < 0$, as $p(N), \mu(N)$ are assumed to be non-increasing and non-decreasing, respectively. Therefore, we have that $c_k^* = 0$, $N^* = \tilde{N}$ is a stable equilibrium solution.

If $\gamma = 0$, the solution $\{c_k(t)\}_{k=1}^M$, $N(t)$, will diverge away from the equilibrium $c_k^* = 0$, $N^* = 0$ and towards the equilibrium $c_k^* = 0$, $N^* = \tilde{N}$. In this instance, the pool of small clones is eradicated due to lack of thymic productivity, and the high lymphopenic proliferation rate pushes existent clones past the truncation threshold M, where they are no longer accounted for in the c_k functions but are accounted for in N, causing $N(t) \to N^*$ despite the fact that $c_k(t) \to 0$ for all k. As before, we wish to explore further the rates at which individual functions c_k diverge from the unstable and towards the stable equilibrium under the linearized and fully nonlinear models. To this end, we study the eigenvalues of the linearization matrix, L_U, evaluated at the two equilibria.

We begin by considering the eigenvalues of L_U evaluated at the unstable equilibrium. In this case, we assume $p(0) > \mu(0)$, as described earlier. Without thymic export, new clones are not generated in the periphery, and existent clones expand due to the high proliferation rate. Under Eqs. 3.2, 3.3, 3.4, this manifests as clones quickly expanding

beyond the small-k compartments and getting "caught" at the boundary at size M, before depleting due to the slow death-induced passage of single cell clones through the boundary at $k = 1$. Under Eq. 3.1, this manifests as the total cell population reaching a natural homeostatic level through peripheral maintenance alone. To investigate the rates at which these processes occur under the linearized model, we derive approximations to the dominant eigenvalues of L_U. Denote the true eigenvalues of L_U under the assumption that $p(0) > \mu(0)$ by λ_k^U for $k = 0, 1, \cdots M$, with corresponding eigenvectors $z_k = (z_k^M, z_k^{M-1}, \cdots, z_k^1, z_k^0)$. Assign to the eigenvalue $u_{(M+1),(M+1)} = p(0) - \mu(0)$ the label λ_k^M, and to its eigenvector $(0, \ldots, 0, 1)$ the label z_M. It remains to find approximations to the other M eigenvalues of L_U, which are precisely the eigenvalues of the $(M+1)\times(M+1)$ minor. For $i = 0, 1, \ldots, M-1$, denote the approximation to the eigenvalue λ_k^U by $\tilde{\lambda}_k^U$, and the approximation to the eigenvector z_k by $\tilde{z}_k = (\tilde{z}_k^M, \tilde{z}_k^{M-1}, \cdots, \tilde{z}_k^1, 0)$. We begin by establishing that the eigenvalue of smallest magnitude, λ_0^U, is well approximated by $\tilde{\lambda}_0^U = 0$.

Proposition 3.4.1. *The eigenvalue of L_U of smallest magnitude, λ_0^U, is well approximated by $\tilde{\lambda}_0^U = 0$, in the sense that there exists a vector $\tilde{z}_0 = (\tilde{z}_0^M, \tilde{z}_0^{M-1}, \cdots, \tilde{z}_0^2, \tilde{z}_0^1, 0)$ such that $||(L_U - \tilde{\lambda}_0^U I)\tilde{z}_0|| \longrightarrow 0$ as $M \longrightarrow \infty$.*

Proof. (Note: The components of $\tilde{z}_0$ are written above in "descending" order for notational convenience, as this reflects the order in which they will be chosen recursively below. The i-th component from the left of $\tilde{z}_0$, denoted explicitly by $\tilde{z}_0^{M-i+1}$, still corresponds to the function c_i.) We begin by considering the matrix $(L_U - \tilde{\lambda}_0^U I) = L_U$ and searching for an appropriate eigenvector, $\tilde{z}_0$. We define $\tilde{z}_0^1 = 1$, and once again choose the components $\tilde{z}_0^i$ inductively via a three-term recurrence relation so as to force the i-th component of $(L_U - \tilde{\lambda}_0^U I)\tilde{z}_0$, which we denote as before by $[(L_U - \tilde{\lambda}_0^U I)\tilde{z}_0]_i$, to satisfy $[(L_U - \tilde{\lambda}_0^U I)\tilde{z}_0]_i = 0$ for $i = 2, 3, \cdots, M+1$. While $[(L_U - \tilde{\lambda}_0^U I)\tilde{z}_0]_1 \neq 0$, we show that $[(L_U - \tilde{\lambda}_0^U I)\tilde{z}_0]_1 \longrightarrow 0$ as $M \longrightarrow \infty$, so that $\tilde{z}_0$ may be regarded formally as an "approximate" eigenvector corresponding to the approximate eigenvalue $\tilde{\lambda}_0^U$.

Defining $\tilde{z}_0^1 = 1$ and $\tilde{z}_0^2 = \frac{M\mu(0)}{(M-1)p(0)}$, we let $\tilde{z}_0$ be defined by solutions to the recurrence relation,

$$\tilde{z}_0^{i+2} = \left(\frac{(M-i)(\mu(0)+p(0))}{(M-(i+1))p(0)}\right)\tilde{z}_0^{i+1} - \left(\frac{(M-(i-1))}{M-(i+1)}\right)\left(\frac{\mu(0)}{p(0)}\right)\tilde{z}_0^{i}, \tag{3.28}$$

for $i = 1, 2, \cdots, M-2$. It may be verified directly that the solution to this recurrence relation is given by,

$$\tilde{z}_0^{i} = \left(\frac{M}{M-(i-1)}\right)\left(\frac{\mu(0)}{p(0)}\right)^{i-1}. \tag{3.29}$$

By construction of the recurrence relation, $[(L_U - \tilde{\lambda}_0^A I)\tilde{z}_0]_i = 0$ for $i = 2, 3, \cdots, M$. The first component, $[(L_U - \tilde{\lambda}_0^A I)\tilde{z}_0]_1$, satisfies,

$$[(L_U - \tilde{\lambda}_0^A I)\tilde{z}_0]_1 = -\mu(0)M\left(\frac{\mu(0)}{p(0)}\right)^{M-1} \longrightarrow 0 \tag{3.30}$$

as $M \longrightarrow \infty$. Thus, when $M \gg 1$, $||(L_U - \tilde{\lambda}_0^U I)\tilde{z}_0|| \approx 0$, and we may conclude that $\tilde{\lambda}_0^U = 0$ and $\tilde{z}_0$ are suitable approximations to λ_0^U and z_0, respectively.

□

Recalling that all eigenvalues of L_U have negative real parts, the true eigenvalue λ_0^U has a negative real part of very small magnitude. We now identify which entries in the eigenvector z_0, as approximated by $\tilde{z}_0$, are particularly large in magnitude in comparison with the others. Recalling that the i-th component of $\tilde{z}_0$ is given by $\tilde{z}_0^i = (M/(M-(i-1)))(\mu(0)/p(0))^{i-1}$, the $\tilde{z}_0^i$ decay nearly exponentially in i, so that components of $\tilde{z}_0$ corresponding to the compartments of very large clones are preserved by this slow eigenvalue, in agreement with the described "build up" of clones at the boundary $k = M$ when $\gamma = 0$.

The eigenvalue λ_1^U of second smallest magnitude is well separated from λ_0^U, and it

encodes information about the movement of smaller size clones. Similar analysis of an approximating eigenvalue $\tilde{\lambda}_1^U$ and eigenvector $\tilde{z}_1$ to λ_1^U and z_1 indicate that compartments containing small clones empty much more rapidly than those containing very large clones, as clones race to the boundary at $k = M$. In particular, all but the compartments of very large clones that had been preserved by the slow eigenvalue λ_0^U empty at nearly the same rate, $\lambda_1^U \approx \tilde{\lambda}_1^U = (\mu(0) - p(0))$.

Proposition 3.4.2. *In the case $p(0) > \mu(0)$, the matrix L_U has an eigenvalue λ_1^U which is well approximated by $\tilde{\lambda}_1^U = (\mu(0) - p(0))$, in the sense that there exists a vector $\tilde{z}_1$ such that $||(L_U - \tilde{\lambda}_1^U I)\tilde{z}_1|| \longrightarrow 0$ as $M \longrightarrow \infty$.*

Proof. First define $\tilde{z}_1^1 = 1$, and $\tilde{z}_1^2 = \left(\frac{M+1}{M-1}\right)\left(\frac{\mu(0)}{p(0)}\right) - \frac{1}{M-1}$. Then for $i = 1, 2, \cdots, M-2$, let $\tilde{z}_0^{i+2}$ be given by the solutions to the following recurrence relation:

$$\tilde{z}_1^{i+2} = \tilde{z}_1^{i+1} + \left(\frac{M-(i-1)}{M-(i+1)}\right)\left(\frac{\mu(0)}{p(0)}\right)\left(\tilde{z}_1^{i+1} - \tilde{z}_1^{i}\right). \tag{3.31}$$

(It is worth nothing that if we were to instead choose $\tilde{z}_1^1 = \tilde{z}_1^2$, then the recurrence relation in Eq. 3.31 would have a constant solution, $\tilde{z}_1^i = \tilde{z}_1^1$ for all $i = 1, 2, \cdots, M$. Although $\tilde{z}_1^1 \neq \tilde{z}_1^2$ for our purposes, solutions of the recurrence relation do converge rapidly to constants, as will be discussed later.)

By construction, $[(L_U - \tilde{\lambda}_1^U I)\tilde{z}_1]_i = 0$ for $i = 2, 3, \cdots, M+1$. Additionally, $[(L_U - \tilde{\lambda}_1^U I)\tilde{z}_1]_1 = 2\mu(0)(\tilde{z}_1^M - \tilde{z}_1^{M-1})$. To show that $[(L_U - \tilde{\lambda}_1^U I)\tilde{z}_1]_1 \longrightarrow 0$ as $M \longrightarrow \infty$, we use Eq. 3.31 to derive an explicit bound on the quantity $2\mu(0)(\tilde{z}_1^M - \tilde{z}_1^{M-1})$.

$$
\begin{aligned}
|\tilde{z}_1^{i+2} - \tilde{z}_1^{i+1}| &= \left(\frac{M-(i-1)}{M-(i+1)}\right)\left(\frac{\mu(0)}{p(0)}\right)|\tilde{z}_1^{i+1} - \tilde{z}_1^{i}| \\
&= \left(\frac{M-(i-1)}{M-(i+1)}\right)\left(\frac{M-(i-2)}{M-i}\right)\left(\frac{\mu(0)}{p(0)}\right)^2|\tilde{z}_1^{i} - \tilde{z}_1^{i-1}| \\
&= \left(\frac{M-(i-2)}{M-(i+1)}\right)\left(\frac{M-(i-3)}{M-i}\right)\left(\frac{\mu(0)}{p(0)}\right)^3|\tilde{z}_1^{i-1} - \tilde{z}_1^{i-2}| \\
&= \cdots \\
&= \left(\frac{M-(i-(j-1))}{M-(i+1)}\right)\left(\frac{M-(i-j)}{M-i}\right)\left(\frac{\mu(0)}{p(0)}\right)^j|\tilde{z}_1^{i+2-j} - \tilde{z}_1^{i+1-j}| \\
&= \cdots \\
&= \left(\frac{M-1}{M-(i+1)}\right)\left(\frac{M}{M-i}\right)\left(\frac{\mu(0)}{p(0)}\right)^i|\tilde{z}_1^{2} - \tilde{z}_1^{1}|. \qquad (3.32)
\end{aligned}
$$

Taking $i = M-2$ in the above relation, we find that,

$$
\begin{aligned}
|[(L_U - \tilde{\lambda}_1^U I)\tilde{z}_1]_1| &= 2\mu(0)|\tilde{z}_1^M - \tilde{z}_1^{M-1}| \\
&= \mu(0)\left(M(M-1)\right)\left(\frac{\mu(0)}{p(0)}\right)^{M-2}|\tilde{z}_1^2 - \tilde{z}_1^1| \\
&\longrightarrow 0
\end{aligned}
$$

as $M \longrightarrow \infty$. Thus, for $M \gg 1$, $||(L_U - \tilde{\lambda}_1^U I)\tilde{z}_1|| \approx 0$, and we find that $\tilde{z}_1$ is "almost" an eigenvector of L_U corresponding to the approximate eigenvalue $\tilde{\lambda}_1^U$. □

We now wish to identify which of the c_k compartments empty at the rate determined by the second approximate eigenvalue, $\tilde{\lambda}_1^U$. As it turns out, the eigenvector $\tilde{z}_1$ corresponding to this eigenvalue is "nearly" constant, and thus all compartments empty at essentially the same rate. We see this by identifying that even though we are only concerned with a finite number (M) of terms of the sequence generated by the recurrence relation in Eq. 3.31, as the index M becomes infinitely large, the sequence $\{z_1^i\}_{i=1}^M$ exhibits "Cauchy-like" behavior, mimicking "convergence" to a limiting value. We make

this more precise in the following Proposition:

Proposition 3.4.3. *Let $\tilde{z}_1$ be an approximate eigenvector of L_U corresponding to approximate eigenvalue $\tilde{\lambda}_1^U$, where $\tilde{z}_1$ is generated by the recurrence relation in Eq. 3.31. Then at large M, the components of $\tilde{z}_1$ exhibit "Cauchy-like" behavior: for any $\varepsilon > 0$ and $0 < c < 1$, we may choose $M \in \mathbf{N}$ such that $|\tilde{z}_1^m - \tilde{z}_1^n| < \varepsilon$ for all $cM \leq m \leq M$ and $cM \leq n \leq M$.*

Proof. Recalling the bound on $|\tilde{z}_1^{i+2} - \tilde{z}_1^{i+1}|$ obtained in Eq. 3.32, we find,

$$
\begin{aligned}
|\tilde{z}_1^m - \tilde{z}_1^n| &= \left| \sum_{i=n}^{m-1} \left(\tilde{z}_1^{i+1} - \tilde{z}_1^i \right) \right| \\
&\leq \sum_{i=n}^{m-1} |\tilde{z}_1^{i+1} - \tilde{z}_1^i| \\
&= \sum_{i=n}^{m-1} \left(\frac{M-1}{M-i} \right) \left(\frac{M}{M-(i-1)} \right) \left(\frac{\mu(0)}{p(0)} \right)^{i-1} |\tilde{z}_1^2 - \tilde{z}_1^1| \\
&\leq M(M-1)|\tilde{z}_1^2 - \tilde{z}_1^1| \sum_{i=n}^{m-1} \left(\frac{\mu(0)}{p(0)} \right)^{i-1} \\
&= M(M-1)|\tilde{z}_1^2 - \tilde{z}_1^1| \left(\frac{\mu(0)}{p(0)} \right)^{n-1} \left(\sum_{j=0}^{m-n-1} \left(\frac{\mu(0)}{p(0)} \right)^{j} \right) \\
&= M(M-1)|\tilde{z}_1^2 - \tilde{z}_1^1| \left(\frac{\mu(0)}{p(0)} \right)^{n-1} \left(\frac{1 - \left(\frac{\mu(0)}{p(0)} \right)^{m-n}}{1 - \frac{\mu(0)}{p(0)}} \right) \\
&\leq \frac{M(M-1)|\tilde{z}_1^2 - \tilde{z}_1^1|}{\left(1 - \frac{\mu(0)}{p(0)} \right)} \left(\frac{\mu(0)}{p(0)} \right)^{n-1} \\
&= \frac{|\tilde{z}_1^2 - \tilde{z}_1^1| \left(\frac{\mu(0)}{p(0)} \right)^{-1}}{\left(1 - \frac{\mu(0)}{p(0)} \right)} \left[M(M-1) \left(\frac{\mu(0)}{p(0)} \right)^{n} \right] \\
&\leq \frac{|\tilde{z}_1^2 - \tilde{z}_1^1| \left(\frac{\mu(0)}{p(0)} \right)^{-1}}{\left(1 - \frac{\mu(0)}{p(0)} \right)} \left[M(M-1) \left(\frac{\mu(0)}{p(0)} \right)^{cM} \right]
\end{aligned}
$$

Recalling that $M(M-1)\left(\frac{\mu(0)}{p(0)}\right)^{cM} \longrightarrow 0$ as $M \longrightarrow \infty$, we may choose M large enough that,

$$M(M-1)\left(\frac{\mu(0)}{p(0)}\right)^{cM} \leq \varepsilon \left(\frac{|\tilde{z}_1^2 - \tilde{z}_1^1| \left(\frac{\mu(0)}{p(0)}\right)^{-1}}{\left(1 - \frac{\mu(0)}{p(0)}\right)} \right)^{-1}, \tag{3.33}$$

allowing us to conclude that $|\tilde{z}_1^m - \tilde{z}_1^n| < \varepsilon$ for all $M \geq m, n \geq cM$. □

By taking $0 < c, \varepsilon \ll 1$, we find that "most" components of $\tilde{z}_1$ are within an ε-distance of each other, so that the eigenvector is nearly constant. (The constancy breaks down at the components representing large-k compartments.) With this, we are able to classify the rates at which clones of all sizes are lost from the pool. As the eigenvector corresponding to the second smallest magnitude eigenvalue, $\lambda_1^A \approx \tilde{\lambda}_1^A$, is nearly constant, all clones except the very largest mentioned previously are lost from the pool at nearly the same rate, on a time scale $\sim |\mu(0) - p(0)|^{-1}$.

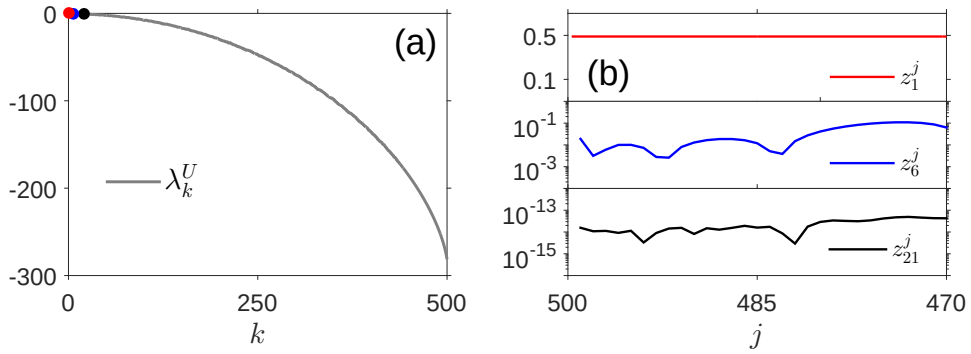

Figure 3.4: **Eigenvalues and eigenvectors of $L_{\tilde{S}}$, $\gamma = 0$** (a) Numerically computed eigenvalue spectrum of the matrix L_U, with $p(N^*) = 0.17$, $\mu(N^*) = 0.12$, and $M = 500$. Dots identify the locations of the eigenvalues λ_1^U (red), λ_6^U (blue), λ_{21}^U (black). (b) First 30 components $(z_k^{500}, \cdots, z_k^{470})$ of the eigenvectors with indices $k = 1, 6, 21$, the eigenvalues corresponding to which are marked on the spectral curve in (a). (Note that the eigenvectors were defined in a "reverse-order", so that z_k^{500} corresponds to compartment c_1, z_k^{495} to compartment c_6, and z_k^{480} to compartment c_{21} (generally: z_k^{M-j+1} corresponds to compartment c_j).

The remaining eigenvalues $\lambda_2^U, \cdots, \lambda_{M-1}^U$ are not treated analytically, but numerical computation indicates that a similar general approximation to the k-th eigenvalue, $\tilde{\lambda}_k^U$, may be made, taking the form $\tilde{\lambda}_k^U = k(\mu(0) - p(0))$. The true eigenvalues, λ_k^U, are depicted in Fig. 3.4(a) (Comparison of the true and approximate spectra is omitted, as the result is similar to that depicted in Fig. 3.1(c). That is, $\lambda_k^U \approx k(\mu(0) - p(0))$ if

$k \lesssim (0.1)M$.). The oscillatory behavior observed in the approximate eigenvectors in the case $p(N^*) < \mu(N^*)$ of section 3.3 is absent here; although the subsequent approximate eigenvectors $\tilde{z}_2, \cdots, \tilde{z}_{M-1}$ do not share the Cauchy-like behavior of $\tilde{z}_1$, the components corresponding to c_k for small k do not vary much in magnitude, and are thus interpreted as being nearly constant themselves (Fig. 3.4(b).) Thus, we conclude that for small k, the functions c_k all have quite similar dynamics, essentially converging at the rate $|\mu(0) - p(0)|$, while for large k, the c_k converge very slowly, at a rate governed by the dominant, near-zero eigenvalue λ_0^U.

We now consider the stable equilibrium solution, $c_k^* = 0$ for $k \geq 1$, $N^* = \tilde{N} > 0$. In this case, the linearization around this equilibrium may be expressed as $p(N^*)L_{U'}$, where $L_{U'} = (u'_{ij})_{1 \leq i,j \leq M+1}$ is the $(M+1) \times (M+1)$ matrix with component u'_{ij} given by,

$$\left\{ \begin{array}{ll} -2j, & \text{if } i = j \leq M-1 \\ -M, & \text{if } i = j = M \\ j, & \text{if } i = j-1;\ 2 \leq j \leq M \\ j, & \text{if } i = j+1;\ 1 \leq j \leq M-1 \\ \frac{p'(N^*)N^* + p(N^*) - \mu'(N^*)N^* - \mu(N^*)}{p(N^*)}, & \text{if } i = j = M+1 \\ 0. & \text{otherwise} \end{array} \right\} \tag{3.34}$$

For reference, an example of the matrix $L_{U'}$, with $M = 4$, is given below:

$$\begin{pmatrix} -2 & 2 & 0 & 0 & 0 \\ 1 & -4 & 3 & 0 & 0 \\ 0 & 2 & -6 & 4 & 0 \\ 0 & 0 & 3 & -4 & 0 \\ 0 & 0 & 0 & 0 & \frac{p'(N^*)N^*+p(N^*)-\mu'(N^*)N^*-\mu(N^*)}{p(N^*)} \end{pmatrix} \tag{3.35}$$

Denote by $\lambda_k^{U'}$ for $k = 1, 2, \cdots, M, M+1$ the eigenvalues of the matrix $L_{U'}$ evaluated at the stable equilibrium solution, and $x_k = (x_k^1, x_k^2, \cdots, x_k^M, x_k^{M+1})$ their corresponding eigenvectors. As before, let $\lambda_{M+1}^{U'} = \frac{p'(N^*)N^*+p(N^*)-\mu'(N^*)N^*-\mu(N^*)}{p(N^*)} < 0$. Then the remaining eigenvalues $\lambda_1^{U'}, \cdots, \lambda_M^{U'}$ are those of the $(M+1) \times (M+1)$ minor of $L_{U'}$, which are independent of the parameters of the system except M. (Of course, the eigenvalues of $p(N^*)L_{U'}$ are then $p(N^*)\lambda_k^{U'}$ for $k = 1, \cdots, M+1$.) These eigenvalues and eigenvectors are not treated analytically. The analysis conducted in section 3.3 does not apply, as it relied on the assumption $p(N^*) < \mu(N^*)$, which no longer holds. However, numerical computation indicates that in the case $p(N^*) = \mu(N^*)$, which applies here, the eigenvalue spectrum and associated eigenvectors qualitatively resemble the λ_k^S, y_k studied analytically in section 3.3. Thus, the convergence of solutions $c_k^i(t), N^i(t)$ to this stable equilibrium is similar to that of solutions to the stable equilibrium that arises when $\gamma > 0$: for small k, c_k converges at the rate given by the dominant eigenvalue, and for larger k, c_k converges at a rate much faster than that given by the dominant eigenvalue.

3.4.3 Behavior of the Linearized and Fully Nonlinear Systems

We now interpret these results in the context of the particular diseased states to which they naturally apply. We first identified an unstable equilibrium solution, $c_k^* = 0$, $N^* = 0$, and studied the linearization of the system around this equilibrium. Under the linearized model, if $\gamma_i = 0$ for some i, the eigenvalue/eigenvectors pairs suggest that solutions

diverge away from this equilibrium, with c_k^i for small k evolving at a rate $\sim \lambda_1^U = (\mu(0) - p(0))$, and c_k^i for $k \sim M$ evolving at the very slow rate given by the small-magnitude eigenvalue, λ_0^U. $N^i(t)$ evolves at the rate $(p(0) - \mu(0))$. This situation represents the start of the repopulation of the T-cell pool from a small number of existent cells via peripheral proliferation in a highly pathological state involving both complete thymic inactivity (e.g. thymectomy or total functional cessation) and near full lymphopenia (as may result from treatment regimens for cancer, etc.). We then identified a stable equilibrium solution, $c_k^* = 0$, $N^* = \tilde{N} > 0$. As $\tilde{N}$ is asymptotically stable, $N^i(t) \to \tilde{N}$ after diverging from $N^* = 0$. Under the linearized model, the eigenvalue/eigenvector pairs predict that $c_k^i(t) \to 0$ slowly for small k, and $c_k^i(t) \to 0$ much more quickly for large k. Simply put, when diverging away from the zero state, c_k travels quickly for small k and very slowly for large k, and when converging towards the stable equilibrium, c_k travels quickly for large k and slowly for small k.

As before, the validity of the eigenvalues in providing accurate convergence rates of c_k^i, N^i to and from equilibria depends on the initial condition $c_k^i(t_i)$ in the full nonlinear model. If the human is in a state of immune health for $t < t_i$, so that $\gamma_{i-1} > 0$ and the initial conditions $c_k^i(t_i), N^i(t_i) > 0$ satisfy $c_k^i(t_i) \sim c_k^*(\gamma_{i-1})$, $N^i(t_i) \sim N^*(\gamma_{i-1})$, we expect that $p(N^i(t_i)) < \mu(N^i(t_i))$. The higher rate of death than proliferation at t_i may cause a transient period of quick collapse, with $N^i(t)$ decreasing to $\tilde{N}$. As $N^i(t) \to \tilde{N}$, convergence occurs at the rates dictated by the linearized eigenvalues. If $\gamma_{i-1} > 0$ but $c_k^i(t_i), N^i(t_i) \sim 0$, so that the thymus is functioning to some extent but the T-cell pool has been eradicated, trajectories first diverge away from the unstable zero equilibrium at rates given by the linearized eigenvalues. As $p(N^i(t_i)) - \mu(N^i(t_i)) \to p(\tilde{N}) - \mu(\tilde{N}) = 0$, the motion of trajectories transitions from being dictated by the eigenvalues of the unstable equilibrium to those of the stable equilibrium.

3.5 Special Cases and Simulations

Using the approximate rates of convergence provided by linearization, we can now study the time scale of the T-cell pool's adjustment to a new export rate. While some T-cell clones will expand and attain a large size, most are small. Thus, in both the cases of

thymic atrophy and recovery, we take as a proxy for the rate at which the full T-cell pool converges to equilibrium the eigenvalue that dictates the rate of convergence of c_1, typically given by the quantity $p(N^*) - \mu(N^*)$ (this tends to also be the dominant eigenvalue). In this section, we study several specific models arising from canonical choices of p and μ, and compute the changing convergence rate as gamma varies.

3.5.1 The Logistic Model

We begin with the canonical logistic growth model, taking $p(N) = p_0(1 - N/K)$, $\mu(N) = \mu_0$, where $p_0, \mu_0 > 0$ are basal rates of cellular proliferation and death, respectively, and $K > 0$ is an inherent carrying capacity. Under this model, Eq. 3.1 has a positive steady state, N^*, given by,

$$N^* = \left(\frac{K}{2p_0}\right)\left((p_0 - \mu_0) + \sqrt{(p_0 - \mu_0)^2 + \frac{4\gamma p_0}{K}}\right). \tag{3.36}$$

In this case, $p(N^*) - \mu(N^*) = p_0\left(1 - \frac{N^*}{K}\right) - \mu_0 = \left(\frac{1}{2}\right)\left((p_0 - \mu_0) - \sqrt{(p_0 - \mu_0)^2 + \frac{4\gamma p_0}{K}}\right) < 0$, so that the assumption $p(N^*) < \mu(N^*)$ always applies. Moreover, $\tilde{\lambda}^S_{M+1} = -\sqrt{(p_0 - \mu_0)^2 + \frac{4\gamma p_0}{K}}$, so it is clear that $0 > \tilde{\lambda}^S_1 > \tilde{\lambda}^S_{M+1}$, and $\tilde{\lambda}^S_1$ is the dominant eigenvalue. Then,

$$|p(N^*) - \mu(N^*)| = \left(\frac{1}{2}\right)\left(-(p_0 - \mu_0) + \sqrt{(p_0 - \mu_0)^2 + \frac{4\gamma p_0}{K}}\right). \tag{3.37}$$

In Fig. 3.5, the quantity $\tilde{\lambda}^S_1$ is plotted against γ for several different combinations of p_0, μ_0, showing the unboundedness of the convergence rate as γ increases. Within this physiological range of γ values, the dependence of $\tilde{\lambda}^S_1$ on γ presents as linear on a loglog plot, indicating a power law relationship. Indeed, the power law is described in detail in the caption of Fig. 3.5.

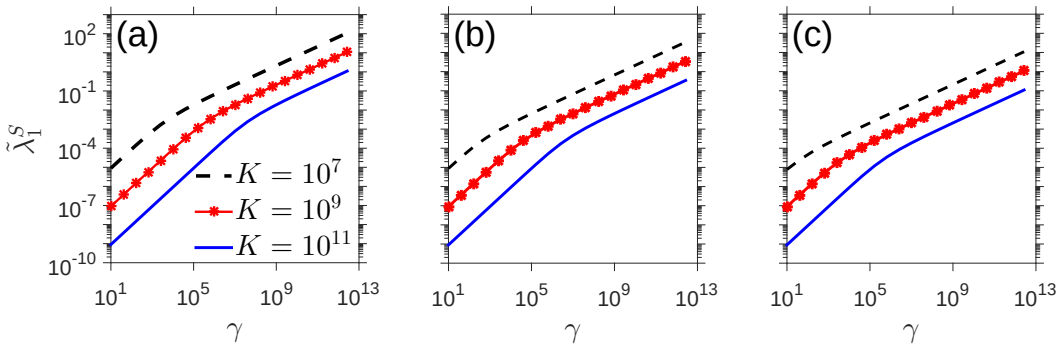

Figure 3.5: **Dominant eigenvalue, $\tilde{\lambda}_1^S$, of $L_{\tilde{S}}$, plotted against γ, Case 1** In (a), $p_0 = 0.18$, $\mu_0 = 0.17$. In (b), $p_0 = 0.018$, $\mu_0 = 0.017$. In (c), $p_0 = 0.0018$, $\mu_0 = 0.0017$. There is an approximate power law relationship between $\tilde{\lambda}_1^S$ and γ within this range of parameter values. In (A), for example, the best fit line to the curve $K = 10^7$ is given by $\log(\tilde{\lambda}_1^S) = (2.673 \times 10^{-11}) \log(\gamma) + 5.594$, with $R^2 = 0.8904$. The curve $K = 10^9$ is fitted by $\log(\tilde{\lambda}_1^S) = (2.672 \times 10^{-12}) \log(\gamma) + 0.558$, with $R^2 = 0.8905$, and the curve $K = 10^{11}$ is fitted by $\log(\tilde{\lambda}_1^S) = (2.67 \times 10^{-13}) \log(\gamma) + 0.05478$, with $R^2 = 0.8911$.

3.5.2 Constant Proliferation, Varying Death

Let us now assume that $p(N) = p_0 > 0$ and $\mu(N) = \mu_0 + \frac{\mu_1 N^2}{K^2+N^2}$, with $\mu_0, \mu_1 > 0$, in the ODEs given by Eqs. 3.1-3.4. (This form was used in Chapter 2.) We make the assumptions that $p_0 > \mu_0$ and $p_0 - (\mu_0 + \mu_1) < 0$, so that the action of the proliferation-death mechanism results in net cellular birth at low cell counts and net cellular death at high cell counts. Explicitly, Eq. 3.1 has the form,

$$\frac{\mathrm{d}N}{\mathrm{d}t} = \gamma + p_0 N - \left(\mu_0 + \mu_1 \left(\frac{N^2}{K^2 + N^2}\right)\right) N. \tag{3.38}$$

The steady states of this ODE are given by the roots of the following cubic, which we denote by $c(N)$,

$$c(N) = (p_0 - (\mu_0 + \mu_1))\, N^3 + \gamma_0 N^2 + (p_0 - \mu_0) K^2 N + \gamma K^2. \tag{3.39}$$

Note first that $c(0) = \gamma K^2 > 0$, and the highest order coefficient satisfies $(p_0 - (\mu_0 + \mu_1)) < 0$ by assumption, so that $c(N) \longrightarrow -\infty$ as $N \longrightarrow \infty$, and $c(N)$ has at least one positive,

real root. From Descartes' rules of signs, the polynomial has at most one positive real root, so we may conclude that it has precisely one positive real root. This root corresponds to the only physically relevant stable fixed point of $\frac{\mathrm{d}N}{\mathrm{d}t}$. By regarding this root, N^*, as the intersection of the line $\gamma + (p_0 - \mu_0)N$ and the rational expression $\mu_1\left(\frac{N^3}{K^2+N^2}\right)$, we see that $N^* \to \infty$ as $\gamma \to 0$.

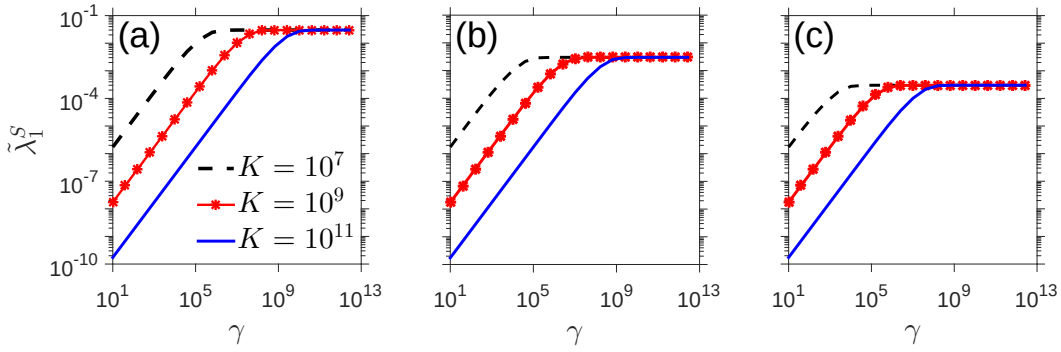

Figure 3.6: **Dominant eigenvalue, $\tilde{\lambda}_1^S$, of $L_{\tilde{S}}$, plotted against γ, Case 2.** In (a), $p_0 = 0.18$, $\mu_0 = 0.17$, and $\mu_1 = 0.004$. In (b), $p_0 = 0.018$, $\mu_0 = 0.017$, and $\mu_1 = 0.004$. In (c), $p_0 = 0.0018$, $\mu_0 = 0.0017$, and $\mu_1 = 0.0004$. The relationship between $\tilde{\lambda}_1^S$ and γ follows a power law for low values of γ, before reaching a plateau for high values of γ. In (A), the best fit line to the curve $K = 10^7$ over the power law region ($\sim \gamma \in [10^1, 2.2\times10^4]$) is given by $\log(\tilde{\lambda}_1^S) = (1.492 \times 10^{-7})\log(\gamma) + 1.972 \times 10^{-5}$, with $R^2 = 0.9979$. The curve $K = 10^9$ over the power law region ($\sim \gamma \in [10^1, 2.1 \times 10^6]$) is fitted by $\log(\tilde{\lambda}_1^S) = (1.505 \times 10^{-9})\log(\gamma) + 1.039 \times 10^{-5}$, with $R^2 = 0.998$, and the curve $K = 10^{11}$ over the power law region ($\sim \gamma \in [10^1, 2.2 \times 10^8]$) is fitted by $\log(\tilde{\lambda}_1^S) = (1.502 \times 10^{-11})\log(\gamma) + 7.6 \times 10^{-6}$, with $R^2 = 0.998$.

We also verify that the eigenvalues $\tilde{\lambda}_1^S, \tilde{\lambda}_{M+1}^S$ satisfy $0 > \tilde{\lambda}_1^S > \tilde{\lambda}_{M+1}^S$, so that $\tilde{\lambda}_1^S$ is, in fact, the dominant eigenvalue. We first check that $0 > \tilde{\lambda}_1^S$. Recalling that $\tilde{\lambda}_1^S = p(N^*) - \mu(N^*) = p_0 - \left(\mu_0 + \mu_1\left(\frac{(N^*)^2}{(K^2+(N^*)^2)}\right)\right)$, we see after some simple algebraic manipulation that the condition $\tilde{\lambda}_1^S < 0$ is equivalent to

$$N^* > \left(\frac{(p_0 - \mu_0)K^2}{|p_0 - (\mu_0 + \mu_1)|}\right)^{\frac{1}{2}} := \overline{N}. \tag{3.40}$$

But $c(\overline{N}) = \frac{\gamma(p_0-\mu_0)K^2}{|p_0-(\mu_0+\mu_1)|} + \gamma K^2 > 0$. That $c(\overline{N}) > 0$ and $c(N) \longrightarrow -\infty$ as $N \longrightarrow \infty$, along with the fact that $c(N)$ has only one real positive root indicates that N^* does, in fact, satisfy Cond. 3.40, so that $\tilde{\lambda}_1^S < 0$. It is easily verified that $-\mu'(N^*)N^* < 0$, and consequently that $\tilde{\lambda}_1^S > \tilde{\lambda}_{M+1}^S$.

From the fact that $N^* \to \infty$ as $\gamma \to \infty$, we have that $|p(N^*) - \mu(N^*)| \to p_0 - (\mu_0 + \mu_1)$ as $\gamma \to \infty$. This limiting behavior is reflected in the eventual plateau seen in Fig. 3.6, which plots the quantity $\tilde{\lambda}_1^S$ in this case. Before the plateau occurs, γ and $\tilde{\lambda}_1^S$ are again related by a power law. The transition from power law to plateau occurs at a "threshold" value, γ^*, of γ, at which the rate of T-cell adjustment becomes sensitive to a changing thymic export rate. If, for some i, $\gamma_{i-1}, \gamma_i \geq \gamma^*$, $\tilde{\lambda}_1^S$ is unaffected by the transition from thymic export rate γ_{i-1} to thymic export rate γ_i–that is, the T-cell pool adjusts to the new thymic export rate γ_i as quickly as it had adjusted to the previous thymic export rate γ_{i-1}. If, however, $(\gamma_i - \gamma^*)(\gamma_{i-1} - \gamma^*) < 0$, then a dramatic shift in the adjustment rate will occur. Thus, parameter choices that result in a low threshold value γ^* might correspond to physiological conditions under which an instance of acute thymic atrophy actually does not affect T-cell adjustment rates. Likewise, a high threshold value of γ^* indicates potential sensitivity of adjustment rates to the changing level of thymic export, with adjustment rates obeying a power law dependence on γ.

3.5.3 Regulation of Proliferation and Death

We conclude with an example in which both peripheral proliferation and death are subject to homeostatic regulation. We adapt forms used by Murray *et al.* in [MKH03], taking $p(N) = p_0 K/(K+N)$ and $\mu(N) = \mu_0(1+\mu_1 N/(K+N))$. The constants $p_0, \mu_0, \mu_1, K > 0$ play the same fundamental roles as in the previous examples. The positive equilibrium solution of Eq. 3.1 under this assumption is given by,

$$N^* = \frac{\gamma + (p_0 - \mu_0)K + \sqrt{(\gamma + (p_0 - \mu_0)K)^2 + 4\mu_0(1+\mu_1)\gamma K}}{2\mu_0(1+\mu_1)}, \tag{3.41}$$

which leads to a dominant eigenvalue $\tilde{\lambda}_1^S$ given by,

$$\tilde{\lambda}_1^S = p(N^*) - \mu(N^*) \tag{3.42}$$

$$= \left[\frac{\mu_0(1+\mu_1)\left(-\gamma + (p_0-\mu_0)K - \sqrt{(\gamma+(p_0-\mu_0)K)^2 + 4\mu_0(1+\mu_1)\gamma K}\right)}{(p_0+\mu_0)K + 2\mu_0\mu_1 K + \gamma + \sqrt{(\gamma+(p_0-\mu_0)K)^2 + 4\mu_0(1+\mu_1)\gamma K}} \right]. \tag{3.43}$$

It is easily verified that $p'(N^*)N^* - \mu'(N^*)N^* < 0$ so that $0 > \tilde{\lambda}_1^S > \tilde{\lambda}_{M+1}^S$, so that $\tilde{\lambda}_1^S$ is, in fact, the dominant eigenvalue. The relationship between γ and $\tilde{\lambda}_1^S$ depicted in Fig. 3.7 is similar to that in Fig. 3.6.

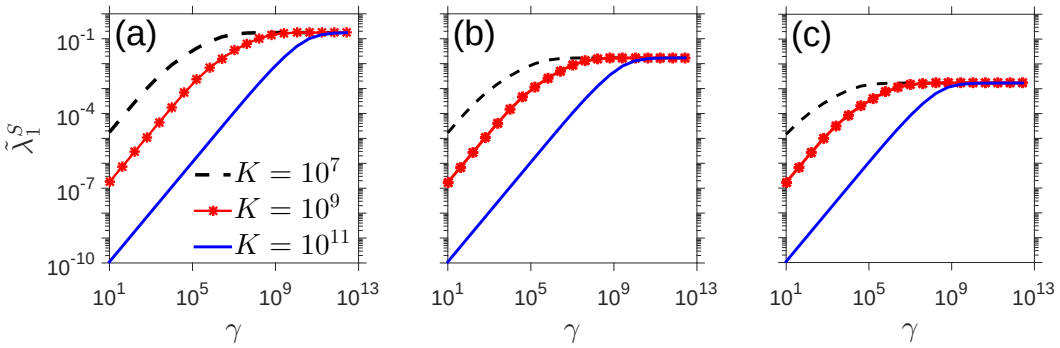

Figure 3.7: **Dominant eigenvalue, $\tilde{\lambda}_1^S$, of $L_{\tilde{S}}$, plotted against γ, case 3** In (a), $p_0 = 0.18$, $\mu_0 = 0.17$, and $\mu_1 = 0.004$. In (b), $p_0 = 0.018$, $\mu_0 = 0.017$, and $\mu_1 = 0.004$. In (c), $p_0 = 0.0018$, $\mu_0 = 0.0017$, and $\mu_1 = 0.0004$. In this case, the power law relationship from Fig. 3.5 and the power law/plateau relationship from Fig. 3.6 break down somewhat, although the qualitative appearance of the curves resembles those of Fig. 3.6.

3.6 Discussion and Conclusions

In this chapter, we formulated a model of how the naive T-cell pool adjusts to changes in the rate of thymic export of new T-cells during a cycle of stress-induced atrophy and recovery, and how it may be reconstituted following an instance of severe lymphopenia induced by a state of immune disease, or treatments such as chemotherapy. In section 3.3, we found that our ODE system admitted one stable equilibrium solution when $\gamma > 0$. From an analysis of the eigenvalues and eigenvectors of the system linearized around this stable equilibrium, we found that for small k, c_k converges to equilibrium at a rate

given by the dominant eigenvalue, $\lambda_1^S = (p(N^*) - \mu(N^*))$. For larger k, c_k converges to equilibrium much faster than $k(p(N^*) - \mu(N^*))$. In section 3.4, we found that the system admits one unstable and one stable equilibrium solution when $\gamma = 0$, so that other solutions converge away from the unstable and towards the stable solution. From a similar eigenvalue and eigenvector analysis, we find that the largest clones move away from the unstable solution very slowly, at a rate given by the near-zero eigenvalue, while the smaller clones tend to travel at the same speed, given predominantly by the eigenvalue $\lambda_1^U = (\mu(0) - p(0))$.

In section 3.5, we take the dominant eigenvalue that arises when $\gamma > 0$ as a proxy for the rate of convergence of the smallest (most common, significant) clones to equilibrium. We compute the dominant eigenvalue as a function of γ for three choices of the functions $p(N), \mu(N)$. In section 3.5.1, we test the logistic model, which assumes a constant rate of proliferation and an N-dependent death rate. From the explicit form of $\tilde{\lambda}_1^S$ in Eq. 3.37, $p(N^*) - \mu(N^*) \to \infty$ as $\gamma \to \infty$ for fixed values of the other parameters, which produces the power-law relationship between γ and $\tilde{\lambda}_1^S$ depicted in Fig. 3.5. In section 3.5.2, we assume a constant rate of cellular proliferation with an N-dependent death rate, and in section 3.5.3, we test a formulation with N-dependent rates of both cellular proliferation and death. In both of these formulations, which differ from the logistic formulation in that regulation is incorporated into $p(N), \mu(N)$ via Hill functions, γ and $\tilde{\lambda}_1^S$ are related by a power law for low γ, before reaching a plateau at higher γ. As the latter formulations are typically used in realistic representations of homeostatic mechanisms, we expect these to be more physiological than the logistic case. That is, jumps in the thymic export rate that either cross the threshold value of γ, or occur between two values of γ both in the power-law region, can be expected to produce changes in both the equilibrium values of c_k and also the convergence rates. If a jump in γ occurs between two values of γ that are both in the plateau region, the equilibrium values shift, but the convergence rates stay the same.

3.7 Appendix: Solution of Recurrence Relation

We verify that Expression 3.21, which we remind the reader was given explicitly by,

$$y_k^i = \sum_{n=1}^{k} \frac{\left[\prod_{j=1}^{n-1}(i-j)\right]\left[\prod_{j=1}^{k-n}(i+j)\right]}{k(-1)^{n-1}(n-1)!(k-n)!}\left(\frac{p(N^*)}{\mu(N^*)}\right)^{i-n}, \tag{3.44}$$

is the solution to Relation 3.20, given by,

$$iy_k^i = \left[(i+(k-1))\left(\frac{p(N^*)}{\mu(N^*)}\right) + (i-(k+1))\right] y_k^{i-1} - [i-2]\left(\frac{p(N^*)}{\mu(N^*)}\right) y_k^{i-2}. \tag{3.45}$$

In what follows, we write $p(N^*)$ as p, and $\mu(N^*)$ as μ for simplicity. Inserting Expression 3.21 into the right side of Relation 3.20, we have,

$$\left[(i+(k-1))\left(\frac{p}{\mu}\right)+(i-(k+1))\right]y_k^{i-1}-[i-2]\left(\frac{p}{\mu}\right)y_k^{i-2}$$

$$=\left[\frac{(i+(k-1))}{i}\left(\frac{p}{\mu}\right)+\frac{i-(k+1)}{i}\right]\left[\left[\left(\prod_{j=1}^{k-1}(i-1+j)\right)\frac{\left(\frac{p}{\mu}\right)^{i-2}}{k!}\right]+\left[\sum_{n=2}^{k-1}\frac{\left[\prod_{m=1}^{n-1}(i-1-m)\right]\left[\prod_{j=1}^{k-n}(i-1+j)\right]\left(\frac{p}{\mu}\right)^{i-1-n}}{(-1)^{n-1}(n-1)!k(k-n)!}\right]+\left[\left[\prod_{j=1}^{k-1}(i-1-j)\right]\frac{\left(\frac{p}{\mu}\right)^{i-1-k}}{(-1)^{k-1}k!}\right]\right]$$

$$-\left(\frac{p}{\mu}\right)\left(\frac{i-2}{i}\right)\left[\left(\prod_{j=1}^{k-1}(i-2-j)\right)\frac{\left(\frac{p}{\mu}\right)}{k!}+\sum_{n=2}^{k-1}\left[\prod_{m=1}^{n-1}(i-2-m)\right]\left[\prod_{j=1}^{k-n}(i-2+j)\right]\frac{\left(\frac{p}{\mu}\right)}{(-1)^{n-1}(n-1)!k(k-n)!}+\left[\prod_{j=1}^{k-1}(i-2-j)\right]\frac{\left(\frac{p}{\mu}\right)^{i-2-k}}{(-1)^{k-1}k!}\right]$$

$$=\left[\prod_{j=0}^{k-1}(i+j)\right]\frac{\left(\frac{p}{\mu}\right)^{i-1}}{k!}+\left[\frac{(i-(k+1))}{k!}\left[\prod_{j=1}^{k-1}(i-1+j)\right]-\frac{(i+(k-1))}{k(k-2)!}\left[\prod_{j=1}^{k-2}(i-1+j)\right]-\frac{(i-2)}{k!}\left[\prod_{j=1}^{k-1}(i-2+j)\right]\right]\left(\frac{p}{\mu}\right)^{i-2}$$

$$+\sum_{n=2}^{k-1}(i-(k+1))\left[\prod_{j=1}^{n-1}(i-1-j)\right]\left[\prod_{j=1}^{k-n}(i-1+j)\right]\frac{\left(\frac{p}{\mu}\right)^{i-1-n}}{(-1)^{n-1}(n-1)!k(k-n)!}+\sum_{n=3}^{k-1}(i+(k-1))\left[\prod_{j=1}^{n-1}(i-1-j)\right]\left[\prod_{j=1}^{k-n}(i-1+j)\right]\frac{\left(\frac{p}{\mu}\right)^{i-n}}{(-1)^{n-1}(n-1)!k(k-n)!}$$

$$+(i+(k-1))\left[\prod_{j=1}^{k-1}(i-1-j)\right]\left[\frac{\left(\frac{p}{\mu}\right)^{i-k}}{(-1)^{k-1}k!}\right]+(i-(k+1))\left[\prod_{j=1}^{k-1}(i-1-j)\right]\frac{\left(\frac{p}{\mu}\right)^{i-1-k}}{(-1)^{k-1}k!}$$

$$-\sum_{n=2}^{k-1}(i-2)\left[\prod_{m=1}^{n-1}(i-2-m)\right]\left[\prod_{j=1}^{k-n}(i-2+j)\right]\frac{\left(\frac{p}{\mu}\right)^{i-1-n}}{(-1)^{n-1}(n-1)!k(k-n)!}-(i-2)\left[\prod_{j=1}^{k-1}(i-2-j)\right]\frac{\left(\frac{p}{\mu}\right)^{i-1-k}}{(-1)^{k-1}k!}$$

$$= \left[\prod_{j=0}^{k-1}(i+j)\right]\frac{\left(\frac{p}{\mu}\right)^{i-1}}{k!} + \left(\frac{p}{\mu}\right)^{i-2}\left[\prod_{j=0}^{k-3}(i+j)\right]\left[\frac{(i+(k-2))(i-(k+1))-(k-1)(i-2)(i+(k-1))-(i-2)(i-1)}{k!}\right]$$

$$+\sum_{s=3}^{k-1}\left(\left[\prod_{j=1}^{s-1}(i-1-j)\right]\left[\prod_{j=1}^{k-s}(i-1+j)\right]\frac{(i+(k-1))}{(-1)^{s-1}(s-1)!k(k-s)!} + \left[\prod_{j=1}^{s-2}(i-1-j)\right]\left[\prod_{j=1}^{k-(s-1)}(i-1+j)\right]\frac{(i-(k+1))}{(-1)^{s-2}(s-2)!k(k-(s-1))!} - (i-2)\left[\prod_{j=1}^{s-2}(i-2-j)\right]\left[\prod_{j=1}^{k-(s-1)}(i-2+j)\right]\frac{1}{(-1)^{s-2}(s-2)!k(k-(s-1))!}\right)\left(\frac{p}{\mu}\right)^{i-s}$$

$$+\left((i-(k+1))\left[\prod_{j=1}^{k-2}(i-1-j)\right]\frac{i}{(-1)^{k-2}(k-2)!k} + (i+(k-1))\left[\prod_{j=1}^{k-1}(i-1-j)\right]\frac{1}{k!} - (i-2)\left[\prod_{j=1}^{k-2}(i-2-j)\right]\frac{(i-1)}{(-1)^{k-2}(k-2)!k}\right)\left(\frac{p}{\mu}\right)^{i-k}$$

$$= \left[\prod_{j=0}^{k-1}(i+j)\right]\frac{\left(\frac{p}{\mu}\right)^{i-1}}{k!} + \left[\prod_{j=0}^{k-3}(i+j)\right]\left[\frac{-(k-1)i^2-(k-1)(k-3)i+(k-2)(k-1)}{k!}\right]\left(\frac{p}{\mu}\right)^{i-2}$$

$$+\sum_{s=3}^{k-1}(-1)^{-s}\left[\prod_{j=2}^{s-1}(i-j)\right]\left[\prod_{j=0}^{k-(s+1)}(i+j)\right]\left[\frac{-(i-s)(i+(k-1))}{(s-1)!k(k-s)!} + \frac{(i-(k+1))(i+(k-s))}{(s-2)!k(k-(s-1))!} - \frac{(i-1)(i-s)}{(s-2)!k(k-(s-1))!}\right]\left(\frac{p}{\mu}\right)^{i-s}$$

$$+\left(\frac{(i+(k-1))}{(-1)^{k-1}k!}\left[\prod_{j=1}^{k-1}(i-1-j)\right] + \frac{(i-(k+1))\left[\prod_{j=1}^{k-2}(i-1-j)\right]i}{(-1)^{k-2}(k-2)!k} - \frac{(i-2)(i-1)\left[\prod_{j=1}^{k-2}(i-2-j)\right]}{(-1)^{k-2}(k-2)!k}\right)\left(\frac{p}{\mu}\right)^{i-k}$$

$$= \left[\prod_{j=0}^{k-1}(i+j)\right]\frac{\left(\frac{p}{\mu}\right)^{i-1}}{k!} + \left[\prod_{j=0}^{k-3}(i+j)\right]\left[\frac{-i^2-(k-3)i+(k-2)}{k(k-2)!}\right]\left(\frac{p}{\mu}\right)^{i-2}$$

$$+\sum_{s=3}^{k-1}(-1)^{-s}\left[\prod_{j=2}^{s-1}(i-j)\right]\left[\prod_{j=0}^{k-(s+1)}(i+j)\right]\left(\frac{p}{\mu}\right)^{i-s}\left[\frac{-(k-(s-1))(i-s)(i+(k-1))+(s-1)(i-(k+1))(i+(k-s))-(s-1)(i-1)(i-s)}{(s-1)!k(k-(s-1))!}\right]$$

$$+\left(\frac{p}{\mu}\right)^{i-k}(-1)^{-k}\left(\prod_{j=2}^{k-1}(i-j)\right)\left[\frac{-(i+(k-1))(i-k)+(k-1)(i-(k+1))i-(i-1)(i-k)(k-1)}{k!}\right]$$

$$= \left[\prod_{j=0}^{k-1}(i+j)\right]\frac{\left(\frac{p}{\mu}\right)^{i-1}}{k!} - \left[\prod_{j=0}^{k-3}(i+j)\right]\left[\frac{(i+(k-2))(i-1)}{k(k-2)!}\right]\left(\frac{p}{\mu}\right)^{i-2} + (-1)^k\left(\prod_{j=2}^{k-1}(i-j)\right)\left[\frac{-i^2+i}{k!}\right]\left(\frac{p}{\mu}\right)^{i-k}$$

$$+\sum_{s=3}^{k-1}\left[\prod_{j=2}^{s-1}(i-j)\right]\left[\prod_{j=0}^{k-(s+1)}(i+j)\right](-1)^{-s}\left(\frac{p}{\mu}\right)^{i-s}\left[\frac{-(k-(s-1))i^2-(k-(s-1))(k-(s+1))i+(k-s)(k-s+1)}{(s-1)!k(k-(s-1))!}\right]$$

$$= \left[\prod_{j=0}^{k-1}(i+j)\right]\frac{\left(\frac{p}{\mu}\right)^{i-1}}{k!} - \left[\prod_{j=0}^{k-2}(i+j)\right]\frac{(i-1)}{k(k-2)!}\left(\frac{p}{\mu}\right)^{i-2} + (-1)^{-(k-1)}\left(\prod_{j=2}^{k-1}(i-j)\right)\frac{i(i-1)}{k!}\left(\frac{p}{\mu}\right)^{i-k}$$

$$+\sum_{s=3}^{k-1}\left[\prod_{j=2}^{s-1}(i-j)\right]\left[\prod_{j=0}^{k-(s+1)}(i+j)\right]\left[\frac{-i^2-(k-(s+1))i+(k-s)}{(s-1)!k(k-s)!}\right]\frac{\left(\frac{p}{\mu}\right)^{i-s}}{(-1)^s}$$

$$= \left[\prod_{j=0}^{k-1}(i+j)\right]\frac{\left(\frac{p}{\mu}\right)^{i-1}}{k!} - \left[\prod_{j=0}^{k-2}(i+j)\right]\frac{(i-1)}{k(k-2)!}\left(\frac{p}{\mu}\right)^{i-2} + (-1)^{-(k-1)}\left(\prod_{j=0}^{k-1}(i-j)\right)\frac{\left(\frac{p}{\mu}\right)^{i-k}}{k!}$$

$$+\sum_{s=3}^{k-1}\left[\prod_{j=1}^{s-1}(i-j)\right]\left[\prod_{j=0}^{k-s}(i+j)\right]\frac{\left(\frac{p}{\mu}\right)^{i-s}}{(-1)^{s-1}(s-1)!k(k-s)!}$$

$$= \left[\prod_{j=0}^{k-1}(i+j)\right]\frac{\left(\frac{p}{\mu}\right)^{i-1}}{k!} + \sum_{s=2}^{k-1}\left[\prod_{j=1}^{s-1}(i-j)\right]\left[\prod_{j=0}^{k-s}(i+j)\right]\frac{\left(\frac{p}{\mu}\right)^{i-s}}{(-1)^{s-1}(s-1)!k(k-s)!} + \left[\prod_{j=0}^{k-1}(i-j)\right]\frac{\left(\frac{p}{\mu}\right)^{i-k}}{(-1)^{k-1}k!}$$

$$= i\left[\left[\prod_{j=1}^{k-1}(i+j)\right]\frac{\left(\frac{p}{\mu}\right)^{i-1}}{k!} + \sum_{s=2}^{k-1}\left[\prod_{j=1}^{s-1}(i-j)\right]\left[\prod_{j=1}^{k-s}(i+j)\right]\frac{\left(\frac{p}{\mu}\right)^{i-s}}{(-1)^{s-1}(s-1)!k(k-s)!} + \left[\prod_{j=1}^{k-1}(i-j)\right]\frac{\left(\frac{p}{\mu}\right)^{i-k}}{(-1)^{k-1}k!}\right]$$

$$= iy_k^i$$

CHAPTER 4

T-cell Populations During HIV Infection and Treatment

4.1 Introduction

In this section, we formulate a model of HIV infection and treatment with bone marrow transplant therapy. This treatment involves transplanting into an HIV-infected individual bone marrow possessing a natural immunity to the HIV virus. After transplant, the thymus would begin to populate with T-cell precursors descended from these HIV-immune stem cells, which possess the same inherent immunity. After maturing into fully functioning T-cells in the thymus, cells from this lineage would exit the thymus and populate the peripheral bloodstream. Ideally, this treatment would lead to a reconstitution of the peripheral T-cell pool sufficient to adequately limit viral loads and restore immune function. However, bone marrow transplant carries with it a risk of graft versus host disease, with the risk increasing as the amount of transplanted tissue increases. As such, we seek to identify the minimum amount of tissue that can be transplanted and still produce an HIV-immune T-cell pool large enough to limit viral loads and adequately preserve immune health.

To realistically model the course of HIV infection and treatment, we develop a piecewise ODE system that describes the changing populations of infected and uninfected T-cells and virus particles during the three qualitatively different stages of infection and treatment. The first stage (Stage 1) is that of health (before infection with HIV), during which we identify healthy equilibrium counts of T-cell progenitors in the bone marrow, developing T-cells in the thymus, and mature T-cells in the periphery. The second stage (Stage 2) begins at the onset of infection, after which we model the depletion of healthy lymphocytes in the thymus and periphery by, and subsequent immune response to, the

HIV virus. The third and final stage (Stage 3) begins at the start of treatment, when the infected individual's bone marrow is ablated and partially replaced with HIV-immune stem cells. During this stage, we observe the repoulation of the bone marrow, thymus, and periphery with ("protected") cells immune to HIV, along with the adjustment of the viral load and HIV-vulnerable ("unprotected") cell populations to the new cell populations.

4.2 Mathematical Model and Analysis

We begin by considering a simple model that accounts for "free-spread" of the virus–that is, infection of healthy CD4 T-cells by virions passing freely through the blood and lymph system. We assume that the bone marrow, thymus, and secondary lymphoid tissues and peripheral blood operate under a homeostatic mechanism to reestablish equilibrium T-cell counts whenever some type of foreign infection disturbs immune cell levels.

We now introduce notation. Let t denote the independent time variable, and assume that the observation of the population of the immune system with T-cells begins at $t = 0$. Let $t_1 > 0$ denote the time at which HIV infection occurs, so that Stage 1 (as described above) occurs over the time period $[0, t_1]$. Analogously, let $t_2 > t_1$ denote the time at which infection is identified and treatment first administered, so that Stage 2 occurs over the time period $[t_1, t_2]$. Finally, let $t_3 > t_2$ denote the time at which we end our observation of the success of the treatment, so that Stage 3 occurs over the time period $[t_2, t_3]$.

4.2.1 Stage 1: Population of Lymphoid Tissues with T-cells Before HIV Infection

Denote by $x(t)$ the total number of T-cell progenitors in the bone marrow, by $y(t)$ the total number of developing T-cells in the thymus, and by $z(t)$ the total number of mature T-cells in the periphery. The time evolution of these cell populations is given by the following system of ODEs:

$$\begin{cases} \dot{x}(t) = \alpha u + p\left(1 - \dfrac{x}{K_{\mathrm{BM}}}\right) x - \beta x & \text{if } \ t \in [0, t_1] \quad (4.1a) \\ \dot{y}(t) = \beta x + q\left(1 - \dfrac{y}{\mathrm{K}_T}\right) y - \gamma y & \text{if } \ t \in [0, t_1] \quad (4.1b) \\ \dot{z}(t) = \gamma y + r\left(1 - \dfrac{z}{\mathrm{K}_P}\right) z & \text{if } \ t \in [0, t_1] \quad (4.1c) \end{cases}$$

In Eq. 4.1a above, the constant u denotes the total number of stem cells in the bone marrow, and the constant α (units time^{-1}, or "cells per capita per unit time") denotes the per-capita rate at which stem cells produce T-cell precursors that travel from the bone marrow to the thymus, so that αu denotes the rate at which T-cell precursors are produced from stem cells in the bone marrow. The coefficient function $p\left(1 - \frac{x}{K_{\mathrm{BM}}}\right)$ (units time^{-1} or "cells per capita per unit time") represents the per-capita rate of cellular division in the bone marrow, with K_{BM} a bone marrow carrying capacity parameter, and p a rate parameter. Note that if $x > K_{\mathrm{BM}}$, this coefficient function is negative, and represents a death rate. The term $p\left(1 - \frac{x}{K_{\mathrm{BM}}}\right) x$ then represents the rate at which stem cells are created in the bone marrow via cellular division. Finally, the constant β (units time^{-1} or "cells per capita per unit time") denotes the per-capita T-cell precursor emigration rate from the bone marrow, so that βx denotes the rate at which T-cell precursors are lost in the bone marrow due to emigration to the thymus.

In Eqs. 4.1b, 4.1c terms are defined analogously. In Eq. 4.1b, the term βx represents the rate at which T-cell precursors enter the thymus from the bone marrow. With K_{T} representing a thymic carrying capacity parameter, and q a thymic division rate parameter, the term $q\left(1 - \frac{y}{K_{\mathrm{T}}}\right) y$ represents the rate at which the T-cell precursor population changes due to cellular division (or death) in the thymus. The constant γ denotes the per-capita rate at which mature T-cells exit the thymus and enter the peripheral blood, so that γy denotes the total rate at which mature T-cells exit the thymus. In Eq. 4.1c, the term $r\left(1 - \frac{z}{K\mathrm{P}}\right) z$ represents the rate at which the peripheral T-cell population changes due to homeostatic cellular division and death, with r a rate parameter and K_{P} a peripheral carrying capacity parameter. In the table below, we summarize quantities appearing in our ODE.

Quantity	Description
$x(t)$	Number of precursors in bone marrow
$y(t)$	Number of progenitors in thymus
$z(t)$	Number of T-lymphocytes in periphery
α	Rate of division in bone marrow
β	Rate of migration from bone marrow to thymus
γ	Rate of migration from thymus to periphery
p	Homeostatic parameter in bone marrow
q	Homeostatic parameter in thymus
r	Homeostatic parameter in periphery
K_{BM}	Carrying capacity in bone marrow
K_T	Carrying capacity in thymus
K_P	Carrying capacity in periphery

Table 4.1: **Functions and Parameters defined in Stage 1**

Denote equilibrium solutions of Eqs. 4.1a, 4.1b, 4.1c by $\overline{x}_1, \overline{y}_1, \overline{z}_1$. As the quantities $\overline{x}_1$, $\overline{y}_1$, and $\overline{z}_1$ represent T-cell population counts, the only relevant equilibria are those satisfying $\overline{x}_1$, $\overline{y}_1$, $\overline{z}_1 \geq 0$. The only physically relevant equilibrium solution of Eqs. 4.1a, 4.1b, 4.1c is then:

$$\overline{x}_1 = \frac{K_{\mathrm{BM}}}{2p}\left(p - \beta + \sqrt{(p-\beta)^2 + \frac{4\alpha u p}{K_{\mathrm{BM}}}}\right), \tag{4.2}$$

$$\overline{y}_1 = \frac{K_{\mathrm{T}}}{2q}\left(q - \gamma + \sqrt{(q-\gamma)^2 + \frac{4\beta \overline{x}_1 q}{K_{\mathrm{T}}}}\right), \tag{4.3}$$

$$\overline{z}_1 = \frac{K_{\mathrm{P}}}{2r}\left(r + \sqrt{r^2 + \frac{4r\overline{y}_1\gamma}{K_{\mathrm{P}}}}\right), \tag{4.4}$$

where we note that $\overline{z}_1$ depends on $\overline{y}_1$, and $\overline{y}_1$ depends on $\overline{x}_1$, as expected. The linearization of Eqs. 4.1a, 4.1b, 4.1c around the equilibrium given by Eqs. 4.2, 4.3, 4.4 is given by:

$$\begin{pmatrix} \frac{\partial \dot{x}}{\partial x} & \frac{\partial \dot{x}}{\partial y} & \frac{\partial \dot{x}}{\partial z} \\ \frac{\partial \dot{y}}{\partial x} & \frac{\partial \dot{y}}{\partial y} & \frac{\partial \dot{y}}{\partial z} \\ \frac{\partial \dot{z}}{\partial x} & \frac{\partial \dot{z}}{\partial y} & \frac{\partial \dot{z}}{\partial z} \end{pmatrix} = \begin{pmatrix} (p-\beta) - \frac{2p}{K_{BM}}\overline{x}_1 & 0 & 0 \\ \beta & (q-\gamma) - \frac{2q}{K_T}\overline{y}_1 & 0 \\ 0 & \gamma & r - \frac{2r}{K_P}\overline{z}_1 \end{pmatrix} \tag{4.5}$$

The linearization has eigenvalues λ_1, λ_2, and λ_3 given by:

$$\begin{aligned} \lambda_1 &= (p-\beta) - \frac{2p}{K_{\mathrm{B}M}}\overline{x}_1 = -\sqrt{(p-\beta)^2 + \frac{4\alpha u p}{K_{\mathrm{B}M}}} \\ \lambda_2 &= (q-\gamma) - \frac{2q}{K_{\mathrm{T}}}\overline{y}_1 = -\sqrt{(q-\gamma)^2 + \frac{4\beta \overline{x}_1 q}{K_{\mathrm{T}}}} \\ \lambda_3 &= r - \frac{2r}{K_{\mathrm{P}}}\overline{z}_1 = -\sqrt{r^2 + \frac{4r\overline{y}_1\gamma}{K_{\mathrm{P}}}} \end{aligned}$$

As each eigenvalue is strictly negative for any combination of strictly positive parameters, our choice of $(\overline{x}_1, \overline{y}_1, \overline{z}_1)$ is a stable equilibrium for Eqs. 4.1a, 4.1b, 4.1c.

4.2.2 Stage 2: Infection with HIV

The next piece of our ODE models Stage 2 of the infection and treatment process: that after which HIV infection has occurred, and before treatment is administered. Denote by $V(t)$ the number of free virions in the system, by $Y(t)$ the number of infected cells in the thymus, and by $Z(t)$ the number of infected cells in the periphery. The ODE system we propose to describe Stage 2 is as follows:

$$
\begin{cases}
\dot{x}(t) = \alpha u + p\left(1 - \dfrac{x}{K_{BM}}\right)x - \beta x & \text{if } \ t \in (t_1, t_2] \qquad (4.6a)\\
\dot{y}(t) = \beta x + q\left(1 - \dfrac{y}{K_T}\right)y - \gamma y - \lambda_y V y & \text{if } \ t \in (t_1, t_2] \qquad (4.6b)\\
\dot{z}(t) = \gamma y + r\left(1 - \dfrac{z}{K_P}\right)z - \lambda_z V z & \text{if } \ t \in (t_1, t_2] \qquad (4.6c)\\
\dot{Y}(t) = \lambda_y V y - k_y Y & \text{if } \ t \in (t_1, t_2] \qquad (4.6d)\\
\dot{Z}(t) = \lambda_z V z - k_z Z & \text{if } \ t \in (t_1, t_2] \qquad (4.6e)\\
\dot{V}(t) = c_y Y + c_z Z - \eta V & \text{if } \ t \in (t_1, t_2] \qquad (4.6f)
\end{cases}
$$

At time t_1, we set the initial conditions $(x(t_1), y(t_1), z(t_1), Y(t_1) = 0, Z(t_1) = 0, V(t_1) = V_0)$, where $x(t_1) \sim \overline{x}_1$, $y(t_1) \sim \overline{y}_1$, and $z(t_1) \sim \overline{z}_1$ are the values of the functions $x(t)$, $y(t)$, and $z(t)$ that resulted at the end of Stage 1 (that is, at t_1, the moment of infection), and V_0 is the starting concentration of virus particles at the moment of infection.

All the quantities (functions and constants) that appear in Eqs. 4.6a–4.6f and already appeared in Eqs. 4.1a–4.1c retain the same interpretation. The effects of viral infection are incorporated into Eqs. 4.6b–4.6f only, as we assume HIV does not infect the bone marrow. In Eq. 4.6b, Vy is taken as a proxy for the number of potential "collisions" between virus particles and healthy T-cells in the thymus, and λ_y represents the rate of infection per collision (units time^{-1}, or "infections per collision per unit time"), so that $-\lambda_y V y$ (units time^{-1}) represents the rate at which healthy cells in the thymus are lost due to infection resulting from collisions with virus particles. In Eq. 4.6c, $-\lambda_z V z$ analogously represents the rate at which healthy cells in the periphery are lost due to infection resulting from collisions with virus particles. In Eq. 4.6d, the term $\lambda_y V y$ indicates that cells lost from the healthy cell pool due to infection in Eq. 4.6b are transferred to the infected cell pool. The constant k_y denotes the per-capita death rate of infected cells in the thymus (units time^{-1}), so that $k_y Y$ represents the total rate at which infected cells die in the thymus. In Eq. 4.6e, terms are defined analogously, with k_z representing the per-capita death rate of infected cells in the periphery. Finally, Eq. 4.6f accounts for changes to the total viral load. The constants c_y, c_z denote the rates at which infected cells produce new virions (units time^{-1}, or "viruses per infected cell per unit time") in the thymus and periphery,

so that c_yY, c_zZ represent the total rate at which new virions are produced by infected cells in the thymus and periphery, respectively. The constant η represents the per-capita rate (units time^{-1}, or "virions cleared per virion per unit time") of clearance of virions by the immune system, so that ηV represents the total rate at which virions are cleared by the immune system (units time^{-1}).

Below is a table summarizing the new quantities appearing in Eqs. 4.6a–4.6f:

Quantity	**Description**
$Y(t)$	Density of infected cells in thymus
$Z(t)$	Density of infected cells in periphery
$V(t)$	Density of virus particles
λ_y	Rate of infection in thymus
λ_z	Rate of infection in periphery
η	Rate of neutralization of viral particles
k_y	Rate of clearance of infected cells in thymus
k_z	Rate of clearance of infected cells in periphery
c_y	Rate of viral production in thymus
c_z	Rate of viral production in periphery

Table 4.2: Functions and parameters new to the Stage 2 ODEs.

The system in Eqs. 4.6a–4.6f presents two distinct equilibrium solutions, one of which corresponds to the disease-free state. The disease-free equilibrium has the form:

$$
\begin{aligned}
\overline{x}_2 &= \frac{K_{\mathrm{B}M}}{2p}\left(p-\beta+\sqrt{(p-\beta)^2+\frac{4\alpha u p}{K_{\mathrm{B}BM}}}\right)\\
\overline{y}_2 &= \frac{K_{\mathrm{T}}}{2q}\left(q-\gamma+\sqrt{(q-\gamma)^2+\frac{4\beta\overline{x}_2 q}{K_{\mathrm{T}}}}\right)\\
\overline{z}_2 &= \frac{K_{\mathrm{P}}}{2r}\left(r+\sqrt{r^2+\frac{4r\overline{y}_2\gamma}{K_{\mathrm{P}}}}\right)\\
\overline{Y}_2 &= 0\\
\overline{Z}_2 &= 0\\
\overline{V}_2 &= 0
\end{aligned}
$$

As one can see, this equilibrium solution in Eqs. 4.7–4.7 essentially reverts to the steady state solution from Stage 1 (Eqs. 4.2–4.4). To study its stability, we first compute the linearization of Eqs. 4.6a–4.6f, evaluated at an arbitrary equilibrium solution:

$$
\begin{pmatrix}
\frac{\partial\dot{x}}{\partial x} & \frac{\partial\dot{x}}{\partial y} & \frac{\partial\dot{x}}{\partial z} & \frac{\partial\dot{x}}{\partial Y} & \frac{\partial\dot{x}}{\partial Z} & \frac{\partial\dot{x}}{\partial V}\\
\frac{\partial\dot{y}}{\partial x} & \frac{\partial\dot{y}}{\partial y} & \frac{\partial\dot{y}}{\partial z} & \frac{\partial\dot{y}}{\partial Y} & \frac{\partial\dot{y}}{\partial Z} & \frac{\partial\dot{y}}{\partial V}\\
\frac{\partial\dot{z}}{\partial x} & \frac{\partial\dot{z}}{\partial y} & \frac{\partial\dot{z}}{\partial z} & \frac{\partial\dot{z}}{\partial Y} & \frac{\partial\dot{z}}{\partial Z} & \frac{\partial\dot{z}}{\partial V}\\
\frac{\partial\dot{Y}}{\partial x} & \frac{\partial\dot{Y}}{\partial y} & \frac{\partial\dot{Y}}{\partial z} & \frac{\partial\dot{Y}}{\partial Y} & \frac{\partial\dot{Y}}{\partial Z} & \frac{\partial\dot{Y}}{\partial V}\\
\frac{\partial\dot{Z}}{\partial x} & \frac{\partial\dot{Z}}{\partial y} & \frac{\partial\dot{Z}}{\partial z} & \frac{\partial\dot{Z}}{\partial Y} & \frac{\partial\dot{Z}}{\partial Z} & \frac{\partial\dot{Z}}{\partial V}\\
\frac{\partial\dot{V}}{\partial x} & \frac{\partial\dot{V}}{\partial y} & \frac{\partial\dot{V}}{\partial z} & \frac{\partial\dot{V}}{\partial Y} & \frac{\partial\dot{V}}{\partial Z} & \frac{\partial\dot{V}}{\partial V}
\end{pmatrix}
\tag{4.7}
$$

$$
= \begin{pmatrix}
(p-\beta)-\frac{2p}{K_{BM}}\overline{x}_2 & 0 & 0 & 0 & 0 & 0\\
\beta & (q-\gamma)-\frac{2q}{K_T}\overline{y}_2-\lambda_y\overline{V}_2 & 0 & 0 & 0 & -\lambda_y\overline{y}_2\\
0 & \gamma & r-\frac{2r}{K_P}\overline{z}_2-\lambda_z\overline{V}_2 & 0 & 0 & -\lambda_z\overline{z}_2\\
0 & \lambda_y\overline{V}_2 & 0 & -k_y & 0 & \lambda_y\overline{y}_2\\
0 & 0 & \lambda_z\overline{V}_2 & 0 & -k_z & \lambda_z\overline{z}_2\\
0 & 0 & 0 & c_y & c_z & -\eta
\end{pmatrix}
\tag{4.8}
$$

To study the linearization matrix at our particular disease-free equilibrium, we first insert

the steady-state components $\overline{Y}_2 = 0$, $\overline{Z}_2 = 0$, and $\overline{V}_2 = 0$ into the linearization, leaving the symbolic expressions for $\overline{x}_2, \overline{y}_2, \overline{z}_2$ at the moment, to keep the matrix simple:

$$\begin{pmatrix} (p-\beta) - \frac{2p}{K_{BM}}\overline{x}_2 & 0 & 0 & 0 & 0 & 0 \\ \beta & (q-\gamma) - \frac{2q}{K_{BM}}\overline{y}_2 & 0 & 0 & 0 & \lambda_y \overline{y}_2 \\ 0 & \gamma & r - \frac{2r}{K_P}\overline{z}_2 & 0 & 0 & -\lambda_z \overline{z}_2 \\ 0 & 0 & 0 & -k_y & 0 & \lambda_y \overline{y}_2 \\ 0 & 0 & 0 & 0 & -k_z & \lambda_z \overline{z}_2 \\ 0 & 0 & 0 & c_y & c_z & -\eta \end{pmatrix}$$

This matrix has eigenvalues $\lambda_1, \cdots, \lambda_6$, and the first three are given explicitly by:

$$\begin{aligned} \lambda_1 &= (p-\beta) - \frac{2p}{K_{\mathrm{BM}}}\overline{x}_2 = -\sqrt{(p-\beta)^2 + \frac{4\alpha u p}{K_{\mathrm{BM}}}} \\ \lambda_2 &= (q-\gamma) - \frac{2q}{K_{\mathrm{T}}}\overline{y}_2 = -\sqrt{(q-\gamma)^2 + \frac{4\beta \overline{x}_2 q}{K_{\mathrm{T}}}} \\ \lambda_3 &= r - \frac{2r}{K_{\mathrm{P}}}\overline{z}_2 = -\sqrt{r^2 + \frac{4r\overline{y}_2\gamma}{K_{\mathrm{T}}}} \end{aligned}$$

The eigenvalues $\lambda_1, \lambda_2,$ and λ_3 are all strictly negative, so the disease-free state will be unstable if at least one of the remaining eigenvalues (λ_4, λ_5, and λ_6) is nonnegative. The three remaining eigenvalues are given by the roots of the following cubic, which we denote by $a(\lambda)$:

$$a(\lambda) = -\lambda^3 - (k_z + \eta)\lambda^2 + (-k_y k_z - (k_z + k_y)\eta + c_z \lambda_z \overline{z}_2 + c_y \lambda_y \overline{y}_2)\,\lambda \tag{4.9}$$

$$+ (k_y c_z \lambda_z \overline{z}_2 + k_z c_y \lambda_y \overline{y}_2 - k_y k_z \eta) \tag{4.10}$$

As $a(\lambda)$ satisfies $a(\lambda) \longrightarrow -\infty$ as $\lambda \longrightarrow \infty$, the condition $a(0) > 0$ is sufficient to guarantee the existence of a positive root of a, and thus a positive eigenvalue, and consequent

instability of the disease-free equilibrium. In terms of the parameters of the system, this amounts to the condition:

$$k_y c_z \lambda_z \overline{z}_2 + k_z c_y \lambda_y \overline{y}_2 > k_y k_z \eta. \tag{4.11}$$

This condition is not necessary to produce a positive root, however, so we now consider what happens when $a(0) < 0$. We first observe that because $a(\lambda) \longrightarrow \infty$ as $\lambda \longrightarrow -\infty$, if $a(0) < 0$, then a must have at least one negative root. From this observation (and basic facts about polynomial roots), we can conclude that in the case $a(0) < 0$, a either has three negative roots, one negative root and 2 positive roots, or one negative root and one pair of complex conjugate roots.

As the coefficients of the third- and second-order terms in a are always negative, and the constant term, $a(0)$, is assumed to be negative, we draw further conclusions about the roots by varying the sign of the coefficient of the first-order term in a. We begin by assuming the first-order term is positive. This condition is given explicitly in terms of the parameters of the system by:

$$c_z \lambda_z \overline{z}_2 + c_y \lambda_y \overline{y}_2 > k_y k_z + (k_z + k_y)\eta. \tag{4.12}$$

If this condition is met, then a cannot have three negative roots. (If all roots of a were negative, then the coefficient of each term in the cubic would have the same sign.) Thus, a has either two positive real roots or a complex conjugate pair of roots. It can be shown that if the other roots consist of a complex conjugate pair, then the real parts of the roots must be positive. Regardless, if the coefficient of the first-order term in the cubic a is positive, then a has two roots with positive real part. In particular, the linearization matrix in Eq. 4.2.2 has two eigenvalues with positive real part, and the disease-free equilibrium is unstable. In addition, Conds. 4.11, 4.12 above are likely to be satisfied in any physically relevant situation, due to the large magnitude of the equilibria $\overline{y}_2$ and $\overline{z}_2$, which appear on the left-hand side of Conds. 4.11, 4.12.

Let's now consider other possible equilibria of Eqs. 4.6a–4.6f, which correspond to persistent infection. Given such equilibrium values of $\overline{x}_2$ and $\overline{y}_2$ to be computed momentarily, it can be shown that equilibrium values $\overline{z}_2,\ \overline{V}_2,\ \overline{Y}_2,$ and $\overline{Z}_2$ are defined in terms of them as follows:

$$\begin{aligned}
\overline{z}_2 &= \frac{k_z\eta}{c_z\lambda_z} - \frac{c_y\lambda_y k_z}{c_z\lambda_z k_y}\overline{y}_2 \ := \ A - B\overline{y}_2 \\
\overline{V}_2 &= \frac{\gamma\overline{y}_2}{\lambda_z(A-B\overline{y}_2)} + \frac{r}{\lambda_z} - \frac{r(A-B\overline{y}_2)}{\lambda_z} \\
\overline{Y}_2 &= \frac{\lambda_y}{k_y}\overline{y}_2\left(\frac{\gamma\overline{y}_2}{\lambda_z(A-B\overline{y}_2)} + \frac{r}{\lambda_z} - \frac{r(A-B\overline{y}_2)}{\lambda_z}\right) \\
\overline{Z}_2 &= \frac{(A-B\overline{y}_2)}{k_z}\left(\frac{\gamma\overline{y}_2}{\lambda_z(A-B\overline{y}_2)} + \frac{r}{\lambda_z} - \frac{r(A-B\overline{y}_2)}{\lambda_z}\right)
\end{aligned}$$

where we define the constants $A := \frac{k_z\eta}{c_z\lambda_z}$ and $B := \frac{c_y\lambda_y k_z}{c_z\lambda_z k_y}$ for simplicity. As we assume the bone marrow itself is immune to infection by HIV, Eq. 4.6a is identical to Eq. 4.1a, and the equilibrium component $\overline{x}_2$ is the same as $\overline{x}_1$:

$$\overline{x}_2 = \frac{K_{\mathrm{BM}}}{2p}\left(p - \beta + \sqrt{(p-\beta)^2 + \frac{4\alpha u p}{K_{\mathrm{BM}}}}\right) \tag{4.13}$$

The equilibrium components $\overline{y_2}$ are given implicitly as roots of the following cubic, which we denote by $b(\overline{y}_2)$:

$$b(\overline{y}_2) = \left(\frac{Bq}{K_{\mathrm{T}}} + \frac{\lambda_y r B^2}{\lambda_z K_{\mathrm{P}}}\right)\overline{y}_2^3 + \left(-B(q-\gamma) - \frac{qA}{K_{\mathrm{T}}} - \frac{\lambda_y\gamma}{\lambda_z} + \frac{B\lambda_y r}{\lambda_z} - \frac{2AB\lambda_y r}{K_{\mathrm{P}}\lambda_z}\right)\overline{y}_2^2 \tag{4.14}$$

$$+ \left(A(q-\gamma) - B\beta\overline{x}_2 + \frac{A\lambda_y r}{\lambda_z}\left(\frac{A}{K_{\mathrm{P}}} - 1\right)\right)\overline{y}_2 + A\beta\overline{x}_2 \tag{4.15}$$

Numerical computations of the three roots for positive, reasonable parameter values generally produce three real roots, two of which are positive, and one of which is negative. The table below includes a sample numerical computation of the roots of this cubic, with

parameter values listed in the caption.

Root 1	Root 2	Root 3
$-3.154570615148978\text{x}10^4$	$1.916591560167755\text{x}10^4$	$4.387979054981225\text{x}10^4$

Table 4.3: **Roots of** $b(\overline{y}_2)$ Parameter values: $\alpha = 1$, $\beta = 0.4$, $\gamma = 0.1$, $u = 2000$, $p = q = r = 1$, $K_{BM} = K_{\mathrm{T}} = K_{\mathrm{P}} = 100,000$, $\lambda_y = \lambda_z = 0.0001$, $k_y = k_z = 0.6$, $c_y = c_z = 0.2$, and $\eta = 0.7$.

Each of the three choices of $\overline{y}_2$ coupled with the single choice of $\overline{x}_2$ produces a set of equilibria $(\overline{x}_2, \overline{y}_2, \overline{z}_2, \overline{Y}_2, \overline{Z}_2, \overline{V}_2)$. A state of productive infection occurs if each component is positive. Our choice of $\overline{x}_2$ satisfies $\overline{x}_2 > 0$, and if we select from the three choices of $\overline{y}_2$ those satisfying $\overline{y}_2 > 0$, then as long as $\overline{z}_2$ and $\overline{V}_2 > 0$, it follows that $\overline{Y}_2, \overline{Z}_2 > 0$ as well. We can impose the conditions $\overline{z}_2, \overline{V}_2 > 0$ by first prescribing that $\overline{z}_2 > 0$, which can be phrased in terms of the original parameters as:

$$\overline{z}_2 > 0 \text{ iff } A - B\overline{y}_2 > 0 \text{ iff } \frac{\eta k_y}{c_y \lambda_y} > \overline{y}_2.$$

With this assumption that $\overline{z}_2 = A - B\overline{y}_2 > 0$, we can guarantee that $\overline{V}_2 > 0$ by imposing the condition:

$$\gamma\overline{y}_2 + r(A - B\overline{y}_2) - \frac{r(A - B\overline{y}_2)^2}{K_{\mathrm{P}}} > 0$$

This expression is quadratic in $(A - B\overline{y}_2) = \overline{z}_2$. In particular, as the coefficient of the highest order term is negative, the relation above is satisfied when $(A - B\overline{y}_2)$ lies between the two roots of the quadratic. Those roots are given by

$$(A - B\overline{y}_2) = \frac{K_{\mathrm{P}}}{2}\left(1 \pm \sqrt{1 + \frac{4\gamma\overline{y}_2}{rK_{\mathrm{P}}}}\right)$$

Notice that, due to the nonnegativity of $r, \gamma, \overline{y}_2, K_{\mathrm{P}}$, one of these roots is negative and the other positive. Earlier we saw that it was necessary to assume $\overline{z}_2 > 0$, so now we make the additional assumption that $\overline{z}_2 = A - B\overline{y}_2 < \frac{K_{\mathrm{P}}}{2}\left(1 + \sqrt{1 + \frac{4\gamma\overline{y}_2}{K_{\mathrm{P}}}}\right)$. This leads

to the constraint on $\overline{y}_2$ given by:

$$\frac{A}{B} - \left(\frac{K_{\mathrm{P}}}{2B}\right)\left(1 + \sqrt{1 + \frac{4\gamma\overline{y}_2}{rK_{\mathrm{P}}}}\right) < \overline{y}_2 < \frac{\eta k_y}{c_y\lambda_y},$$

which can be written in terms of the original parameters as,

$$\frac{\eta k_y}{c_y\lambda_y} - \frac{K_{\mathrm{P}}c_z\lambda_z k_y}{2c_y\lambda_y k_z}\left(1 + \sqrt{1 + \frac{4\gamma\overline{y}_2}{rK_{\mathrm{P}}}}\right) < \overline{y}_2 < \frac{\eta k_y}{c_y\lambda_y}.$$

Numerical simulations show that the small positive root $\overline{y}_2$ of the cubic b generally satisfies the above relation, and so we look to this choice of $\overline{y}_2$ to produce an equilibrium solution corresponding to a state of persistent infection, and study its stability numerically.

4.2.3 Stage 3: After Treatment

The final part of the piecewise ODE models Stage 3, treatment of the HIV infection with bone marrow transplant. Denote by $x^*(t)$ the number of HIV-immune T-cell precursors in the bone marrow, by $y^*(t)$ the number of developing HIV-immune T-cells in the thymus, and by $z^*(t)$ the number of mature HIV-immune T-cells in the periphery. Assuming occasional infection of defective HIV-immune cells with the HIV virus, denote by $Y^*(t)$ the total number of infected HIV-immune cells in the thymus, and by $Z^*(t)$ the total number of infected HIV-immune cells in the periphery. The ODE we propose to describe Stage 3 is as follows:

$$
\begin{cases}
\dot{x}(t) = \alpha u + p\left(1 - \dfrac{x + x^*}{K_{BM}}\right) x - \beta x & \text{if } t \in [t_2, t_3] \quad (4.16a) \\
\dot{y}(t) = \beta x + q\left(1 - \dfrac{y + y^*}{K_T}\right) y - \gamma y - \lambda_y V y & \text{if } t \in [t_2, t_3] \quad (4.16b) \\
\dot{z}(t) = \gamma y + r\left(1 - \dfrac{z + z^*}{K_P}\right) z - \lambda_z V z & \text{if } t \in [t_2, t_3] \quad (4.16c) \\
\dot{x^*}(t) = \alpha u^* + p\left(1 - \dfrac{x + x^*}{K_{BM}}\right) x^* - \beta x^* & \text{if } t \in [t_2, t_3] \quad (4.16d) \\
\dot{y^*}(t) = \beta x^* + q\left(1 - \dfrac{y + y^*}{K_T}\right) y^* - \gamma y^* - \lambda_{y^*} V y^* & \text{if } t \in [t_2, t_3] \quad (4.16e) \\
\dot{z^*}(t) = \gamma y^* + r\left(1 - \dfrac{z + z^*}{K_P}\right) z^* - \lambda_{z^*} V z^* & \text{if } t \in [t_2, t_3] \quad (4.16f) \\
\dot{Y}(t) = \lambda_y V y - k_y Y & \text{if } t \in [t_2, t_3] \quad (4.16g) \\
\dot{Z}(t) = \lambda_z V z - k_z Z & \text{if } t \in [t_2, t_3] \quad (4.16h) \\
\dot{Y^*}(t) = \lambda_{y^*} V y^* - k_y Y^* & \text{if } t \in [t_2, t_3] \quad (4.16i) \\
\dot{Z^*}(t) = \lambda_{z^*} V z^* - k_z Z^* & \text{if } t \in [t_2, t_3] \quad (4.16j) \\
\dot{V}(t) = c_y Y + c_z Z + c_{y^*} Y^* + c_{z^*} Z^* - \eta V & \text{if } t \in [t_2, t_3] \quad (4.16k) \\
 & \quad (4.16l)
\end{cases}
$$

The dynamics of the HIV-immune and HIV-susceptible cell populations are coupled via the logistic growth coefficients $\left(1 - \frac{x+x^*}{K_{BM}}\right)$ in Eqs. 4.16a, 4.16d and the analogous terms that appear in Eqs. 4.16b, 4.16c, 4.16e, 4.16f. These coefficient functions are "symmetric" in x, x^*, y, y^*, z, z^*, to reflect the identical effect the homeostatic mechanism has on protected and unprotected cell populations. Aside from the added representation of protected cell populations to the logistic growth coefficients, Eqs. 4.16a–4.16c are unchanged from their forms in Eqs. 4.1a–4.1c and Eqs. 4.6a–4.6c.

Eqs. 4.16d–4.16f, 4.16i, 4.16j describe the time evolution of the new functions z^*, y^*, z^*, Y^*, Z^*. In Eq. 4.16d, the constant u^* represents the total number of HIV-immune stem cells in the bone marrow, and in Eqs. 4.16e, 4.16f, the constants $\lambda_{y^*}, \lambda_{z^*}$ represent the rates of infection of HIV-immune cells in the thymus and periphery, respectively. As the immune system's homeostatic mechanism operates on the protected and unprotected T-cell populations in the same fashion, and HIV infection results from physical colli-

sions between virions and either protected or unprotected cells (albeit at different rates), Eqs. 4.16d–4.16f are formulated in direct analogue with Eqs. 4.16a–4.16c. Eqs. 4.16i, 4.16j are also formulated in effigy of Eqs. 4.16g, 4.16h, under the assumption that protected thymic and peripheral cells die at the same rates (k_y, k_z, respectively) as unprotected cells. In Eq. 4.16k, we modify Eq. 4.6f to account for production of new virions from infected protected cells in the thymus and periphery, with new virions produced from infected protected thymic and peripheral cells at rates c_{y^*}, c_{z^*}, respectively.

In the table below, we introduce the new quantities that appear in Eqs. 4.16a–4.16k, but did not appear in Eqs. 4.16a–4.16f.

Quantity	**Description**
$x^*(t)$	Number of protected cells in bone marrow
$y^*(t)$	Number of protected cells in thymus
$z^*(t)$	Number of protected cells in periphery
$Y^*(t)$	Number of infected protected cells in thymus
$Z^*(t)$	Number of infected protected cells in periphery
u^*	Number of protected stem cells in bone marrow
λ_{y^*}	Rate of infection of protected cells in thymus
λ_{z^*}	Rate of infection of protected cells in periphery
c_{y^*}	Rate of viral production (in protected cells) in thymus
c_{z^*}	Rate of viral production (in protected cells) in periphery

Table 4.4: Functions and Parameters Introduced in Stage 3

We define the initial conditions of those functions that were defined in Stage 2–$(x(t), y(t), z(t), Y(t), Z(t), V(t))$–to be the values that resulted at the end of Stage 2, at time t_2. We assign to the five new functions the initial conditions: $(x^*(t_2) = 0, y^*(t_2) = 0, z^*(t_2) = 0, Y^*(t_2) = 0, Z^*(t_2) = 0)$, because we are introducing a new type of protected cell not already be present in the tissues of the immune system.

We begin by analyzing the Stage 3 equilibrium corresponding to the disease-free state, which is given below:

$$\overline{x}_3 = \frac{2\alpha u}{\sqrt{(p-\beta)^2 + \frac{4p\alpha(u+u^*)}{K_{\mathrm{B}M}}} - (p-\beta)} \qquad \overline{x}_3^* = \frac{2\alpha u^*}{\sqrt{(p-\beta)^2 + \frac{4p\alpha(u+u^*)}{K_{\mathrm{B}M}}} - (p-\beta)}$$

$$\overline{y}_3 = \frac{2\beta\overline{x}_3}{\sqrt{(q-\gamma)^2 + \frac{4q\beta(\overline{x}_3+\overline{x}_3^*)}{K_{\mathrm{T}}}} - (q-\gamma)} \qquad \overline{y}_3^* = \frac{2\beta\overline{x}_3^*}{\sqrt{(q-\gamma)^2 + \frac{4q\beta(\overline{x}_3+\overline{x}_3^*)}{K_{\mathrm{T}}}} - (q-\gamma)}$$

$$\overline{z}_3 = \frac{\gamma\overline{y}_3}{\sqrt{r^2 + \frac{4r\gamma(\overline{y}_3+\overline{y}_3^*)}{K_{\mathrm{P}}}} - r} \qquad \overline{z}_3^* = \frac{\gamma\overline{y}_3^*}{\sqrt{r^2 + \frac{4r\gamma(\overline{y}_3+\overline{y}_3^*)}{K_{\mathrm{P}}}} - r}$$

$$\overline{Y}_3 = 0 \qquad \overline{Z}_3 = 0 \qquad \overline{V}_3 = 0 \qquad \overline{Y}_3^* = 0 \qquad \overline{Z}_3^* = 0$$

Due to the nonnegativity of the parameters, all eleven components of the equilibrium solution above are nonnegative. To study the stability of this equilibrium solution, we begin by computing the linearization of the system in Eqs. 4.16a–4.16k around an arbitrary point $(x, x^*, y, y^*, z, z^*, Y, Z, Y^*, Z^*, V)$:

$$
\begin{pmatrix}
\left[(p-\beta) - \frac{p(2x+x^*)}{k_{\mathrm{B}M}}\right] & 0 & 0 & \frac{-px}{K_{\mathrm{B}M}} & 0 & 0 & 0 & 0 & 0 & 0 & \\
\beta & \begin{matrix}(q-\gamma) \\ -\frac{q(2y+y^*)}{K_{\mathrm{T}}} \\ -\lambda_y V\end{matrix} & 0 & 0 & \frac{-qy}{K_{\mathrm{T}}} & 0 & 0 & 0 & 0 & 0 & -\lambda_y y \\
0 & \gamma & \begin{matrix}r \\ -\frac{r(2z+z^*)}{K_{\mathrm{P}}} \\ -\lambda_z V\end{matrix} & 0 & 0 & \frac{-rz}{K_{\mathrm{P}}} & 0 & 0 & 0 & 0 & -\lambda_z z \\
\frac{-px^*}{K_{\mathrm{B}M}} & 0 & 0 & (p-\beta) - \frac{p(2x^*+x)}{K_{\mathrm{B}M}} & 0 & 0 & 0 & 0 & 0 & 0 & 0 \\
0 & \frac{-qy^*}{K_{\mathrm{T}}} & 0 & \beta & (q-\gamma) - \frac{q(2y^*+y)}{K_{\mathrm{T}}} - \lambda_{y^*} V & 0 & 0 & 0 & 0 & 0 & -\lambda_{y^*} y^* \\
0 & 0 & \frac{-rz^*}{K_{\mathrm{P}}} & 0 & \gamma & r - \frac{r(2z^*+z)}{K_{\mathrm{P}}} & 0 & 0 & 0 & 0 & \lambda_{z^*} z^* \\
0 & \lambda_y V & 0 & 0 & 0 & 0 & -k_y & 0 & 0 & 0 & \lambda_y y \\
0 & 0 & \lambda_z V & 0 & 0 & 0 & 0 & -k_z & 0 & 0 & \lambda_z z \\
0 & 0 & 0 & 0 & \lambda_{y^*} V & 0 & 0 & 0 & -k_y & 0 & \lambda_{y^*} y^* \\
0 & 0 & 0 & 0 & 0 & \lambda_{z^*} V & 0 & 0 & 0 & -k_z & \lambda_{z^*} \\
0 & 0 & 0 & 0 & 0 & 0 & c_y & c_z & c_{y^*} & c_{z^*} & -\eta
\end{pmatrix}
$$

We now insert our equilibrium solution into the linearization matrix, taking $Y = Z = Y^* = Z^* = V = 0$, and taking $x \to \overline{x}_3$, $y \to \overline{y}_3$, $z \to \overline{z}_3$, $x^* \to \overline{x}_3^*$, $y^* \to \overline{y}_3^*$, and $z^* \to \overline{z}_3^*$ to keep the matrix simple. We obtain:

$$\begin{pmatrix}
(p-\beta)-\frac{p(2\overline{x}_3+\overline{x}_3^*)}{K_{BM}} & 0 & 0 & \frac{-p\overline{x}_3}{K_{BM}} & 0 & 0 & 0 & 0 & 0 & 0 & 0 \\
\beta & (q-\gamma)-\frac{q(2\overline{y}_3+\overline{y}_3^*)}{K_T} & 0 & 0 & \frac{qy}{K_T} & 0 & 0 & 0 & 0 & 0 & -\lambda_y\overline{y}_3 \\
0 & \gamma & r-\frac{r(2\overline{z}_3+\overline{z}_3^*)}{K_P} & 0 & 0 & \frac{-rz}{K_P} & 0 & 0 & 0 & 0 & -\lambda_z\overline{z}_3 \\
\frac{-p\overline{x}_3^*}{K_{BM}} & 0 & 0 & (p-\beta)-\frac{p(2\overline{x}_3^*+\overline{x}_3)}{K_{BM}} & 0 & 0 & 0 & 0 & 0 & 0 & 0 \\
0 & \frac{-q\overline{y}_3^*}{K_T} & 0 & \beta & (q-\gamma)-\frac{q(2\overline{y}_3^*+y)}{K_T} & 0 & 0 & 0 & 0 & 0 & -\lambda_{y^*}\overline{y}_3^* \\
0 & 0 & \frac{-r\overline{z}_3^*}{K_P} & 0 & \gamma & r-\frac{r(2\overline{z}_3^*+\overline{z}_3)}{K_P} & 0 & 0 & 0 & 0 & -\lambda_{z^*}\overline{z}_3^* \\
0 & 0 & 0 & 0 & 0 & 0 & -k_y & 0 & 0 & 0 & \lambda_y\overline{y}_3 \\
0 & 0 & 0 & 0 & 0 & 0 & 0 & -k_z & 0 & 0 & \lambda_z\overline{z}_3 \\
0 & 0 & 0 & 0 & 0 & 0 & 0 & 0 & -k_y & 0 & \lambda_{y^*}\overline{y}_3^* \\
0 & 0 & 0 & 0 & 0 & 0 & 0 & 0 & 0 & -k_z & \lambda_{z^*}\overline{z}_3^* \\
0 & 0 & 0 & 0 & 0 & 0 & c_y & c_z & c_{y^*} & c_{z^*} & -\eta
\end{pmatrix}$$

If this matrix has eigenvalues $\lambda_1, \lambda_z, \cdots, \lambda_{11}$, the first eight $(\lambda_1, \lambda_2, \cdots, \lambda_8)$ are given by:

$$\lambda_1 = \frac{1}{2}\left((p-\beta) - \sqrt{(p-\beta)^2 + \frac{4\alpha p(u+u^*)}{K_{\mathrm{B}M}}}\right) \qquad \lambda_2 = -\sqrt{(p-\beta)^2 + \frac{4\alpha p(u+u^*)}{K_{\mathrm{B}M}}}$$

$$\lambda_3 = \frac{1}{2}\left((q-\gamma) - \sqrt{(q-\gamma)^2 + \frac{4q\beta(\overline{x}_3+\overline{x}_3^*)}{K_{\mathrm{T}}}}\right) \qquad \lambda_4 = -\sqrt{(q-\gamma)^2 + \frac{4q\beta(\overline{x}_3+\overline{x}_3^*)}{K_{\mathrm{T}}}}$$

$$\lambda_5 = \frac{1}{2}\left(r - \sqrt{r^2 + \frac{4r\gamma(\overline{y}_3+\overline{y}_3^*)}{K_{\mathrm{P}}}}\right) \qquad \lambda_6 = -\sqrt{r^2 + \frac{4r\gamma(\overline{y}_3+\overline{y}_3^*)}{K_{\mathrm{P}}}}$$

$$\lambda_7 = -k_y \qquad \lambda_8 = -k_z$$

All of these eigenvalues are negative, and the solution can only be unstable if one of the three remaining eigenvalues is nonnegative. The remaining three eigenvalues, $\lambda_9, \lambda_{10}, \lambda_{11}$, are roots of the following cubic, which we denote by $c(\lambda)$:

$$c(\lambda) = -\lambda^3 - (k_y + k_z + \eta)\,\lambda^2 + (C + D - k_y k_z - \eta k_z - \eta k_y)\,\lambda + (Ck_y + Dk_z - \eta k_y k_z) \tag{4.17}$$

In Eq. 4.17 above, $C := c_{z^*}\lambda_{z^*}\overline{z}_3^* + c_z\lambda_z\overline{z}_3$ and $D := c_{y^*}\lambda_{y^*}\overline{y}_3^* + c_y\lambda_y\overline{y}_3$. The cubic satisfies $c(\lambda) \longrightarrow -\infty$ as $\lambda \longrightarrow \infty$, thus if $c(0) > 0$, there is guaranteed to be at least one positive real root of $c(\lambda)$, thus at least one positive eigenvalue. The condition $c(0) > 0$ is given explicitly as:

$$\left(c_{z_3^*}\lambda_{z_3^*}\overline{z}_3^* + c_z\lambda_z\overline{z}_3\right)k_y + \left(c_{y_3^*}\lambda_{y_3^*}\overline{y}_3^* + c_y\lambda_y\overline{y}_3\right)k_z > \eta k_y k_z \tag{4.18}$$

By the same reasoning used in the analysis of the disease-free steady state in Stage 2, if $c(0) < 0$, then c is guaranteed to have at least one negative real root. In particular, if $c(0) < 0$, the cubic c possesses either three negative roots, one negative root and two

positive roots, or one negative root and one pair of complex conjugate roots. In particular, knowing that the coefficients of the third- and second-order terms in c are always negative allows us to conclude that if, additionally, the first-order term is positive, then c has two roots with positive real parts, and thus the disease-free steady-state is unstable. The condition that the first-order term in c is positive is given explicitly in terms of the parameters of the system by:

$$c_{z_3^*}\lambda_{z_3^*}\overline{z}_3^* + c_z\lambda_z\overline{z}_3 + c_{y_3^*}\lambda_{y_3^*}\overline{y}_3^* + c_y\lambda_y\overline{y}_3 > \eta k_y + \eta k_z + k_y k_z \tag{4.19}$$

Cond. 4.19 is likely to be satisfied in a physically realistic situation, because the terms $\overline{y}_3$, $\overline{y}_3^*$, $\overline{z}_3$, and $\overline{z}_3^*$ are quite large in magnitude.

4.2.4 Asymptotic Behavior in the Absence of Infection.

We now consider the asymptotic behavior of the quantities $\frac{x^*}{x}$, $\frac{y^*}{y}$, and $\frac{z^*}{z}$, the ratios of HIV-immune to HIV-susceptible cells in the bone marrow, thymus, and periphery, respectively. We first imagine that the treatment is administered absent of infection, and identify the proportions of protected and unprotected cells that naturally arise in each compartment via the homeostatic mechanism after such a transplant takes place. In doing so, we establish a basis of comparison for the protected and unprotected cell dynamics when treatment is administered after infection takes place (and the viral presence disturbs the balance of protected and unprotected cells).

We begin by modifying the ODE system in Eqs. 4.16a–4.16k to describe post-transplant populations of protected and unprotected cells in the absence of HIV infection. To do so, we omit Eqs. 4.16g–4.16k entirely, as well as the terms in Eqs. 4.16a–4.16f that contain the viral load function, V.

$$\begin{cases} \dot{x}(t) = \alpha u + p\left(x, x^*\right) x - \beta x & \text{(4.20a)} \\ \dot{y}(t) = \beta x + q\left(y, y^*\right) y - \gamma y & \text{(4.20b)} \\ \dot{z}(t) = \gamma y + r\left(z, z^*\right) z & \text{(4.20c)} \\ \dot{x^*}(t) = \alpha u^* + p\left(x, x^*\right) x^* - \beta x^* & \text{(4.20d)} \\ \dot{y^*}(t) = \beta x^* + q\left(y, y^*\right) y^* - \gamma y^* & \text{(4.20e)} \\ \dot{z^*}(t) = \gamma y^* + r\left(z, z^*\right) z^* & \text{(4.20f)} \end{cases}$$

In Eqs. 4.20a–4.20f, we replace the logistic terms used earlier with general growth/decay coefficient functions, $p(x, x^*)$, $q(y, y^*)$, and $r(z, z^*)$. Each of the functions p, q, r, may assume either positive or negative values, indicating homeostasis-based growth or decay, respectively. As we are no longer modeling the infection and treatment process described earlier, we may take the ODEs in Eqs. 4.20a–4.20f to be defined for $t \in [0, \infty)$, with initial conditions $x(0), y(0), z(0) > 0$, $x^*(0), y^*(0), z^*(0) = 0$.

We first introduce notation, under the assumption that each of the quantities x, x^*, y, y^*, z, z^* is bounded both above and away from zero. (This can be shown easily, but the proof is tedious and uninteresting.) Define the constants $m_x, m_y, m_z > 0$, and $M_x, M_{x^*}, \cdots M_{z^*} > 0$ to satisfy:

$$m_x \leq x \leq M_x \qquad 0 \leq x^* \leq M_{x^*} \tag{4.21}$$

$$m_y \leq y \leq M_y \qquad 0 \leq y^* \leq M_{y^*} \tag{4.22}$$

$$m_z \leq z \leq M_z \qquad 0 \leq z^* \leq M_{z^*} \tag{4.23}$$

We are most interested in the asymptotic behavior of $\frac{z^*}{z}$, which describes the ratio of protected to unprotected cells. To do this, we first identify the asymptotic behavior of $\frac{x^*}{x}$ and $\frac{y^*}{y}$.

Proposition 4.2.1. *Let $x(t)$ and $x^*(t)$ be solutions of the ODE system in Eq. 4.20a–4.20f. Then either $\frac{x^*(t)}{x(t)} = \frac{u^*}{u}$ for all $t \geq 0$, or $\frac{x^*(t)}{x(t)} \neq \frac{u^*}{u}$ for all $t \geq 0$. Additionally, under*

the physically intuitive assumptions that u, u^*, $x(0) > 0$, *and* $x^*(0) = 0$, *we discern that* $\frac{x^*(t)}{x(t)} \leq \frac{u^*}{u}$ *for all* $t \geq 0$.

Proof. Consider Eqs. 4.20a, 4.20b:

$$\begin{aligned} \dot{x} &= \alpha u + p(x, x^*)x - \beta x \\ \dot{x^*} &= \alpha u^* + p(x, x^*)x^* - \beta x^* \end{aligned}$$

By dividing the first by u and the second by u^*, we see that the functions $\frac{x}{u}$ and $\frac{x^*}{u^*}$ satisfy the system:

$$\frac{\dot{x}}{u} = \alpha + p(x, x^*)\left(\frac{x}{u}\right) - \beta\left(\frac{x}{u}\right) \tag{4.24}$$

$$\frac{\dot{x^*}}{u^*} = \alpha + p(x, x^*)\left(\frac{x^*}{u^*}\right) - \beta\left(\frac{x^*}{u^*}\right) \tag{4.25}$$

In particular, $\frac{x}{u}$ and $\frac{x^*}{u^*}$ satisfy the same ODE. But solutions to this ODE are unique, so there exists no time t at which $\frac{x(t)}{u} = \frac{x^*(t)}{u^*}$, or, by simple rearrangement, $\frac{x^*(t)}{x(t)} = \frac{u^*}{u}$, unless $\frac{x(t)}{u} = \frac{x^*(t)}{u^*}$ for all t in the first place. By subtracting Eq. 4.25 from Eq. 4.24, we find that the function $x_{aux}(t) := x/u - x^*/u^*$ satisfies the ODE,

$$\dot{x}_{aux} = (p(x, x^*) - \beta)\, x_{aux}, \tag{4.26}$$

which has solution,

$$x_{aux}(t) = x_{aux}(0)e^{\int_0^t p(x(s),x^*(s))-\beta ds} = \frac{x(0)}{u}e^{\int_0^t p(x(s),x^*(s))-\beta ds} > 0. \tag{4.27}$$

After rearranging the expression in Eq. 4.27, we have that $\frac{x^*}{x} \leq \frac{u^*}{u}$. □

Proposition 4.2.2. *Let* $x(t)$ *and* $x^*(t)$ *be defined by Eqs. 4.20a, 4.20b. Then the quantity*

$\left|\frac{x^*}{x} - \frac{u^*}{u}\right|$ *decays to zero exponentially as* $t \longrightarrow \infty$*, at a rate directly proportional to* au*, and inversely proportional to* M_x*.*

Proof. We begin by computing $\frac{d}{dt}\frac{1}{2}\left(\frac{x^*}{x} - \frac{u^*}{u}\right)^2$:

$$\begin{aligned}
\frac{d}{dt}\frac{1}{2}\left(\frac{x^*}{x} - \frac{u^*}{u}\right)^2 &= \left(\frac{x^*}{x} - \frac{u^*}{u}\right)\frac{d}{dt}\left(\frac{x^*}{x}\right) \\
&= \left(\frac{x^*}{x} - \frac{u^*}{u}\right)\left(\frac{x\dot{x}^* - x^*\dot{x}}{x^2}\right) \\
&= \left(\frac{x^*}{x} - \frac{u^*}{u}\right)\left(\frac{\alpha x u^* - \alpha x^* u}{x^2}\right) \\
&= \frac{\alpha u}{x}\left(\frac{x^*}{x} - \frac{u^*}{u}\right)\left(\frac{u^*}{u} - \frac{x^*}{x}\right) \\
&= -\left(\frac{\alpha u}{x}\right)\left(\frac{x^*}{x} - \frac{u^*}{u}\right)^2 \\
&\leq -\left(\frac{\alpha u}{M_x}\right)\left(\frac{x^*}{x} - \frac{u^*}{u}\right)^2
\end{aligned}$$

In the last line above, we used that $x \leq M_x$. We have arrived at the Gronwall-type differential inequality:

$$\frac{d}{dt}\left(\frac{x^*}{x} - \frac{u^*}{u}\right)^2 \leq -\left(\frac{2\alpha u}{M_x}\right)\left(\frac{x^*}{x} - \frac{u^*}{u}\right)^2,$$

which can be solved to obtain:

$$\left(\frac{x^*(t)}{x(t)} - \frac{u^*}{u}\right)^2 \leq \left(\frac{x^*(0)}{x(0)} - \frac{u^*}{u}\right)^2 e^{\frac{-2\alpha u}{M_x}t}.$$

Thus, $\left|\frac{x^*(t)}{x(t)} - \frac{u^*}{u}\right| \longrightarrow 0$ as $t \longrightarrow \infty$, and in particular, $\frac{x^*(t)}{x(t)} \longrightarrow \frac{u^*}{u}$ as $t \longrightarrow \infty$. We obtain the following bound on the decay:

$$\left|\frac{x^*(t)}{x(t)} - \frac{u^*}{u}\right| \leq \left|\frac{x^*(0)}{x(0)} - \frac{u^*}{u}\right| e^{\frac{-\alpha u}{M_x}t}, \tag{4.28}$$

which will be used in the next computation. □

We now show that $\frac{y^*}{y} \longrightarrow \frac{x^*}{x}$ as $t \longrightarrow \infty$.

Proposition 4.2.3. *Let $x(t)$, $x^*(t)$, $y(t)$ and $y^*(t)$ be defined by Eqs. 4.20a–4.20f. Then $\left|\frac{y^*}{y} - \frac{x^*}{x}\right|$ decays exponentially to 0 as $t \longrightarrow \infty$. From this and Proposition 4.2.2, it follows that $\left|\frac{y^*}{y} - \frac{u^*}{u}\right| \longrightarrow 0$ as $t \longrightarrow \infty$. Additionally, under the assumptions that $u, u^*, x(0), y(0) > 0$, and $x^*(0), y^*(0) = 0$, we deduce that $\frac{y^*(t)}{y(t)} \leq \frac{u^*}{u}$ for $t \geq 0$.*

Proof. In analogue with the proof of Proposition 4.2.2, we begin by computing $\frac{d}{dt}\frac{1}{2}\left(\frac{y^*}{y} - \frac{x^*}{x}\right)^2$.

$$\begin{aligned}
\frac{d}{dt}\frac{1}{2}\left(\frac{y^*}{y} - \frac{x^*}{x}\right)^2 &= \left(\frac{y^*}{y} - \frac{x^*}{x}\right)\frac{d}{dt}\left(\frac{y^*}{y} - \frac{x^*}{x}\right) \\
&= \left(\frac{y^*}{y} - \frac{x^*}{x}\right)\left(\beta\left(\frac{x^*y - xy^*}{y^2}\right) - \alpha\left(\frac{xu^* - ux^*}{x^2}\right)\right) \\
&= \left(\frac{y^*}{y} - \frac{x^*}{x}\right)\left(\left(\frac{\beta x}{y}\right)\left(\frac{x^*}{x} - \frac{y^*}{y}\right) - \left(\frac{\alpha u}{x}\right)\left(\frac{u^*}{u} - \frac{x^*}{x}\right)\right) \\
&= -\frac{\beta x}{y}\left(\frac{y^*}{y} - \frac{x^*}{x}\right)^2 - \frac{\alpha u}{x}\left(\frac{u^*}{u} - \frac{x^*}{x}\right)\left(\frac{y^*}{y} - \frac{x^*}{x}\right) \\
&\leq -\frac{\beta x}{y}\left(\frac{y^*}{y} - \frac{x^*}{x}\right)^2 + \frac{\alpha u}{x}\left|\frac{u^*}{u} - \frac{x^*}{x}\right|\left|\frac{y^*}{y} - \frac{x^*}{x}\right| \\
&\leq -\frac{\beta x}{y}\left(\frac{y^*}{y} - \frac{x^*}{x}\right)^2 + \frac{\alpha u}{x}\left|\frac{u^*}{u} - \frac{x^*}{x}\right|\left(\left|\frac{y^*}{y}\right| + \left|\frac{x^*}{x}\right|\right) \\
&\leq -\frac{\beta x}{y}\left(\frac{y^*}{y} - \frac{x^*}{x}\right)^2 + \frac{\alpha u}{x}\left|\frac{x^*(0)}{x(0)} - \frac{u^*}{u}\right| e^{\frac{-\alpha u}{M_x}t}\left(\left|\frac{y^*}{y}\right| + \left|\frac{x^*}{x}\right|\right) \\
&\leq \frac{-\beta m_x}{M_y}\left(\frac{y^*}{y} - \frac{x^*}{x}\right)^2 + \frac{\alpha u}{m_x}\left|\frac{x^*(0)}{x(0)} - \frac{u^*}{u}\right| e^{\frac{-\alpha u}{M_x}t}\left(\frac{M_{y^*}}{m_y} + \frac{M_{x^*}}{m_x}\right).
\end{aligned}$$

The second-to-last inequality above comes from Eq. 4.28, and the last inequality comes from Eqs. 4.21, 4.22. Now, for simplicity, define the constant $R := \frac{\alpha u}{m_x}\left|\frac{x^*(0)}{x(0)} - \frac{u^*}{u}\right|\left|\frac{M_{y^*}}{m_y} + \frac{M_{x^*}}{m_x}\right|$, and consolidate the computations above into the differential inequality:

$$\frac{d}{dt}\left(\frac{y^*}{y} - \frac{x^*}{x}\right)^2 \leq \frac{-2\beta m_x}{M_y}\left(\frac{y^*}{y} - \frac{x^*}{x}\right)^2 + 2Re^{\frac{-\alpha u}{m_x}t},$$

which can be solved to obtain the inequality,

$$\left(\frac{y^*}{y} - \frac{x^*}{x}\right)^2 \leq e^{\frac{-2\beta m_x}{M_y}t}\left(\left(\frac{y^*(0)}{y(0)} - \frac{x^*(0)}{x(0)}\right) - \frac{2R}{\left(\frac{2\beta m_x}{M_y} - \frac{\alpha u}{m_x}\right)}\right) + \frac{2R}{\left(\frac{2\beta m_x}{M_y} - \frac{\alpha u}{m_x}\right)}e^{\frac{-\alpha u}{m_x}t}, \tag{4.29}$$

from which it follows that $\left|\frac{y^*}{y} - \frac{x^*}{x}\right| \longrightarrow 0$ as $t \longrightarrow \infty$, and thus that $\frac{y^*}{y} \longrightarrow \frac{x^*}{x}$ as $t \longrightarrow \infty$. In conjunction with Proposition 4.3.2, this implies that $\frac{y^*}{y} \longrightarrow \frac{u^*}{u}$ as $t \longrightarrow \infty$.

From Proposition 4.2.1, we know that under the assumptions $u, u^*, x(0) > 0$, and $x^*(0) = 0$, $\frac{x^*(t)}{x(t)} \leq \frac{u^*}{u}$, or $x^*(t)u \leq x(t)u$, for $t \geq 0$. Multiply Eq. 4.20b by the constant u^*, and Eq. 4.20e by the constant u to rewrite Eqs. 4.20b, 4.20e as:

$$\frac{d}{dt}(u^*y) = \beta x u^* + q(u^*y) - \gamma(u^*y), \tag{4.30}$$

$$\frac{d}{dt}(uy^*) = \beta x^* u + q(uy^*) - \gamma(uy^*). \tag{4.31}$$

By subtracting Eq. 4.31 from Eq. 4.30, the quantity $y_{aux}(t) := u^*y(t) - uy^*(t)$ satisfies the ODE,

$$\dot{y}_{aux} = (q(y, y^*) - \gamma)\, y_{aux} + \beta(xu^* - x^*u), \tag{4.32}$$

which can be solved to obtain,

$$y_{\text{aux}}(t)e^{-\int_0^t (q(y(s),y^*(s))-\gamma)ds} = y_{\text{aux}}(0) + \beta\int_0^t x_{\text{aux}}(s)e^{-\int_0^s (q(y(w),y^*(w))-\gamma)dw}ds. \tag{4.33}$$

From the fact that $x_{\text{aux}}(t) \geq 0$, and $y_{\text{aux}}(0) = u^*y(0) > 0$, we have $y_{\text{aux}}(t) \geq 0$.

We now simplify the bound in Eq. 4.29. Define the constants S, T, Q as such:

$$
\begin{aligned}
S &:= \left(\left(\frac{y^*(0)}{y(0)} - \frac{x^*(0)}{x(0)} \right)^2 - \frac{2R}{\left(\frac{2\beta m_x}{M_y} - \frac{\alpha u}{m_x} \right)} \right) \\
T &:= \frac{2R}{\left(\frac{2\beta m_x}{M_y} - \frac{\alpha u}{m_x} \right)} \\
Q &:= \min \{ \frac{2\beta m_x}{M_y}, \frac{\alpha u}{m_x} \}
\end{aligned}
$$

Then Eq. 4.29 may be modified and expressed more simply in terms of these constants as follows:

$$
\begin{aligned}
\left(\frac{y^*}{y} - \frac{x^*}{x} \right)^2 &\leq e^{\frac{-2\beta m_x}{M_y} t} \left(\left(\frac{y^*(0)}{y(0)} - \frac{x^*(0)}{x(0)} \right) - \frac{2R}{\left(\frac{2\beta m_x}{M_y} - \frac{\alpha u}{m_x} \right)} \right) + \frac{2R}{\left(\frac{2\beta m_x}{M_y} - \frac{\alpha u}{m_x} \right)} e^{\frac{-\alpha u}{m_x} t} \\
&= S e^{\frac{-2\beta m_x}{M_y} t} + T e^{\frac{-\alpha u}{m_x} t} \\
&\leq |S| e^{\frac{-2\beta m_x}{M_y} t} + |T| e^{\frac{-\alpha u}{m_x} t} \\
&\leq (|S| + |T|) \, e^{-Qt}
\end{aligned}
$$

which can be simplified to:

$$
\left| \frac{y^*}{y} - \frac{x^*}{x} \right| \leq (|S| + |T|)^{\frac{1}{2}} \, e^{\frac{-Q}{2} t} \tag{4.34}
$$

□

We now proceed to the most essential result, that $\frac{z^*}{z} \longrightarrow \frac{u^*}{u}$ as $t \longrightarrow \infty$.

Proposition 4.2.4. *Let $z(t)$, $z^*(t)$, $y(t)$, $y^*(t)$, $x(t)$, and $x^*(t)$ be defined by Eqs. 4.20a–4.20f. Then $\left| \frac{z^*}{z} - \frac{y^*}{y} \right| \longrightarrow 0$ as $t \longrightarrow \infty$, and thus $\frac{z^*}{z} \longrightarrow \frac{u^*}{u}$ as $t \longrightarrow \infty$. If, in addition, $u, u^*, x(0), y(0), z(0) > 0$, and $x^*(0), y^*(0), z^*(0) = 0$, then $\frac{z^*(t)}{z(t)} \leq \frac{u^*}{u}$ for all $t \geq 0$.*

Proof. We begin by computing $\frac{d}{dt} \frac{1}{2} \left(\frac{z^*}{z} - \frac{y^*}{y} \right)^2$:

$$
\begin{aligned}
\frac{d}{dt}\frac{1}{2}\left(\frac{z^*}{z}-\frac{y^*}{y}\right)^2 &= \left(\frac{z^*}{z}-\frac{y^*}{y}\right)\frac{d}{dt}\left(\frac{z^*}{z}-\frac{y^*}{y}\right) \\
&= \left(\frac{z^*}{z}-\frac{y^*}{y}\right)\left(\left(\frac{z\dot{z^*}-z^*\dot{z}}{z^2}\right)-\left(\frac{y\dot{y^*}-y^*\dot{y}}{y^2}\right)\right) \\
&= \left(\frac{z^*}{z}-\frac{y^*}{y}\right)\left(\left(\frac{\gamma y^* z-\gamma y z^*}{z^2}\right)-\left(\frac{\beta x^* y-\beta x y^*}{y^2}\right)\right) \\
&= \left(\frac{z^*}{z}-\frac{y^*}{y}\right)\left(\left(\frac{\gamma y}{z}\right)\left(\frac{y^*}{y}-\frac{z^*}{z}\right)-\left(\frac{\beta x}{y}\right)\left(\frac{x^*}{x}-\frac{y^*}{y}\right)\right) \\
&= -\left(\frac{\gamma y}{z}\right)\left(\frac{z^*}{z}-\frac{y^*}{y}\right)^2-\left(\frac{\beta x}{y}\right)\left(\frac{x^*}{x}-\frac{y^*}{y}\right)\left(\frac{z^*}{z}-\frac{y^*}{y}\right) \\
&\leq -\left(\frac{\gamma y}{z}\right)\left(\frac{z^*}{z}-\frac{y^*}{y}\right)^2+\frac{\beta|x|}{|y|}\left|\frac{x^*}{x}-\frac{y^*}{y}\right|\left(\left|\frac{z^*}{z}\right|+\left|\frac{y^*}{y}\right|\right) \\
&\leq -\left(\frac{\gamma y}{z}\right)\left(\frac{z^*}{z}-\frac{y^*}{y}\right)^2+\frac{\beta|x|}{|y|}\left(|S|+|T|\right)^{\frac{1}{2}}e^{-\frac{Q}{2}t}\left(\left|\frac{z^*}{z}\right|+\left|\frac{y^*}{y}\right|\right) \\
&\leq -\left(\frac{\gamma m_y}{M_z}\right)\left(\frac{z^*}{z}-\frac{y^*}{y}\right)^2+\left(\frac{\beta M_x}{m_y}\right)\left(|S|+|T|\right)^{\frac{1}{2}}e^{\frac{-Q}{2}t}\left(\frac{M_{z^*}}{m_z}+\frac{M_{y^*}}{m_y}\right)
\end{aligned}
$$

The second-to-last inequality follows from Eq. 4.34, and the very last inequality follows from Eqs. 4.21, 4.22, 4.23. Rearranging terms in the derivation above, we obtain the differential inequality:

$$
\frac{d}{dt}\left(\frac{z^*}{z}-\frac{y^*}{y}\right)^2 \leq -\left(\frac{2\gamma m_y}{M_z}\right)\left(\frac{z^*}{z}-\frac{y^*}{y}\right)^2+\left(\frac{2\beta M_x}{m_y}\right)\left(|S|+|T|\right)^{\frac{1}{2}}e^{\frac{-Q}{2}t}\left(\frac{M_{z^*}}{m_z}+\frac{M_{y^*}}{m_y}\right).
$$

This can be solved to obtain the inequality:

$$
\left(\frac{z^*}{z}-\frac{y^*}{y}\right)^2 \leq e^{\frac{-2\gamma m_y}{M_z}t}\left(\frac{z^*(0)}{z(0)}-\frac{y^*(0)}{y(0)}\right)^2 \tag{4.35}
$$

$$
+\left(\frac{2\beta M_x}{m_y\left(\frac{2\gamma m_y}{M_z}-Q\right)}\right)\left(|S|+|T|\right)\left(\frac{M_{z^*}}{m_z}+\frac{M_{y^*}}{m_y}\right)\left(e^{\frac{-Q}{2}t}-e^{\frac{-2\gamma m_y}{M_z}t}\right) \tag{4.36}
$$

from which it follows that $\left|\frac{z^*}{z}-\frac{y^*}{y}\right| \longrightarrow 0$ as $t \longrightarrow \infty$. Thus, $\frac{z^*}{z} \longrightarrow \frac{y*}{y}$ as $t \longrightarrow \infty$, and

in conjunction with Proposition 4.3.3, $\frac{z^*}{z} \longrightarrow \frac{u^*}{u}$ as $t \longrightarrow \infty$.

In a process similar to that used to establish Eq. 4.33, we can show that $z_{aux}(t) := u^*z - uz^* \geq 0$, from which it follows that $\frac{z^*}{z} \leq \frac{u^*}{u}$. □

4.2.5 Asymptotic Behavior with Virus Present

We established in the previous section that if the bone marrow transplant were administered in the absence of infection, the ratio of protected to unprotected cells that would arise in the thymus and peripheral blood would equal the ratio of protected to unprotected stem cells. We now consider how this ratio is disturbed by the presence of virus at the time of transplant. Numerical simulation indicates that in general, $\lim_{t\to\infty} z^*(t)/z(t) \gg u^*/u$ in the presence of virus, but that the behavior of $z^*(t)$ and $z(t)$ is highly sensitive to the parameters of the system.

The presence of virus complicates the dynamical interactions between the HIV-immune and HIV-susceptible cell populations. The presence of the HIV-immune cell pool confers a certain degree of protection on the HIV-susceptible pool, as HIV-immune cells are infected–and release new virions–only rarely, if ever. This may allow for growth of the HIV-susceptible population. However, both cell populations are treated as one unified pool by the homeostatic mechanism, and expansion of the HIV-immune cell pool leaves less room for the HIV-susceptible pool to expand. To investigate this, we consider how the asymptotic behavior of the functions $z^*(t)$, $z(t)$ varies as the parameter η, which represents the viral clearance rate, changes. In Fig. 4.1, we plot the asymptotic values of $z(t)$, $z^*(t)$, and $z^*(t)/z(t)$ for different choices of u^*/u varying from $u^*/u = 0.01$ to $u^*/u = 1.04$, with the sum $u+u^*$ (total stem cells) preserved. In Figs. 4.1(a)-(c), $\eta = 0.3$, and in Figs. 4.1(d)-(f), $\eta = 0.6$. (All other parameter values are identical in Figs. 4.1(a)-(f), as described in the caption.) When the viral clearance rate is low, $z(t)$ decreases, while $z^*(t)$ and $z^*(t)/z(t)$ increase, with increasing u^*/u, as shown in Figs. 4.1(a)-(c). In this situation, the body eradicates virus less effectively, and the growing HIV-immune cell population is less capable of protecting the susceptible cell population and allowing it to expand, resulting in a decrease in $z(t)$ as u^*/u increases. When the viral clearance rate is high, however, $z(t)$ and $z^*(t)$ both increase with increasing u^*/u, while $z^*(t)/z(t)$

decreases, as shown in Figs. 4.1(d)-(f). In this case, the body clears the virus more effectively, and thus the added protected afforded by the presence of a growing HIV-immune cell population allows for expansion of the HIV-susceptible cell pool. Future work on this model will consist of investigations into sensitivity to other parameters.

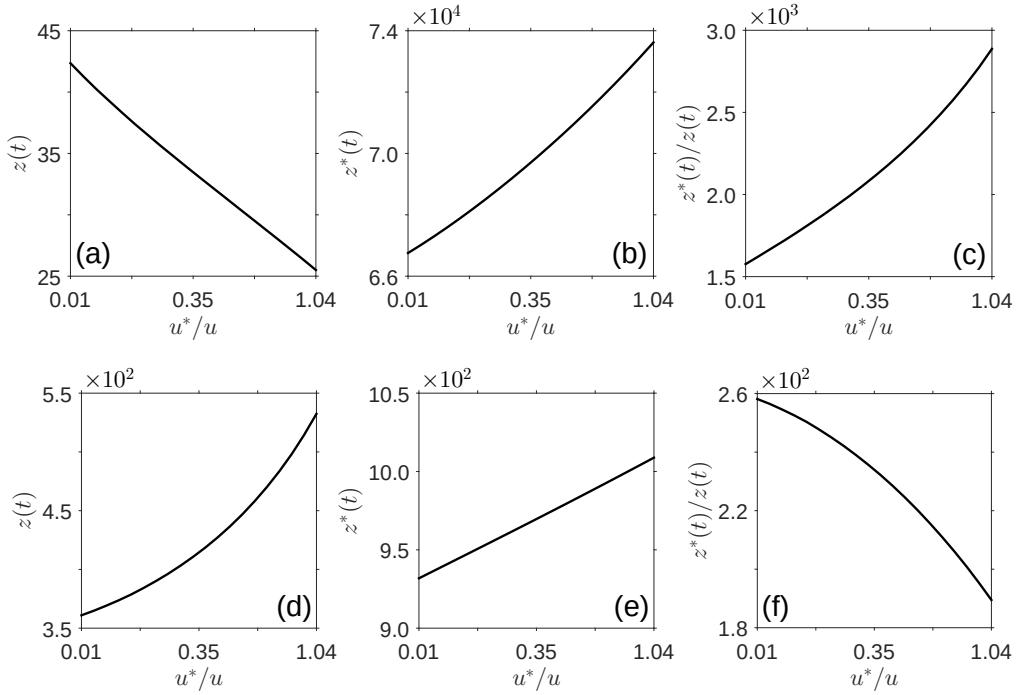

Figure 4.1: **Simulation of Stage 3 with virus** (a)-(c) Plots of $z(3000)$, $z^*(3000)$, and $z^*(3000)/z(3000)$, respectively, for varying u^*/u with $\eta = 0.3$. (d)-(f) Plots of $z(3000)$, $z^*(3000)$, and $z^*(3000)/z(3000)$, respectively, for varying u^*/u with $\eta = 0.6$. Other parameter values: $\lambda_y = \lambda_z = 10^{-4}$, $\lambda_{y^*} = \lambda_{z^*} = 5 \times 10^{-6}$, $k_y = k_z = 0.6$, $c_y = c_z = 0.2$, $\alpha = 1$, $\beta = 0.4$, $\gamma = 0.1$, $u + u^* = 2 \times 10^3$. Initial conditions were produced as described in this chapter, by evaluating the full ODE system starting at $t = 0$, with initial conditions $x(0) = y(0) = z(0) = 0$ at the start of Stage 1. We took $t_1 = 200$, $t_2 = 500$, and $t_3 = 3000$. Thus, initial conditions for Stage 3 were taken from the values that resulted at t_2.

[AJL02] Bruce Alberts, Alexander Johnson, Julian Lewis, Martin Raff, Keith Roberts, and Peter Walter. *Molecular Biology of the Cell*. Garland Science, 2002.

[ALV00] Jonathan D. Ashwell, Frank W. M. Lu, and Melanie S. Vacchio. "Glucocorticoids in T Cell Development and Function." *Annual Review of Immunology*, **18**:309–345, 2000.

[AS14] Victor Appay and Delphine Sauce. "Naive T cells: The crux of cellular immune aging?" *Experimental Gerontology*, **54**:90–93, 2014.

[ASR86] A K Ageev, V S Sidorin, M V Rogachev, and I V Timofeev. "Morphologic characteristics of the changes in the thymus and spleen during alcoholism." *Arkhiv Patologii*, **48**(10):33–39, 1986.

[BAC09] Iren Bains, Rustom Antia, Robin Callard, and Andrew J. Yates. "Quantifying the development of the peripheral naive CD4+ T-cell pool in humans." *Immunobiology*, **113**(22):5480–5487, 2009.

[BBM98] S. P. Berzins, R.I. Boyd, and J. F. Miller. "The role of the thymus and recent thymic migrants in the maintenance of the adult peripheral lymphocyte pool." *The Journal of Experimental Medicine*, **187**(11):1839–1848, 1998.

[BHS05] Linda M. Bradley, Laura Haynes, and Susan L. Swain. "IL-7: maintaining T-cell memory and achieving homeostasis." *Trends in Immunology*, **26**(3):172–176, 2005.

[BMS14] Dawn Brass, Pam McKay, and Fiona Scott. "Investigating an incidental finding of lymphopenia." *British Medical Journal*, **348**:1–3, 2014.

[BPS14] Olga V. Britanova, Ekaterina V. Putintseva, Mikhail Shugay, Ekaterina M. Merzlyak, Maria A. Turchaninova, Dmitriy B. Staroverov, Dmitriy A. Bolotin, Sergey Lukyanov, Ekaterina A. Bogdanova, Ilgar Z. Mamedov, Yuriy B. Lebedev, and Dmitriy M. Chudakov. "Age-related decrease in TCR repertoire diversity measured with deep and normalized sequence profiling." *The Journal of Immunology*, **192**(6):2689–2698, 2014.

[BSA02] Craig H. Bassing, Wojciech Swat, and Frederick W. Alt. "The Mechanism and Regulation of Chromosomal V(D)J Recombination." *Cell*, **109**(2):S45–S55, 2002.

[BSR89] Joop van Baarlen, Henk-Jan Schuurman, Roelie Reitsma, and Jonne Huber. "Acute Thymuc Involution During Infancy and Childhood: Immunohistology of the Thymus and Peripheral Lymphoid Tissues after Acute Illness." *Pediatric Pathology*, **19**(10):261–275, 1989.

[BTY09] Iren Bains, Rodolphe Thiébaut, Andrew J. Yates, and Robin Callard. "Quantifying thymic export: Combining models of naive T cell proliferation and TCR excision circle dynamics gives an explicit measure of thymic output." *The Journal of Immunology*, **183**(7):4329–4336, 2009.

[CC94] Robert K. Colwell and Jonathan A. Coddington. "Estimating terrestrial biodiversity through extrapolation." *Philosophical Transactions of the Royal Society B*, **345**(1311):101–118, 1994.

[Cha84] Anne Chao. "Nonparametric estimation of the number of classes in a population." *Scandanavian Journal of Statistics*, **11**(4):265–270, 1984.

[CHC80] Michael Cohen, Charles A. Hill, Ayten Cangir, and Margaret P. Sullivan. "Thymic rebound after treatment of childhood tumors." *American Journal of Roentgenology*, **135**(1):151–156, 1980.

[CL92] Anne Chao and Shen-Ming Lee. "Estimating the number of classes via sample coverage." *Journal of the American Statistical Association*, **87**(417):210–217, 1992.

[Cor09] A Corthday. "How do Regulatory T Cells Work?" *Scandanavian Journal of Immunology*, **70**(4):326–336, 2009.

[CSA06] Daniella Arêas Mendes da Cruz, João Santana Silva, Vinícius Cotta de Almeida, and Wilson Savino. "Altered thymocyte migration during experimental acute Trypanosoma cruzi infection: combined role of fibronectin and the chemokines CXCL12 and CCL4." *European Journal of Immunology*, **36**(6):1486–1493, 2006.

[CVD16] Mohammed S. Chaudhry, Enrico Velardi, Jarrod A. Dudakov, and Marcel R.M. van den Brink. "Thymus: The Next (Re)Generation." *Immunological Reviews*, **271**(1):56–71, 2016.

[CYB13] Jian L. Campian, Xiaobu Ye, Malcolm Brock, and Stuart A. Grossman. "Treatment-related Lymphopenia in Patients With Stage III Non-Small-Cell Lung Cancer." *Cancer Investigation*, **31**(3):183–188, 2013.

[CZG87] Peter L. Choyke, Robert K. Zemon, Joseph E. Gootenberg, Jay N. Greenberg, Frederic Hoffer, and Joseph A. Frank. "Thymic atrophy and regrowth in response to chemotherapy: CT evaluation." *American Journal of Roentgenology*, **149**(2):269–272, 1987.

[DCW01] D. E. DeFriend, J. M. Coote, M. P. Williams, and J. A. Copplestone. "Thymic Enlargement in an Adult Following a Severe Infection." *Clinical Radiology*, **56**(4):331–333, 2001.

[DL12] James Dooley and Adrian Liston. "Molecular control over thymic involution: From cytokines and microRNA to aging and adipose tissue." *European Journal of Immunology*, **42**(5):1073–1079, 2012.

[DMM17] Jonathan Desponds, Andreas Mayer, Thierry Mora, and Aleksandra M. Walczak. "Population dynamics of immune repertoires." *ArXiv e-prints*, 2017.

[DMW15] Jonathan Desponds, Thierry Mora, and Aleksandra Walczak. "Fluctuating fitness shapes the clone-size distribution of immune repertoires." *Proceedings of the National Academy of Sciences*, **113**(2):274–279, 2015.

[dP13] Rob J. de Boer and Alan S. Perelson. "Quantifying T lymphocyte turnover." *Journal of Theoretical Biology*, **327**:45–87, 2013.

[Ewe72] W.J. Ewens. "The sampling theory of selectively neutral alleles." *Theoretical Population Biology*, **3**(1):87–112, 1972.

[FE08] Douglas M. Fleming and Alex J. Elliot. "The impact of influenza on health and health care utilisation of elderly people." *Vaccine*, **32**(1):S1–S9, 2008.

[FJB14] S. M. Falkenberg, C. Johnson, F.V. Bauermann, J. McGill, M.V. Palmer, R.E. Sacco, and J.F. Ridpath. "Changes observed in the thymus and lymph nodes 14 days after exposure to BVDV field strains of enhanced or typical virulence in neonatal calves." *Veterinary Immunology or Immunopathology*, **160**(1–2):70–80, 2014.

[FM05] Terry J. Fry and Crystal L. Mackall. "The many faces of IL-7: from lymphopoesis to peripheral T cell maintenance." *The Journal of Immunology*, **174**(11):6571–6576, 2005.

[FVP00] Francesco F. Fagnoni, Rosanna Vescovini, Giovanni Passeri, Goivanni Bologna, Mario Pedrazzoni, Giampaolo Lavagetto, Amos Casti, Claudio Franceschi, Mario Passeri, and Paolo Sansoni. "Shortage of circulating naive CD8+ T cells provides new insights on immunodeficiency in aging." *Blood*, **95**(9):2860–2868, 2000.

[FYR14] Donna L. Farber, Naomi A. Yudanin, and Nicholas P. Restifo. "Human memory T cells: generation, compartmentalization and homeostasis." *Nature Reviews Immunology*, **14**(1):24–35, 2014.

[GE00] Amiela Globerson and Rita B. Effros. "Aging of Lymphocytes and Lymphocytes in the Aged." *Immunology Today*, **21**(10):515–521, 2000.

[GEC15] Stuart A. Grossman, Susannah Ellsworth, Jian Campian, Aaron T. Wild, Joseph M. Herman, Dan Laheru, Malcolm Brock, Ani Balmanoukian, and Xiaobu Ye. "Survival in patients with severe lymphopenia following treatment with radiation and chemotherapy for newly diagnosed solid tumors." *Journal of the National Comprehensive Cancer Network*, **13**(10):1225–1231, 2015.

[Ger99] Peter Gergely. "Drug-Induced Lymphopenia." *Drug Safety*, **21**(2):91–100, 1999.

[GFN85] WW Grody, S Fliegiel, and F Naeim. "Thymus involution in the acquired immunodeficiency syndrome." *American Journal of Clinical Pathology*, **84**(1):85–95, 1985.

[GGL72] David W. Gelfand, Armond S. Goldman, Edward J. Law, Bruce G. Macmillan, Duane Larson, Sally Abston, and J. Tracy Schreiber. "Thymic Hyperplasia in Children Recovering from Thermal Burns." *The Journal of Trauma*, **12**(9):813–817, 1972.

[GHS07] AL Gruver, LL Hudson, and JD Sempowski. "Immunosenescence of Aging." *The Journal of Pathology*, **211**(2):144–156, 2007.

[GKC15] Sidhartha Goyal, Sanggu Kim, Irvin S Y Chen, and Tom Chou. "Mechanisms of blood homeostasis: lineage tracking and a neutral model of cell populations in rhesus macaques." *BMC Biology*, **13**(85):1–14, 2015.

[GLC01] Lia Ginaldi, Maria Francesca Loreto, Maria Pia Corsi, Marco Modesti, and Massimo de Martinis. "Immunosenescence and Infectious Diseases." *Microbes and Infection*, **3**(10):851–857, 2001.

[GLW07] Jörg J. Goronzy, Won-Woo Lee, and Cornelia M. Weyland. "Aging and T-cell Diversity." *Experimental Gerontology*, **42**(5):400–406, 2007.

[GNV10] Jacy Gameiro, Patrïcia Nagib, and Liana Verinaud. "The thymus microenvironment in regulating thymocyte differentiation." *Cell Adhesion and Migration*, **4**(3):382–390, 2010.

[GQO15] Jörg J. Goronzy, Qian Qi, Richard A. Olshen, and Cornelia M. Weyland. "High-throughput sequencing insights into T-cell receptor diversity in aging." *Genome Medicine*, **7**:1–3, 2015.

[GS08] Amanda L. Gruver and Gregory D. Sempowski. "Cytokines, leptin, and stress-induced thymic atrophy." *Journal of Leukocyte Biology*, **84**(4):915–923, 2008.

[GSC03] Merica Glavina-Durdov, Oskar Springer, Vesna Ćapkun, Žana Saratlija-Novaković, Damir Rozić, and Miroslava Barle. "The Grade of Acute Thymus Involution in Neonates Correlates with the Duration of Acute Illness and with the Percentage of Lymphocytes in Peripheral Blood Smear." *Biology of the Neonate*, **83**(4):229–234, 2003.

[HLC13] Tharindi Hapuarachchi, Joanna Lewis, and Robin E. Callard. "A mechanistic mathematical model for naive CD4 T cell homeostasis in healthy adults and children." *Frontiers in Immunology*, **4**(366):1–6, 2013.

[HMK06] Jason Hataye, James J. Moon, Alexander Khoruts, Cavan Reilly, and Marc K. Jenkins. "Naïve and Memory CD4+ T Cell Survival Controlled by Clonal Abundance." *Science*, **312**(5770):114–116, 2006.

[JCM09] Marc K. Jenkins, H. Hamlet Chu, James B. McLachlan, and James J. Moon. "On the composition of the preimmune repertoire of T cells specific for peptide-major histocompatibility ligands." *Annual Review of Immunology*, **28**:275–294, 2009.

[JJU01] E. Juretić, A. Juretić, B. Užarević, and M. Petrovečki. "Alterations in Lymphocyte Phenotype of Preterm Infected Newborns." *Biology of the Neonate*, **80**(3):223–227, 2001.

[KHC02] Fan kun Kong, Chen lo H. Chen, and Max D. Cooper. "Reversible Disruption of Thymic Function by Steroid Treatment." *The Journal of Immunology*, **168**(12):6500–6505, 2002.

[LAG15] Jessica P. Levya-Rangel, Maria de los Angeles Hernández-Cueto, Carlos-Samuel Galan-Enriquez, Marcela López-Medina, and Vianney Ortiz-Navarrete. "Bacterial clearance reverses a skewed T-cell repertoire induced by

Salmonella infection." *Immunity, Inflammation and Disease*, **3**(3):209–223, 2015.

[LBA15] Daniel J. Laydon, Charles R. M. Bangham, and Becca Asquith. "Estimating T-cell repertoire diversity: limitations of classical estimators and a new approach." *Philosophical Transactions of the Royal Society B*, **370**(1675):1–11, 2015.

[LCH16] Grant Lythe, Robin E. Callard, Rollo L. Hoare, and Carmen Molina-Par'ıs. "How many TCR clonotypes does a body maintain?" *Journal of Theoretical Biology*, **389**:214–224, 2016.

[Lon12] Sara S. Long. *Principles and Practice of Pediatric Infectious Diseases (Fourth Edition)*, chapter Laboratory Manifestations of Infectious Disease, pp. 1400–1412. Elsevier, 2012.

[MAL13] Marco Antonio Moro-García, Rebeca Alonso Arias, and Carlos López-Arrea. "When aging reaches CD4+ T-cells: Phenotypic and functional changes." *Frontiers in Immunology*, **4**(107):1–12, 2013.

[Mas98] Don Mason. "A very high level of crossreactivity is an essential feature of the T-cell receptor." *Trends in Immunology*, **19**(9):395–404, 1998.

[MCB14] E. Kathryn Morris, Tancredi Caruso, François Buscot, Markus Fischer, Christine Hancock, Tanja S. Maier, Torsten Meiners, Caroline Müller, Elisabeth Obermaier, Daniel Prati, Stephanie A. Socher, Ilja Sonnemann, Nicole Wäschke, Tesfaye Wubet, Susanne Wurst, and Matthias C. Rillig. "Choosing and using diversity indices: Insights for biological applications from the German Biodiversity Exploratories." *Ecology and Evolution*, **4**:3514–3524, 2014.

[MD08] Janet A. McElhaney and Jan P. Dutz. "Better Influenza Vaccines for Older People: What Will it Take?" *The Journal of Infectious Diseases*, **198**(5):632–634, 2008.

[Met63] Donald Metcalf. "The autonomous behavior of normal thymus grafts." *Australian Journal of Experimental Biology and Medical Sciences*, **41**:437–444, 1963.

[MFB95] Crystal L. Mackall, Thomas A. Fleischer, Margaret R. Brown, Mary P. Andrich, Clara C. Chen, Irwin M. Feuerstein, Marc E. Horowitz, Ian T. Magrath, Aziza T. Shad, Seth M. Steinberg, Leonard H. Wexler, and Ronald E. Gress. "Age, Thymopoiesis, and CD4+ T-Lymphocyte Regeneration after Intensive Chemotherapy." *The New England Journal of Medicine*, **332**(3):143–149, 1995.

[MGL16] Joe S. Mendez, Ashwin Govindan, Jacqueline Leong, Feng Gao, Jiayi Huang, and Jian L. Campian. "Association between treatment-related lymphopenia and overall survival in elderly patients with newly diagnosed glioblastoma." *Journal of Neuro-Oncology*, **127**(2):329–335, 2016.

[MKH03] John M. Murray, Gilbert R. Kaufmann, Philip D. Hodgkin, Sharon R. Lewin, Anthony D. Kelleher, Miles P. Davenport, and John J. Zaunders. "Naive T-cells are maintained by thymic output in early ages but by proliferation without phenotypic change after age 20." *Immunology and Cell Biology*, **81**(6):487–495, 2003.

[MPF96] Ramit Mehr, Alan S. Perelson, Masha Fridkis-Hareli, and Amiela Globerson. "Feedback regulation of T cell development: manifestations in aging." *Mechanisms of Ageing and Development*, **91**(3):195–210, 1996.

[MPF97] Ramit Mehr, Alan S. Perelson, Masha Fridkis-Harelic, and Amiela Globersond. "Regulatory feedback pathways in the thymus." *Immunology Today*, **18**(12):581–585, 1997.

[Mur12] Kenneth Murphy. *Immunobiology*. Garland Science, Taylor and Francis Group, LLC, 2012.

[MW16] Thierry Mora and Aleksandra Walczak. "Quantifying lymphocyte receptor diversity." *ArXiv e-prints*, 2016.

[NLV05] Keither Naylor, Guangjin Li, Abbe N. Vallejo, Won-Won Lee, Kerstin Koetz, Ewa Bryl, Jacek Witkowski, James Fulbright, Cornelia M. Weyand, and Jörg J. Goronzy. "The influence of age on T cell generation and TCR diversity." *The Journal of Immunology*, **174**(11):7446–7452, 2005.

[NSM04] Janko Nicolić-Žugić, Mark K. Slifka, and Ilhem Messaoudi. "The many important facets of T-cell repertoire diversity." *Nature Reviews Immunology*, **4**(2):123–132, 2004.

[PLM10] Greory A. Poland, Joan Langley, Jean pierre Michel, Pierre Van Damme, and Sabine Wicker. "A global prescription for adult immunization: Time is catching up with us." *Vaccine*, **28**(44):7137–7139, September 2010.

[PMI00] José A. Guevara Patiño, Michael W. Marino, Vladimir N. Ivanov, and Janko Nicolić-Žugić. "Sex steroids induce apoptosis of CD8+ CD4+ double positive thymocytes via TNF-α." *European Journal of Immunology*, **30**(9):2586–2592, 2000.

[PML04] Jared F. Purton, Julie A. Monk, Douglas R. Liddicoat, Konstantinos Kyparissoudas, Samy Sakkal, Samantha J. Richardson, Dale I. Godfrey, and Timothy J. Cole. "Expression of the Glucocorticoid Receptor from the 1A Promotor Correlates with T Lymphocyte Sensitivity to Glucocorticoid–Induced Cell Death." *The Journal of Immunology*, **173**(6):3816–3824, 2004.

[QLC14] Qian Qi, Yi Liu, Yong Cheng, Jacob Glanville, David Zhang, Ji-Yeun Lee, Richard A. Olshen, Cornelia M. Weyand, Scott D. Boyd, and Jörg J. Goronzy. "Diversity and clonal selection in the human T-cell repertoire." *Proceedings of the National Academy of Sciences*, **111**(36):13139–13144, 2014.

[RCL13] Joseph Reynolds, Mark Coles, Grant Lythe, and Carmen Molina-París. "Mathematical model of naive T cell division and IL-7 survival thresholds." *Frontiers in Immunology*, **4**(434):1–13, 2013.

[RP07] Ruy M. Ribeiro and Alan S. Perelson. "Determining thymic output quantitatively: Using models to interpret experimental T-cell receptor excision circle (TREC) data." *Immunological Reviews*, **216**(1):21–34, 2007.

[RTB96] Asha G. Rijhsinghani, Kristin Thompson, and Sudershan K. Bhatia. "Estrogen Blocks Early T Cell Development in the Thymus." *American Journal of Reproductive Immunology*, **36**(5):269–277, 1996.

[SAM09] Daryl P. Shanley, Daniella Aw, Nancy R. Manley, and Donald B. Palmer. "An evolutionary perspective on the mechanisms of immunosenescence." *Trends in Immunology*, **30**(7):374–381, 2009.

[Sav06] Wilson Savino. "The thymus is a common target organ in infectious diseases." *PLoS Pathogens*, **2**(6):0472–0483, 2006.

[SDV07] Wilson Savino, Mireille Dardenne, Licio A. Velloso, and Suse Dayse Silva-Barbosa. "The thymus is a common target in malnutrition and infection." *British Journal of Nutrition*, **98**(S1):S11–S16, 2007.

[Sel36] Hans Selye. "Thymus and the adrenals in the response of the organ to injuries and intoxications." *British Journal of Experimental Pathology*, **17**(3):234–248, 1936.

[SKM85] GG Steinmann, B Klaus, and HK Müller-Hermelink. "The involution of the ageing human thymic epithelium is independent of puberty." *Scandanavian Journal of Immunology*, **22**(5):563–575, 1985.

[SMK93] Sharilyn K. Stanley, Joseph M. McCune, Hideto Kaneshima, J. Shawn Justement, Margery Sullivan, Elizabeth Boone, Michael Baseler, Joe Adelsberger, Mark Bonyhadi, Jan Orenstein, Cecil H. Fox, and Anthony S. Fauci. "Human Immunodeficiency Virus Infection of the Human Thymus and Disruption of the Thymic Microenvironment in the SCID-hu Mouse." *The Journal of Experimental Medicine*, **178**(4):1151–1163, 1993.

[SRD13] Nasir Salam, Sanket Rane, Rituparna Das, Matthew Faulkner, Rupali Gund, Usha Kandpal, Virginia Lewis, Hamid Mattoo Savit Prabhu, Vidya Ranganathan, Jeannine Durdik, Anna George, Satyajit Rath, and Vineeta Bal. "T cell ageing: Effects of age on development, survival, function." *Indian Journal of Medical Research*, **138**(5):595–608, 2013.

[Ste86] G. G. Steinmann. *The Human Thymus*, volume 75 of *Current Topics in Pathology*, chapter Changes in The Human Thymus During Aging, pp. 43–88. Springer Berlin Heidelberg, 1986.

[SWS95] J Storek, RP Witherspoon, and R Storb. "T cell reconstitution after bone marrow transplantation into adult patients does not resemble T cell development in early life." *Bone Marrow Transplant*, **16**(3):413–425, 1995.

[SY67] Aaron Strauss and James A. Yorke. "Perturbation Theorems for Ordinary Differential Equations." *Journal of Differential Equations*, **3**(1):15–30, 1967.

[Tak06] Yousuke Takahama. "Journey through the thymus: stromal guides for T-cell development and selection." *Nature Reviews Immunology*, **6**(2):127–135, 2006.

[TDL01] Joyce T. Tan, Eric Dudl, Eric LeRoy, Richard Murray, Jonathan Sprent, Kenneth I. Weinberg, and Charles D. Surh. "IL-7 is critical for homeostatic proliferation and survival of naive T cells." *Proceedings of the National Academy of Sciences*, **98**(15):8732–8737, 2001.

[TDR99] Todd A. Tibbetts, Franco DeMayo, Susan Rich, Orla M. Conneely, and Bert W. O'Malley. "Progesterone receptors in the thymus are required for thymic involution during pregnancy and for normal fertility." *PNAS*, **96**(21):12021–12026, 1999.

[TMA12] Judith Thomas-Crussels, Janet E. McElhaney, and M. Theresa Aguado. "Report of the ad-hoc consultation on aging and immunization for a future WHO research agenda on life-course immunization." *Vaccine*, **40**(32):6007–6012, 2012.

[Tre74] F Trepel. "Number and distribution of lymphocytes in man." *Klinische Wochenschrift*, **52**(11):511–515, 1974.

[VBB08] Nienke Vrisekoop, Ineke den Braber, Anne Bregje de Boer, An F. C. Ruiter, Mariëtte T. Ackermans, Saskia N. van der Crabben, Elise H. R. Schrijver, Gerrit Spierenburg, Hans P. Sauerwein, Mette D. Hazenberg, Rob J. de Boer, Frank Miedema, José A. M. Borghans, and Kiki Tesselaar. "Sparse production but preferential incorporation of recently produced naive T-cells in the human peripheral pool." *Proceedings of the National Academy of Sciences*, **105**(16):6115–6120, 2008.

[VBM01] Laëtitia Vivien, Christophe Benoist, and Diane Mathis. "T lymphocytes need IL-7 but not IL-4 or IL-6 to survive in vivo." *International Immunology*, **13**(6):763–768, 2001.

[Wan05] Michael Wang. *"Nonhomogenous Birth-Death Processes."*. Master's thesis, California State Polytechnic University, Pomona, 2005.

[WDB00] Georg Wick, Pidder Jansen Dürr, Peter Berger, Imrich Blasko, and Beatrix Grubeck-Loebenstein. "Diseases of Aging." *Vaccine*, **18**(16):1567–1583, 2000.

[WHD15] Liset Westera, Vera van Hoeven, Julia Drylewicz, Gerrit Spierenburg, Jeroen F. van Velzen, Rob J. de Boer, Kiki Tesselaar, and José A. M. Borghans. "Lymphocyte Maintenance during healthy aging requires no substantial alterations in cellular turnover." *Aging Cell*, **14**(2):219–227, 2015.

[WHL94] S D Wang, K J Huang, Y S Lin, and H Y Lei. "Sepsis-induced apoptosis of the thymocytes in mice." *The Journal of Immunology*, **152**(10):5014–5021, 1994.

[WP90] Jürgen Westermann and Reinhard Pabst. "Lymphocyte subsets in the blood: A diagnostic window on the lymphoid system?" *Immunology Today*, **11**(11):406–410, 1990.

[YAL08] Eric J. Yagger, Mushtaq Ahmed, Kathleen Lanzer, Troy D. Randall, David L. Woodland, and Marcia A. Blackman. "Age-associated decline in T cell repertoire diversity leads to holes in the repertoire and impaired immunity to the influenza virus." *The Journal of Experimental Medicine*, **205**(3):711–723, 2008.

[Yat14] Andrew J. Yates. "Theories and quantification of thymic selection." *Frontiers in Immunology*, **5**(13):1–15, 2014.

[YKG13] Susannah Yovino, Lawrence Kleinberg, Stuart A. Grossman, Manisha Narayanan, and Eric Ford. "The Etiology of Treatment-related Lymphopenia in Patients with Malignant Gliomas: Modeling Radiation Dose to Circulating Lymphocytes Explains Clinical Observations and Suggests Methods of Modifying the Impact of Radiation on Immune Cells." *Cancer Investigation*, **31**(2):140–144, 2013.

[ZSK07] Allison L Zoller, Frederick J Schnell, and Gilbert J Kersh. "Murine pregnancy leads to reduced proliferation of maternal thymocytes and decreased thymic emigration." *Immunology*, **121**(2):207–215, 2007.